The Lithosphere of the East African Rift and Plateau (Afar-Ethiopia-Turkana): Insights from Integrated 3-D Density Modelling

Dissertation

Zur Erlangung des Grades eines
Doktors der Naturwissenschaften

an der Mathematisch-Naturwissenschaftlichen Fakultät
der Christian-Albrechts-Universität zu Kiel, Germany

Vorgelegt von
Girma Woldetinsae
aus Addis Ababa, Äthiopien

Kiel 2005

Referent: Prof. Dr. H.-J. Götze
Korreferenten: Prof. Dr. Ron Hackney

Tag der mündlichen Prüfung: 12. Juli 2005

Zum Druck genehmigt: 24. August 2005

Table of Contents

List of figures page

List of tables page

Important abbreviations

AAMP:African Magnetic Mapping Project
ANS: Arabo Nubin Shield
APM: Absolute Plate Motion
BGI: Buerau Gravimetric International
CARS: Central Africa Rift System
CASZ: Central Africa Shear Zone
CMER: Central Main Ethiopian Rift
EARS: East African Rift System
EAGLE: Ethiopia Afar Geoscientific Lithospheric Experiment
EAO: East African Orogen
EEP: Eastern Ethiopian Plateau
GBR: Gofa Basin and Range
GRACE: Gravity Recovery and Climate Experiment
GSE: Geological Survey of Ethiopia.
IGF: International Gravity Formula
IGSN71: International Gravity Standardization Net 71
IGMAS: Interactive Gravity and Magnetic Analysis System
KRISP: Kenya Rift International Seismic Project
KR: Kenya Rift
MER: Main Ethiopian Rift
NMER: North Main Ethiopian Rift
MB: Mozambique Belt
WEP: Western Ethiopian Plateau

Acknowledgement

I had very successful years in Germany. Truthfully, without the support of many institutions and individuals my dream would have remained in air. This work was started at Freie Universität Berlin, Institut für Geowissenschaften and completed at the Christian Albrecht Universität zu Kiel, Institut für Geowissenschaften, Geophysik with the support of Katholischer Akademischer Ausländer-Dienst (KAAD). I am very much thankful to KAAD for financing my stay in Germany.

I am very grateful to my advisor Prof. Dr. H.-J Götze for introducing to me the wide range of applications of gravity field and three dimensional modelling, useful suggestions, support and constant encouragement throughout the work. I am very much indebted to the reviewer of this work, Prof. Dr. Ron Hackney for his valuable suggestions and critical comments, which have greatly improved the work. I would also like to thank all the members of the PhD commission: Priv.-Doz. Dr. Bohlen, Prof. Dr. Böning, Prof. Dr. Grotemeyer, Prof. Dr. Janle, and Prof. Dr. Rabbel.

I wish to thank the Geological Survey of Ethiopia (GSE) for permission to use the data sets from Ethiopia and for allowing me to remain absent for such an extended period in order to complete the work. Many thanks are due to Mamushet Zewge, Ketsela Tadesse and all staff members in the GSE and Ministry of Mines for their support. GETECH and the Sudan Geological Authority and BGI are acknowledged for the gravity data sets. I would like to thank Prof. R.G. Keller for allowing to use the recent EAGLE velocity data from the Main Ethiopian Rift, Dr. Jeron Ritesma for sending the tomographic data sets of EARS, Dr. Lithgow-Berteloni for the dynamic topographic model data of Africa, Dr. Andy Nyblade and Mullugeta Dugda for sharing their recent results and Dr. Tanya Furman for chemical compositions of Main Ethiopian Rift lavas.

I would like to extend very sincere thanks to all academic and technical staff of the Institut für Geowissenschaften in Berlin and Kiel for their friendship and support. C. Prezzi and A. Tassara, are thanked for their interest in my work and many useful discussions.

Very special thanks go to Dr. Sabine Schmidt for helping me to use the compute programs. Without the use of her programs this work would have not been realised.

I am very much grateful to Tolla Gillo and Amelework Kassa in Berlin for their constant support and encouragement and in Addis to my mother, brothers and sisters. Many thanks Etenesh for your encouragement.

Abstract

The area encompassing the Eastern branch of the East African Rift System (EARS: Afar-Ethiopia-Turkana) and associated plateaux is an ideal region to investigate extension and magmatism associated with rupturing continental lithosphere. Ethiopia covers an important part of the EARS. It contains the major section of the ca. 5000 km Afro-Arabian rift and includes the transition between the Arabo-Nubian-Shield and the Mozambique Belt.

A compilation of over 45000 onshore and offshore gravity stations covering the EARS and adjacent regions (Eastern Sudan, Red Sea and Gulf of Aden margins) has been made and forms the major data set upon which this study is based. The database is re-evaluated and re-processed using consistent procedures and has an estimated Bouguer gravity error of 1.5-4.5 $x10^{-5}m/s^2$. An attempt has been made to fill data gaps by merging the terrestrial data with GRACE satellite data.

Different regional isostatic Mohos with and without dynamic corrections are produced, interpreted and integrated into a 3D density model. Isostatic residual fields are used to delineate upper crustal structures. The isostatic analysis leads to the conclusion that the broad negative Bouguer anomaly observed in the EARS and adjoining plateau is due to upwelling of the asthenosphere complemented by local crustal thinning and/or underplating. The application of different isostatic models with or without dynamic compensation could not completely explain the Bouguer gravity anomalies under the rifts.

A regional 3D density model is developed using the GIS functionalities of a potential field-modelling program (IGMAS) and integrates seismic constraints with information from isostatic models, global seismic tomography, geological, geochemical, petrological and experimental results. Thirty parallel east-west sections through the EARS are modelled to a depth of 150 km. The 3D density structure reproduces the Bouguer gravity anomaly with a high accuracy (standard deviation of $16x10^{-5}$ m/s^2). Misfits are attributed to errors in the gravity database and unconsidered structures. Sensitivity analysis shows that the allowable density variation for the modelled units ranges from 0.003 to 0.1609 Mg/m^3.

Density and other elastic properties determined from bulk chemical compositions show distinct patterns (bimodality) for pre-rift and post-rift lavas that have crustal and lithospheric origins respectively. The differences imply modification of the lower crust. A rough estimate in the EARS suggests that about 60% of the lower crust under rifts has been modified. Modelled upper crustal thickness is very thin in Afar and Turkana (6-10 km). It increases from the southern terminus of the northern main Ethiopian rift to the central main Ethiopian rift and also further southwards. Very thick upper crust has developed under the western Ethiopian plateau (15-18 km), whereas under the eastern Ethiopian plateau it is relatively thin and localized (12-15). At a depth of 25 km, a large area is represented by middle crustal composition. In central Afar, at the northern end of main Ethiopian rift and Turkana, lower crustal modification due to asthenospheric processes is evident. The anomalous mantle material at a depth of 35 km replaces a significant part of the lower crust under the rift, with complete replacement at a depth of 39 km. The intensive modification in Afar may indicate that the Afar plume is hot and shallow, whereas the Kenya plume is less hot or deeply seated.

The Moho is shallowest (about 16 km) under central and northern Afar, and deepest (48 km) beneath the western Ethiopian plateau. The mean Moho depth is 30 km for the whole region. The maximum load (internal and external) acting in the western Ethiopian plateau is about $8x10^{18}$ kg/m^2. This load has induced a downward flexure of the Moho from a mean depth of 35km to about 45 km. The variation of loads from north to south in the EARS has partly controlled the general rift and lithospheric architecture. The roughly north-south trending Moho gradient near 34°E marks a suture zone. The area between ~8°N and north of Turkana is characterized by relatively deeper Moho. Narrowing of the region of shallow Moho from Afar

to about 8°N in the main Ethiopian rift could be related to the direction of propagation of the Afar plume.

Gravity modelling shows that a significant part of the Bouguer gravity field is generated by density contrasts within the crust. An average density contrast of 0.148 Mg/m^3 is applied to simulate the positive gravity field due to dyke injection under the rifts. A negative density contrast of -0.114 Mg/m^3 is used to model the gravity effect of the upwelling mantle material. Eliminating both these long-wavelength components from the Bouguer gravity anomaly produces a residual Bouguer gravity map that reliably explains the crustal Bouguer gravity effects under the rifts. The basement topography varies from a depth of a few hundred meters to 7 km, and basement highs and lows are related to Precambrian domains and sedimentary basins, respectively. Three broad sedimentary basins, of potential interest for hydrocarbon exploration are identified in the western Ethiopian plateau. A basement high between Turkana and Southern Ethiopian rift might have blocked the further development of the Turkana rift in Ethiopia.

Elastic thickness is calculated using combined topographic loads (corrected by dynamic topographic models) and subsurface loads, and the Moho geometry from the model. Highly tectonized zones in Afar and Turkana are marked by consistently low elastic thickness (less than 15 km), while Precambrian/basement areas are characterized by medium to high elastic thickness (15-35 km). Differences between the elastic thickness estimated during this work and using other methods (e.g. coherence and admittance) are observed in the main Ethiopian rift. Possible explanations include: a) the methods applied here may not be suitable to areas like the main Ethiopian rift, b) the Ethiopian rift is relatively intact/rigid, c) the current locus of the strain shifted from border faults towards the centre of the rift and, as a result, elastic thickness is dominated by the high rigidity of the adjacent plateau.

Analysis of the new gravity database and 3D modelling offers new information on the EARS, namely the isostatic state of the region, crust and upper mantle structures, basement and optimised Moho maps, quantification of modelled units and estimation of rigidity, among others. Based on the present data and new additional data sets, short and long-term scientific goals can be identified. Some of the most important are: further rigidity calculations using the 3D density model, joint modelling of gravity and magnetic data in selected areas, updating of the gravity network in Ethiopia, heat flow measurements in the Main Ethiopian rift and adjacent plateau, and integrated geoscientific experiments in the broadly-rifted region of southern Ethiopia.

Zusammenfassung

Der östliche Teil des Ostafrikanischem Riftsystems (East African Rift system, EARS, im Gebiet von Afar, Äthiopien und Turkana) und die mit dem Rift verbundenen Plateaus sind ein ausgezeichnetes Untersuchungsgebiet zum Studium von Extensionsphänomenen und Magmatismus in zerbrochenen Lithosphärenplatten. Das Gebiet von Äthiopien überdeckt einen wichtigen Teilbereich des Systems, da 5000 km des Afro-Arabischen Rifts in diesem Land liegen. Zum Gebiet von Äthiopien gehört auch das Übergangsgebiet zwischen dem Arabisch-Nubischen Schild und dem Mosambik-Gürtel.

Die Kompilation von über 45000 land- und seegestützten Schwerestationen im Ostafrikanischem Rift und seinen Nachbargebieten (östlicher Sudan, Rotes Meer and Ränder des Golf von Aden) war ein Hauptbestandteil der vorliegenden Arbeit und bildet den Hauptbestandteil des zur Verfügung stehenden Datensatzes. Die Kompilation erforderte die Evaluierung und das erneute Prozessing älterer Daten, sowie in einem erheblichen Umfang Konsistenzprüfungen; nach den vorliegenden Abschätzungen liegt der Fehler für die reprozessierten Bouguer-Schwerewerte bei 1.5 bis 4.5×10^{-5} m/s^2. Versuchsweise wurden zur Auffüllung existierender Datenlücken im Schwerefeld Feldkompilationen aus Satellitendaten verwendet.

Verschiedene Kompilationen von isostatischen Regionalfeldern mit und ohne dynamischer Korrektur sind berechnet worden, um aus ihnen Karten der Ausgleichstiefe zu berechnen, die als MOHO-Tiefen interpretiert werden. Isostatische Restfeldkarten werden verwendet, um Dichteinhomogenitäten in der Kruste zu kartieren. Die Analyse der isostatischen Modellrechnungen legt die Interpretation nahe, dass der breite Gürtel negativer Anomalien im Ostafrikanischen Riftsystem und dem benachbarten Plateau durch eine Aufwölbung der Asthenosphäre (Ausdünnung der Kruste und/oder "underplating") hervorgerufen wird. In diesem Zusammenhang ist darauf hinzuweisen, dass die Bougueranomalien unter der Riftstruktur den durchgeführten Modellierungen nach nicht vollständig durch Effekte isostatischer Ausgleichsvorgänge erklärt werden können.

Für die Konzeption des 3D Dichtemodells wurde die GIS-Funktionalität des Modellierpakets ausgenutzt. Dabei wurden die seismischen Informationen zusammen mit den Befunden zur Isostasie, der globalen Tomographie und den Ergebnissen geochemischer, petrologischer und experimenteller Studien zusammengeführt. Es galt, die regionale Struktur des Modells festzulegen. Diese ist definiert auf 30 vertikalen Modellebenen, die das ostafrikanische Rift überdecken und das Modell bis in eine Tiefe von 150 km aufspannen. Die Standardabweichung zwischen modellierter und gemessener Schwere beträgt 16×10^{-5} m/s^2. Hauptursache für die Abweichungen sind in der Schweredatenbasis und in nicht berücksichtigten Dichtekörpern begründet. Das Programmpaket ermöglicht es, auch Sensitivitätsrechnungen der Modellierung durchzuführen. Dichtevariationen von 0.003 bis 0.1609 Mg/m^3 verschiedener Modellkörper rufen Abweichungen im Modellschwerefeld hervor, die im Fehlerbereich der Schwerewerte liegen.

Die Berechnung von Modelldichten und anderer elastischer Eigenschaften der Lithosphäre basiert auf Auswertungen des Chemismus der Gesteine und belegt die Bimodalität für Prä- und Postrift Laven, die entweder krustalen oder lithosphärischen Ursprung haben. Ferner belegen sie durch Überschlagsrechnungen, dass 60 % der Unterkruste im Riftbereich modifiziert worden ist. Die Dicke der oberen Kruste variiert von sehr geringen Werten im Afar und in der Turkana zu größeren Dicken Im Zentralen Athiopischen Rift und weiter südwärts. In einer Tiefe von 25 km haben große Volumina eine typische Mittelkrustenkomposition. In den Gebieten im Zentral-Afar-Gebiet, dem nördlichen Teil des Rifts und in der Turkana ist die Modifikation der tieferen Kruste mit Transportprozessen aus der Asthenosphäre verknüpft. Ab 35 km Tiefe wird Unterkrustenmaterial im Bereich des Rifts durch anomales Mantelmaterial verdrängt und ab 39

km Tiefe komplett ersetzt. Die intensiven Modifikationen im Bereich des Afargebietes weisen darauf hin, dass der postulierte Afar-Plume heiß ist und in geringer Tiefe liegt, während der Kenia-Plume weniger heiß ist und tiefer liegt.

Geringe MOHO-Tiefen von 16 km werden im Gebiet des nördlichen und zentralen Afars beobachtet, die größten Tiefen von 48 km liegen im Bereich des West Äthiopischen Plateaus; die Durchschnittstiefen für die Gesamtregion liegen nach der Modellierung bei 30 km. Die erreichten Maximaltiefen deuten darauf hin, dass interne und externe Auflasten (loads) von 8 x 10^{18} kg/m^3 eine Flexur der MOHO-Topographie hervorgerufen haben; das Mittel beträgt nach den Rechnungen 35 km, mit Werten bis zu 45 km. Die beobachtete Mohostruktur entlang des Meridians 34°E markiert die Suturzone. Das Gebiet zwischen ca. 8°N und dem Gebiet nördlich der Turkana ist durch eine tiefere MOHO-Lage ausgezeichnet. Die relativ flache Lage der MOHO in der Region zwischen Afar und ca. 8°N im nördlichen Äthiopischen Riftsystem könnte auf die Ausweitung des Afar-Plumes hinweisen. Weiter südlich geht der Trend in der MOHO zu größeren Tiefen, um im südlichen Äthiopischen Rift diffus zu werden.

Die gravimetrische Modellierung zeigt, dass ein erheblicher Beitrag zum Gesamtschwerefeld durch die Dichtekontraste in der Kruste zustande kommt. Ein Durchschnittsdichtekontrast von 0.148 Mg/m^3 musste verwendet werden, um die gemessene positive Schwereanomalie zu modellieren. Die positiven Anomalien werden durch dichtes Material unter dem Rift verursacht. Mit einem negativen Kontrast von -0.114 Mg/m^3 wurde der aufgewölbte Mantel modelliert. Nach Abzug dieser beiden langwelligen Anteile vom Bouguer-Schwerefeld konnte mit dem verbleibenden Residualfeld das Schwerefeld der Kruste interpretiert werden. Die Topographie des Basements variiert danach zwischen Tiefen von einigen 100 Metern bis zu 7 km. Basement Hoch- und Tieflagen korrelieren mit Präkambrischen Domänen, bzw. mit Sedimentbecken. Drei breite Sedimentbecken mit einem erheblichen Potenzial für Kohlenwasserstoff Exploration sind auf diese Weise im Gebiet des westlichen Äthiopischen Plateaus identifiziert worden. Eine Basementaufwölbung zwischen der Turkana und dem südlichen Äthiopischen Rift könnte dafür verantwortlich sein, dass das Turkana Rift sich nicht in Richtung Äthiopien entwickeln konnte.

Die elastische Dicke wurde unter Zuhilfenahme der internen und externen Auflasten, sowie unter Berücksichtigung von dynamischen Topographiemodellen berechnet. Die tektonisch aktiven Zonen von Afar und der Turkana sind durch niedrige Werte für die elastische Dicke gekennzeichnet, während Präkambrische und Basement-Regionen von mittleren bis hohen Werten überdeckt werden. Im Vergleich mit anderen Arbeiten zur Berechnung der elastischen Dicke (etwa durch Kohärenz- oder Admittanzmodelle) kommt es im Gebiet des Äthiopischen Rifts zu größeren Abweichungen. Mögliche Gründe sind: (a) die verwendeten Methoden können generell nicht auf Gebiete wie das Äthiopische Riftsystem angewendet werden, (b) das Äthiopische Riftsystem ist von Natur aus rigide und (c) der aktuelle Strain wird durch die Randverwerfungen in das Zentrum des Rifts transferiert and wird durch die hohe Rigidität der benachbarten Plateaus beeinflusst.

Die Analyse der neuen Schweredatenbasis und die 3D-Modellrechnungen erlauben es, neue Informationen zur Struktur und Entwicklung des Ostafrikanischen Riftsystems zu gewinnen und zwar durch die Untersuchung des isostatischen Zustandes der Lithosphäre, sowie der Basementstrukturen. Hierzu tragen neue optimale Karten der MOHO bei, ebenso wie die Untersuchungen zur Rigidität der Lithosphäre. Auf der Grundlage der erarbeiteten neuen Informationen werden Aspekte kurz- und längerfristiger wissenschaftlicher Zielstellungen diskutiert.

1 Introduction

1.1 Overview

The Afro-Arabian plate, with its unique combination of triple junction (Red Sea, Gulf of Aden and Afar depression of Ethiopia), Cenozoic rifts, Precambrian structures, and multiphase and multidimensional geodynamic episodes, has attracted the attention of many Earth scientists worldwide. The geo-scientific research in this region consists of geodynamic studies in the rift and adjacent plateau, resource exploration and geological mapping in the rift, sedimentary basins and Precambrian areas. The results of studies from topographic, geodetic, archaeological and natural history have also contributed to current geo-scientific thinking in this region.

The study area under consideration specifically covers a large section of the Eastern branch of the East African Rift System (EARS), namely Afar, the Main Ethiopian Rift (MER), Turkana and associated Ethiopian and Northern Kenyan Plateau (Fig. 1). It is an ideal region to investigate extension and magmatism in an environment of rupturing continental lithosphere, in this case using integrated three-dimensional density modelling. In spite of the numerous geoscientific studies both at small and large scales, the interdisciplinary geoscientific experiments are the most relevant to the objective of this work.

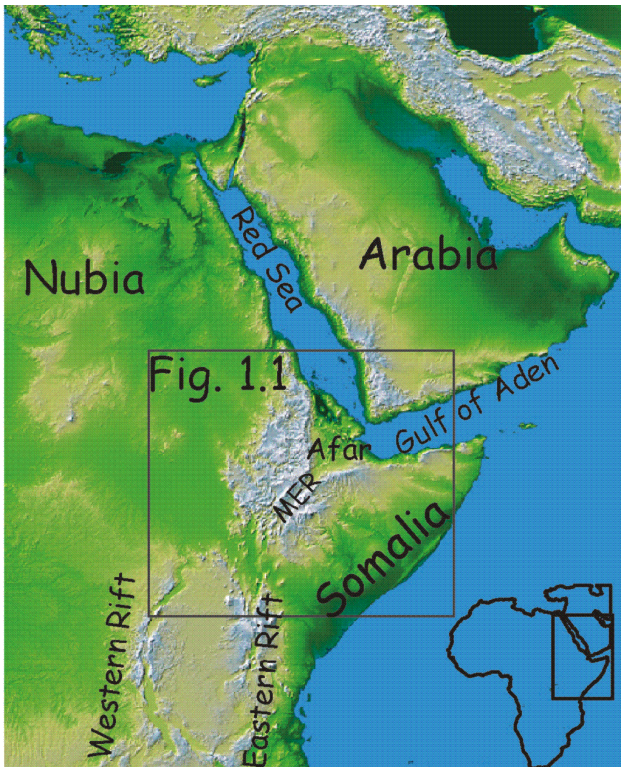

Figure 1. Regional setting of the study area showing the interplay of the three plates (Nubia Arabia and Somalia) at Afar. The image is from the Shuttle Radar Topography Mission (SRTM). More details of the study area are shown in Figs. 1.1, and 2a, b.

The first interdisciplinary geoscientific work in Afar and western Ethiopia was carried out in the early 1970s by a group of German, French and Italian Scientists (Berckhemer et al., 1975). In the early 1990s, a joint German and UK Research group conducted similar experiments in the Northern Kenya rift (KRISP, 1991). Recently, a multi disciplinary project, Ethiopia-Afar-Geoscientific-Experiment (EAGLE), was conducted between 2001 and 2003 by a consortium of European and US institutions (Maguire et al., 2003).

The present work makes use of the results of the above-mentioned major experiments, that span over 1500 km of the plateau and rift region, to broadly assess the East African lithosphere. Compilation of both published and new gravity data sets and 3-dimensional density modelling are also undertaken. The work to be presented here encompasses a substantial region of the EARS with its diverse geologic environments and deals with integration of data across many disciplines. The integrated density modelling contributes to the understanding of upper crustal and deep-seated structures and associated processes. The 3-D modelling has two major purposes: (1) to investigate the various stages of development and different forms of rifting from Turkana to Afar. To the south, basins are intimately associated with rift structures (Turkana and Southern Ethiopian rift system) and to the north the Main Ethiopian rift (MER) joins the mature spreading zone of Afar; (2) to suggest some possible density models prior to continental break up.

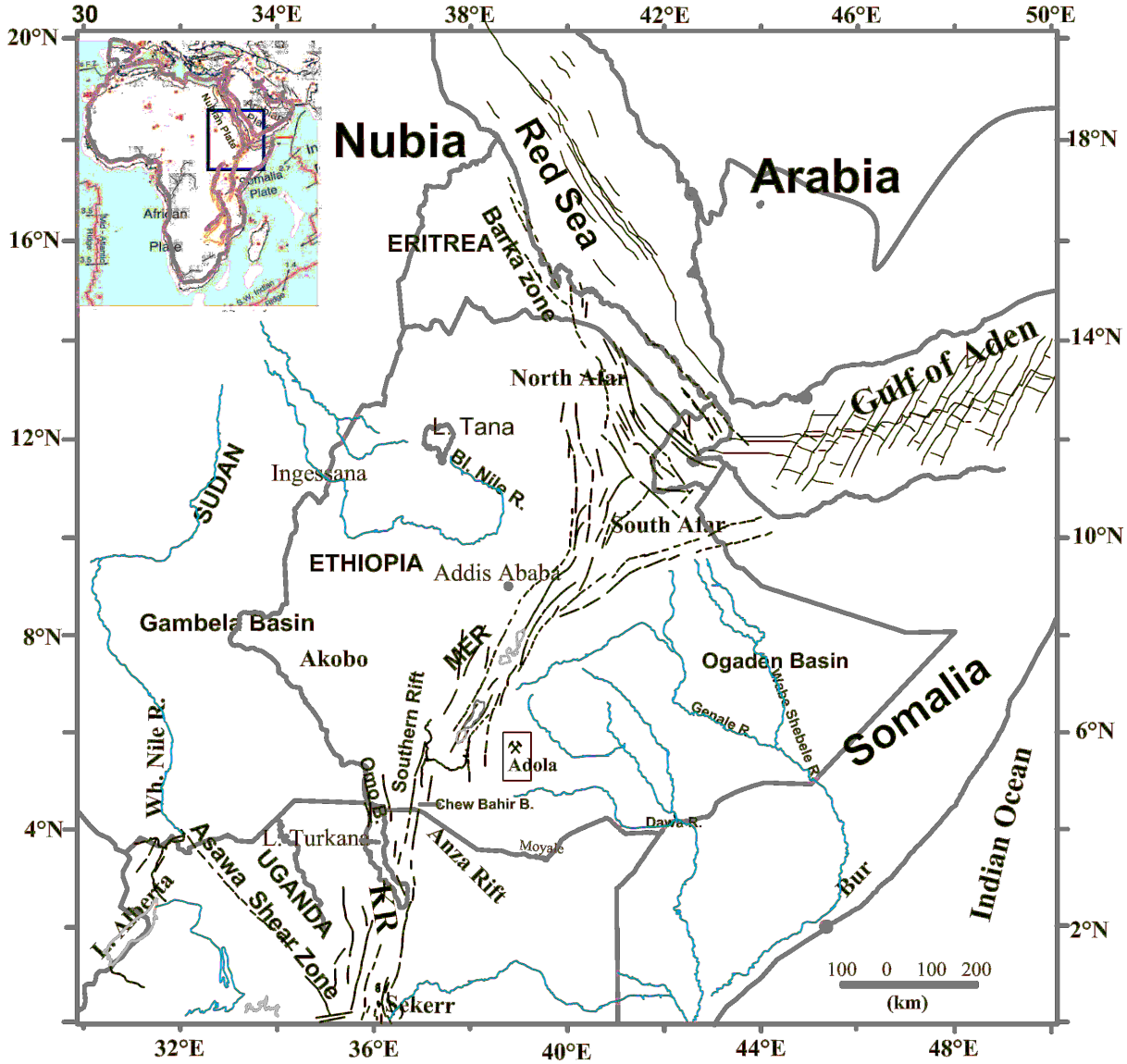

Figure 1.1 Inset shows the location of the study area between 20°N and the equator. It comprises the Arabia, Somalia and Nubian plates that are dissected by the Arabo-African Rift system (Red Sea, Gulf of Aden, Main Ethiopian Rift (MER), Southern Rift, Kenya Rift (KR) and Western Rift systems). The major rivers (light blue lines) flow NW-SE and E-W. The fault systems in Afar, MER, KR, Gulf of Aden, and Red Sea are from CGMW (1968).

The thesis is composed of seven chapters. In the first chapter, the main objectives of the study are outlined. The second chapter discuss topography, geological and tectonic settings. Constraints from ancillary information such as volcanoes, earthquakes, boundary fault systems, and boundaries of major geological units are described. In Chapter 3 major constraining information and additional data sets (e.g. petrophysical data) and different approaches for converting seismic velocity to density are described. Here, densities for the lower crust are calculated using a method that uses chemical composition of lavas, xenoliths and known chemical composition of mantle minerals and also thermodynamic principles. The calculated densities and some elastic parameters are compared and interpreted.

Chapter 4 and 5 deal with the potential field database. The aeromagnetic data coverage in Ethiopia is shown and the gravity database is discussed in detail. Data sources, processing, evaluation, interpretations of Bouguer and free air anomalies, analysis of isostatic models for Precambrian and rift structures and insights on subcrustal lithospheric processes are all dealt with in detail. New isostatic residual maps that make use of dynamic topography models based on subduction history and global tomography are tested to improve the isostatic residual maps. In all cases, the derived Moho, together with the seismically defined Moho, are integrated into the three-dimensional model to aid interactive modification of model geometry. The core of the work is dealt with in Chapter 6, which first presents a short review of forward modelling and interpretation in potential field (gravity) applications, then deals with different types of data integration and the state of the art in the 3D IGMAS modelling system. The final three-dimensional model and important derivatives from this model are shown and the rigidity of the East African lithosphere is computed and interpreted. Chapter 7 discusses the contributions of this work to the current and ongoing debates on the nature of the East African lithosphere and deep structure.

Aim and scope of the study

This work has the following major objectives:

(1) homogenise existing gravity surveys to a common datum (IGSN71) and prepare an error-reduced database that covers a large part of the East African rift and plateau areas;

(2) compile a database for an interdisciplinary interpretation using IGMAS;

(3) investigate the local and regional isostatic state of the lithosphere and perform geologic correlations by removing deep-crustal effects to study the linkage between rift systems;

(4) investigate the influence of dynamic topography on isostasy and compile new isostatic maps corrected for dynamic compensation;

(5) re-assess previous interpretations and forward new ones through integrated three-dimensional density modelling of the East African lithosphere;

(6) study the rigidity of the lithosphere.

2 Topography, geological and tectonic setting

The region under consideration is dominated by plateaux, extensive rifting, complex geology and tectonic history imprinted from the disintegration of Gondwanaland to the present Cenozoic volcanism. During this period, periodic rifting, uplift, marine transgression and regression played the dominant role in the development of the modern East African rift and plateau topography. In this section, the topography and geological and tectonic settings are presented. This is important to consider when constructing the initial model geometry and for interpreting potential field data.

2.1 Topography

The topography data for the continental regions were taken from GTOPO30 and, for oceanic regions, bathymetry data are from Smith and Sandwell (1997). Recently, the Shuttle Radar Topography Mission (SRTM) has released 3-arc second (90 metre) resolution topography data for the entire globe. The part of the image that covers the East African rift and Plateau area is shown in Figure 1. The resolution of the GTOPO30 data is sufficient for the purpose of isostatic calculation and other analysis and interpretation made in this work. The earthquake epicentres for the years 1973-2002 and volcanoes used are accessed at URL: http://wwwneic.cr.usgs.gov/neis/epic/database.htm and http://wwwvolcano.si.edu/gvp/volcano/index.htm, respectively. The Great Rift Valley of Africa that extends through the mid-section of Ethiopia can be traced as elevated plateaus in the central part and as an extensive depression between Kenya and Southern Ethiopia. The filtered topography (using upward continuation to a level of eight km) of the Afro Arabian shield (Fig. 2b) is to emphasize the broad uplifted part of the region (see Fig. 2a for the topographic image and Fig. 1.1 for locations). North of the Main Ethiopian Rift (MER), the rift extends into the Afar depression. To the northeast and east, the Red Sea and Gulf of Aden spreading zones delineate the plate boundaries of Africa and Arabia respectively. Earthquake epicentres (Fig. 2, white circles) coincide with the rift systems and delineate the boundaries between the Arabian, Nubian and Somalian plates (e.g. Kebede and Kulhanek, 1991).

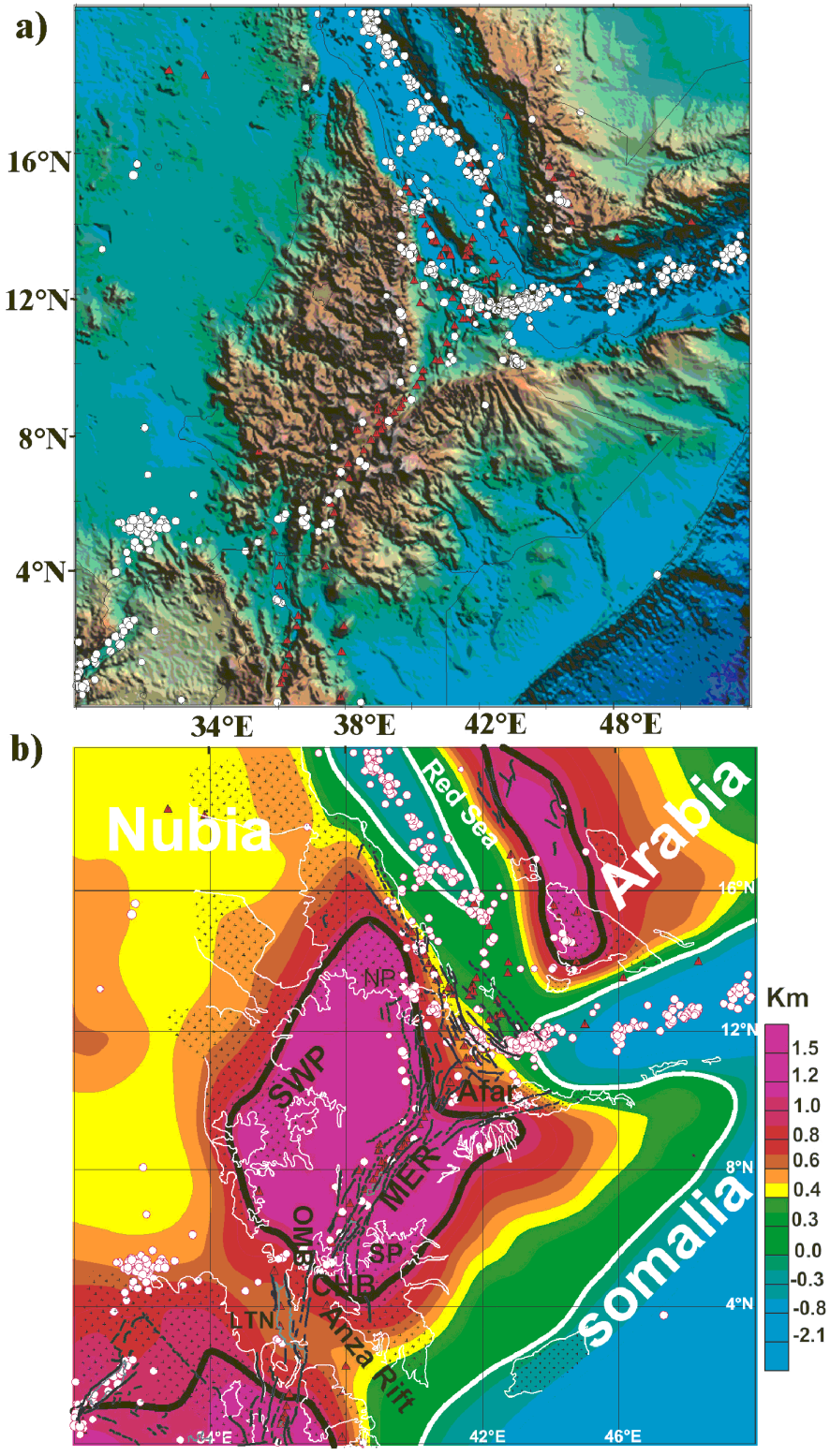

Figure 2 (a) Merged topography and bathymetry sets from GTOP30 and Smith and Sandwell (1997). (b) Low-pass filtered to enhance major long-wavelength features (see text). The area covering the highlands of Ethiopia, Main Ethiopian Rift (MER), East African Plateau areas and elevated areas in Arabian plates are approximately bounded by the 1 km contour (heavy black line). Overlain are earthquakes (white circles) and volcanoes (red triangles) spanning the entire rift system (see text for reference). The fault systems (black lines) and Precambrian boundaries (white lines and dark crosses) are from CGMW (1968). The Precambrian domains include: NP= Northern Precambrian, SP=Southern Precambrian (spanning areas in Kenya and limited by Anza Rift to the south and MER in the north), SWP=Southwestern Precambrian. White thick lines are boundaries for areas below sea levels. Bk=Barka zone, LTN=Lake Turkana, CHB=Chew-Bahir Basin, OMB=Omo Basin.

Within the broad region of the Ethiopian and Kenyan Plateaus, approximated by the 1 km elevation contour (thick black line in Fig. 2b), the average elevation near the central rift valley of Ethiopia reaches about 1500 meters. It is drastically reduced as it merges with the Afar depression to the north and Lake Turkana (LTN), Chew Bahir (CHB) and Omo basins (OMB) to the south (Fig. 2 and Fig. 1.1). The floor of the rift valley is characterized by extensive depressions forming elongated lakes of different size. The lowest inland depression (ca. 100 meters below sea level) is in the Afar area (Dallol). The maximum water depth in the Gulf of Aden reaches 1800 m near 46°E, deepening towards the Afar depression (Hébert et al., 2001).

2.2 Geological and tectonic setting

Knowledge of the geological history is key for constructing a three-dimensional (3D) initial density model and detailed interpretation of the resulting structure. Therefore, this section describes briefly the major geological features, Precambrian/basement structure and Cenozoic history of the crust.

To the northeast, the Arabian plate is bounded by the submerged Red Sea and Gulf of Aden oceanic spreading ridges (see Fig. 1.1). The other boundary that forms the continental boundary is the Afar triangle. The part of the Earth's crust which combines the eastern section of Africa (Horn of Africa) and part of the Arabian plate could be termed as the Afro-Arabian plate (Fig. 1.1). In this region, the East African Orogen (EAO) and the mainly basement areas (Figs. 2b, 2.1) represented by the Mozambique belt (MB) and the Arabo-Nubian Shield (ANS) and the Eastern branch of the East African Rift system, are the most important geological features. The difference between the two is partly related to metamorphic grade, otherwise there is no distinct boundary, and both are part of the EAO.

The Mozambique belt (MB) and the Arabo-Nubian Shield (ANS) represent Neoproterozoic orogenic belts in northeast Africa (e.g. Vail 1983; Berhe, 1990; Stern, 1994, see also Fig. 2.1). The Mozambique belt can be traced along the eastern margin of the African continent to the north of Kenya and Uganda (e.g. Vail, 1983; Kröner, 1985) and may extend through southern Ethiopia as far as Egypt (see Fig. 2.1). The MB is the result of Precambrian deformation and metamorphism that led to observed variations in composition of rocks of different ages (e.g. Vail, 1983). The ANS covers large sections of the Red Sea and extends along East Africa into Sudan, Eritrea and Ethiopia. It is characterized by juvenile island arc associations and ophiolitic complexes and is largely composed of volcanic rocks of calc-alkaline affinity, metasediments and low-grade metamorphism (e.g. Berhe, 1990; Abdelsalam and Stern, 1996, and Fig. 2.1).

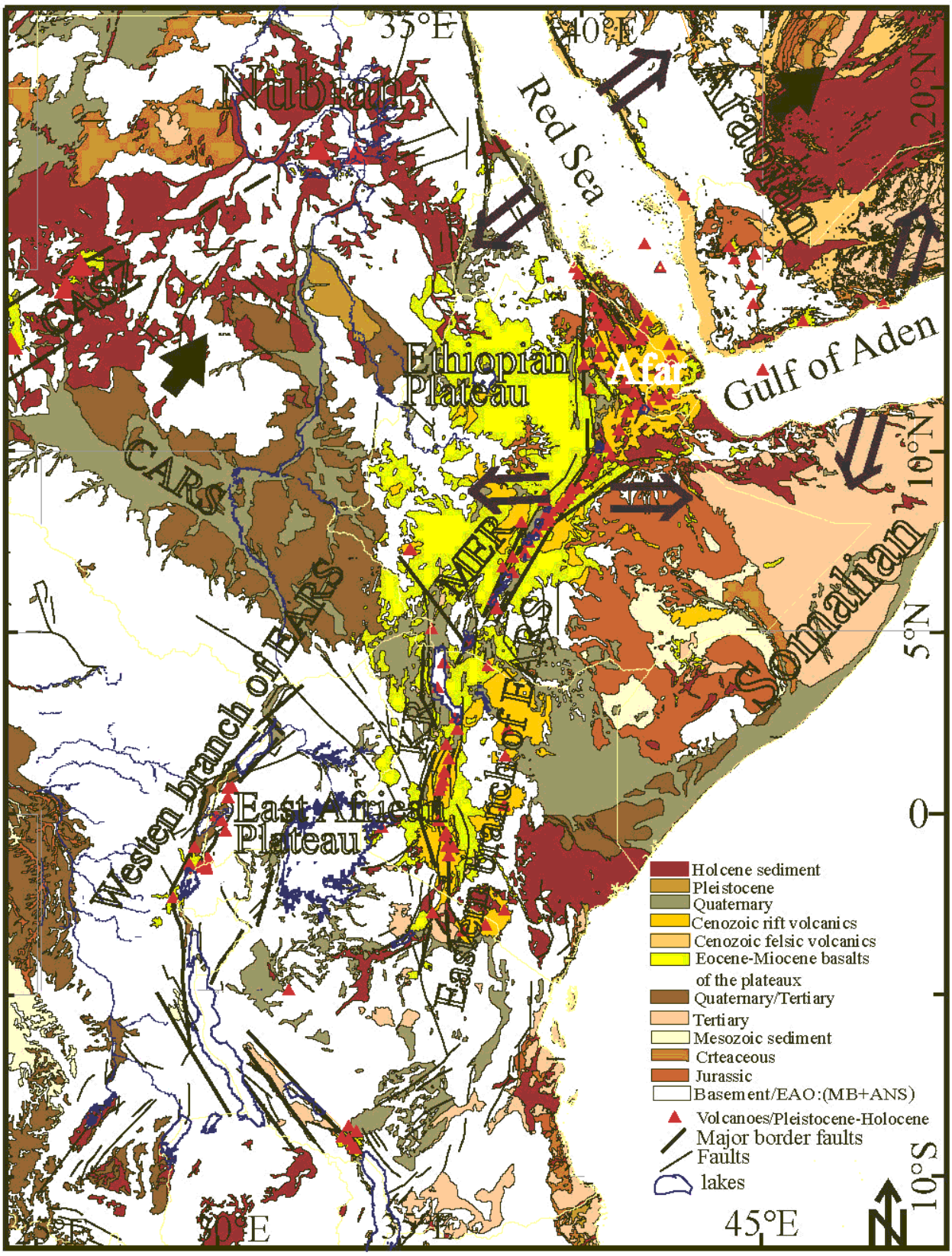

Figure 2.1 Regional geology showing major lithological units and tectonic features. The map is largely modified from different sources: CGMW (1968); Woldegabriel et al. (1990); Ebinger and Ibrahim (1994); Tefera et al. (1996); Hearn et al. (2001). CARS: Central Africa Rift system (Mesozoic), CASZ: Central Africa Shear Zone, KR=Kenya Rift, MER= Main Ethiopian Rift. Solid arrows: Absolute Plate Motion (APM) directions: Nubia plate=10 mm/yr; Arabia plate=30 mm/yr (Argus and Gordon, 1991). Brown Arrows: direction and relative plate velocities (MER= 7 mm/yr, Fernandes et al. (2004); Red Sea area= 20 mm/yr, Joffe and Garfunkel (1987); Gulf of Aden= 23 mm/yr, Jestin et al. (1994).

Mafic-ultramafic rocks are widely distributed in northern (e.g. Berhe, 1990; Tadesse, 1996), western (Mogessie et al., 2000; Braathen et al., 2001; Allen and Tadesse, 2003), and southern (Worku, 1996; Yibas et al., 2002) Ethiopia, and in Eritrea along the Barka zone (e.g. Berhe, 1990).

The Cenozoic history of the crust in Ethiopia was affected by a major change after the onset of rifting between the Nubian and Arabian plates ca. 25 million years ago (e.g. Ukstins et al., 2002). The rifting and sea-floor spreading along the Red Sea and Gulf of Aden, the displacement of Arabia northward and collision with Eurasia culminated in the formation of a broad zone of extension across the Afar depression as well as sedimentary basins in the Red Sea and Gulf of Aden. A broad thermal anomaly and associated buoyancy due to low density material (e.g. Lithgow-Bertelloni and Silver, 1998) vis a vis a single plume model (e.g. Ebinger and Sleep, 1998), two plumes (e.g. George et al., 1998) or separation of deeper mantle upwelling into three currents (e.g. Davis and Slack, 2002) may have triggered rifting in the entire Precambrian plate and the adjoining marginal parts of the Arabian and African plates were uplifted. The domal uplift in the early Tertiary and the Cretaceous and early Tertiary rifts are imprinted on erosion surfaces and form the main physiographic elements (Kazmin, 1972).

In the Oligocene (~26 Ma) and Pleistocene, the major fault scarps (grabens) formed (e.g. Davidson and Rex, 1980). The rift margin is characterized by Miocene volcanic construction (e.g. Tesfaye et al., 2003), relatively high seismicity (e.g. Kebede and Kulhanek, 1991) and geothermal activity (e.g. Berktold et al. 1975). In the Oligocene and Miocene, a marine trough formed in the Red Sea by the rupturing of the Precambrian lithosphere (Cochran, 1983, Cochran, 2005).

Figure 2.1 shows the distribution of Pleistocene to Holocene volcanoes. They range from massive central volcanoes over the plateau to small volcanic vents or edifices in the depressions (Tefera et al., 1996 and Fig. 2.1). Davidson and Rex (1980) argue that volcanism in the Ethiopian rift has migrated southwards and that Quaternary volcanism is not limited to the rift, but also extends beyond it and is related to newly developing fracture zones. The systematic younging of the Ethiopian volcanism from north to south (e.g. George et al., 1998; Ukstins et al., 2002) probably indicates the direction of influence of the mantle material or plume (see also Ebinger and Sleep, 1998; George et al., 1998; Knox, et al., 1998). Detailed study of the Ertale and Ayala ranges in Afar by Barberi et al. (1970); Barrat et al. (1998) and historic flows at Fantale, show that volcanism is continuing in Afar and northern MER.

3 Constraining information and data

This chapter brings together available geo-constraints and shows how the initial structure of the 3D model (Chapter 6) was derived. The major constraints from surface (geothermal manifestations, temperature and heat flow data) to deep probing methods (lithospheric seismic experiments and tomography models) are presented here and used to calculate the densities of the lower crust or convert seismic velocities to densities.

3.1 Regional heat flow and temperature

How do we estimate the density contrast at the mantle lithosphere/asthenosphere boundary? Where is this boundary located? How thick is the lithosphere and what are the approximate temperatures underlying the enigmatic East African lithosphere? These are at least some of the fundamental questions that need to be addressed to prepare the initial geometry of the three dimensional model. These problems at the first hand could be tackled by re-assessing the available heat flow and temperature data.

Temperature is a critical parameter that has a profound effect on the rheology of rocks and minerals. The heat flow data available in this region (e.g. see the global distribution: http://www.heatflow.und.edu/index2.html and Fig. 3a extracted for east and south Africa) does not allow well constrained modelling of appropriate geotherms. However, the scarce regional heat flow data is subjected to a large interpolation distance in order to give and indication of possible geotherms that represent the temperature distribution in the rift and adjacent plateau regions. The regional heat flow map (Fig. 3a) for eastern and southern Africa displays a 70-80 mW/m^2 trend in the rift zones of Ethiopia and Kenya and 40-50 mW/m^2 in the adjacent plateau regions. Based on this average trend and an assumption of a steady-state thermal condition and mantle adiabats of 1300°C; two geotherms: 45 mW/m^2 and 75 mW/m^2 corresponding to the plateau and active rift zones respectively are calculated using the relation and constants from Turcotte and Schubert (2002) for the study area (Fig. 3b).

Fadaie and Ranalli (1990) use the heat flow (106± 21) for the east African rift south of Turkana in order to develop reheological properties of the lithosphere of EARS. Rheological analysis from their work shows a thickness of the most brittle layer of 10-12 km and in shield/craton area it reaches 53-64 km, whereas the rheological thickness of the lithosphere (the lower limit of strength) is 23-30 km for EARS and ca.135 km for adjacent cratons. The geotherm for the rift zones show a temperature variation from 220°C at 10km to 572°C at 40km

and reach about 1000°C at a depth of 85km, whereas the geotherm for the plateau display a slight variation of 213°C at 15km, 474°C at 40km and about 1000°C at 95km (Fig. 3b).

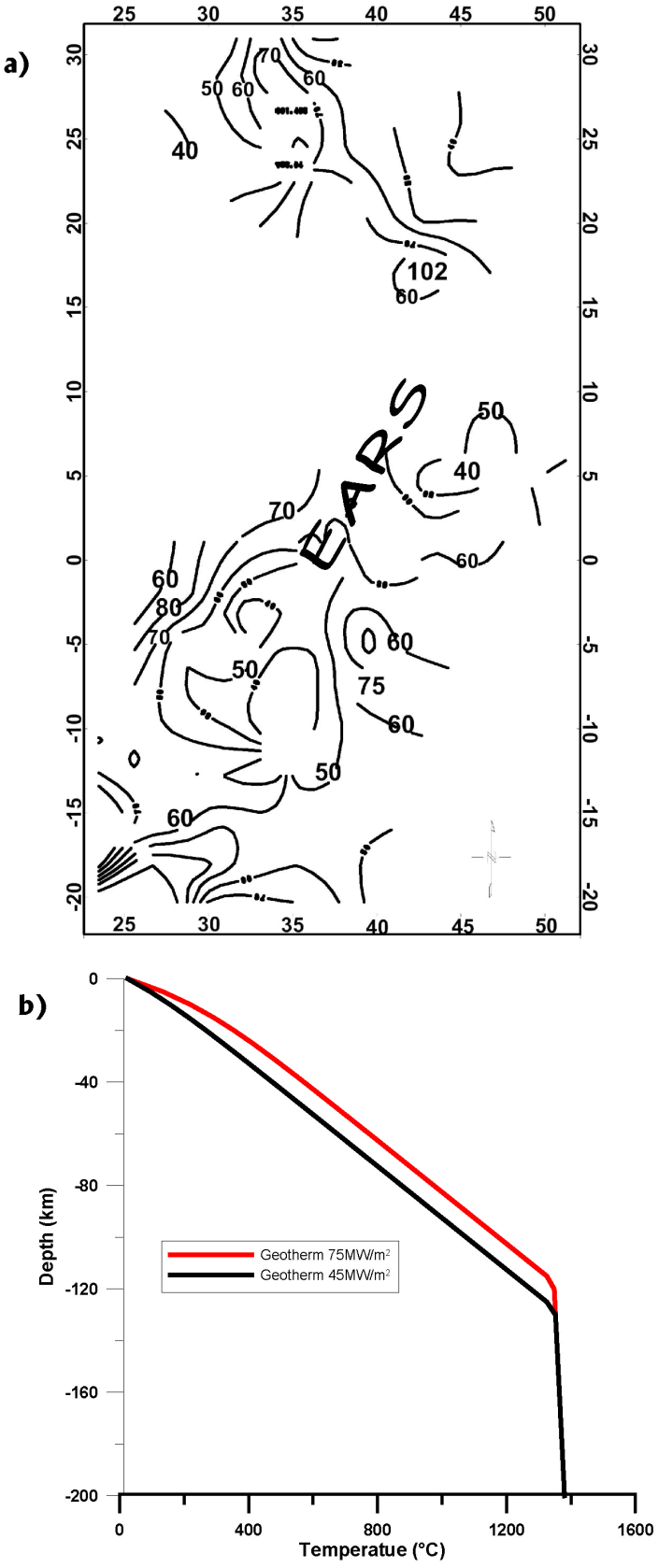

Figure 3. a) Regional heat flow for Eastern and Southern Africa (data source Global heat flow database (see text). b) Geotherms calculated using average heat flow data for East Africa (see text).

The geotherms and the assumed mantle adiabats of 1300°C intersect at a depth of about 110 km and 122 km. These depths could represent the approximate thickness of the thermal lithosphere in this region. Global thermal structure modelling (e.g. Artmieva and Mooney, 2001) that is based on compilations of the heat flow data (Pollack et al. 1993; and for up to date information, see www.heatflow.und.edu/index2.html), estimates two typical thicknesses of 200-220km for the Southern hemisphere and 300-350km for the Northern hemisphere. Being an area between early Proterozoic and middle to late Proterozoic (Goodwin, 1996), the thickness of the East African lithosphere could be 140±50 km.

Independent estimations of temperature based on petrological modelling and seismic refraction data, though highly variable in the entire rift region, show about 800°C at a depth of 6-14 km below Afar (Berckhemer et al., 1975, Berktold et al., 1975). This may be accepted in Afar, where oceanic crust is expected or maximum thinning is observed. It is also associated with low resistivity from 10-50 ohm-m at about 15 km (Berktold et al., 1975). Makris (1974) parallels the phenomena in Afar with the mid-oceanic ridge systems of Iceland where temperatures of 800°C to 1000°C occur at 10 to 15 km depth and high thermal gradients of the order of 50°C to 60°C/km are estimated. Recent geothermal drilling by the Geological Survey of Ethiopia (GSE) shows a maximum reservoir temperature of about 350°C at a depth of 2.5 km in Langano-MER and 270°C at a depth of 2.1 km in Tendaho-Northern Afar (Teklemariam, 2004). Xenolith data are very scarce in the Ethiopian rift. However, studies of xenolith from southern Ethiopia (adjacent to the southern Rift system, Mega area) by Bedini et al. (1997) shows an equilibrium temperature of 850°C-1040°C using the pyroxene method. Other geothermometer yield a temperature range of 1130°C ±10 for deformed peridotite and 1210°C (+20) for granular peridotite (Bedini et al. 1997).

Based on the above results, the thickness of the thermal lithosphere is assumed to be 110 km under the rift and 120 km beneath the plateau. The base of the seismic lithosphere, or top of the convective mantle (Goodwin, 1996), may be as deep as about 150 km below the East African rift and plateau. Therefore, a thickness of 150 km is used for the lithosphere in the 3-D model.

The geotherms discussed above are used to make density calculations and other elastic properties are estimated from seismic velocities and using the bulk chemical compositions of various rock types in the region.

3.2 Constraints from lithospheric scale seismic studies

3.2.1 Seismic studies

Deep probing data sets (e.g. seismic refraction experiments, shear wave tomography models and geochemical data) consistently show a low velocity region probably stemming out from the 440 km mantle boundary. The low velocity region at least underlies the rift region in the upper mantle.

Important data about the deep crustal/lithospheric structure mainly comes from seismic experiments in the Afar (Berckhemer et al., 1975), Djibouti region (Ruegg, 1975), MER (Maguire et al., 2003) and Kenya (KRISP Working Group, 1991) and global seismic tomography (e.g. Ritsema and Van Heijst, 2000). Crustal thickness from gravity and seismic data show 5 to 6 km thick oceanic crust in the centre of the Red Sea (e.g. Prodehl et al., 1997), 15 to 25 km beneath the NMER and Afar (e.g., Makris, 1975; Prodehl et al., 1997), 35 to 40 km beneath the Ethiopian plateau, and in the northern Afar the crust thins to 10-18 km (Berckhemer et al., 1975). The deep-seismic studies of Berckhemer et al. (1975) across the Ethiopian rift, Afar and adjacent highlands identified low seismic velocity anomalies (7.4-7.8 km/s) beneath the rift. To the south, the KRISP project in the Kenyan rift revealed that the crust of the Kenyan rift thins along axis (N-S) from about 35 km near the Kenya dome (about the equator) to 20 km towards the Lake Turkana area (e.g. Keller et al., 1994). Like the Turkana KRISP experiment, the recent EAGLE geoscientific experiment in the MER, particularly the axial seismic profile, show similar axial thinning along the 450 km length of the rift. A low velocity (~ 7.5 km/s) under Southern Afar could be interpreted as mafic lower crust (Keller et al., 2004, Fig. 3.5a), and similar velocities in the uppermost mantle beneath the Kenya dome (Mechie et al., 1994; Keller et al., 2004). The cross-rift profile about 400 km long shows a significant crustal asymmetry with a 48 km thick crust to the west of the rift and a 38 km thick crust to the east of the rift (Mackenzie et al., 2004). Beneath the western edge of the model, a velocity of 7.5 km/s is interpreted as a lower crustal body (Mackenzie et al., 2004). Both velocity models (KRISP and EAGLE) are integrated into the 3D density model (chapter 6) and other results from shear wave splitting, receiver functions and magnetotelluric studies are discussed in the interpretations.

3.2.2 Global shear wave structures

An analysis of shear waves demonstrates that the low velocity structures extend to a depth of 250 km under the Mid Ocean Ridge and the Afro-Arabian Rift (Ritsema and Van Heijst, 2000) and reach down to the depth of the 660 km discontinuity (Debayle et al., 2001) beneath the northeastern Afro/Arabian continent. The global seismic tomography indicates the existence of a large-scale low-velocity anomaly beneath the African plate, which dynamically supports

the excess elevation in the East African Plateau (e.g. Grand et al., 1997; Lithgow–Bertelloni and Silver, 1998; Ritsema and Van Heijst, 2000; Gurnis et al., 2000).

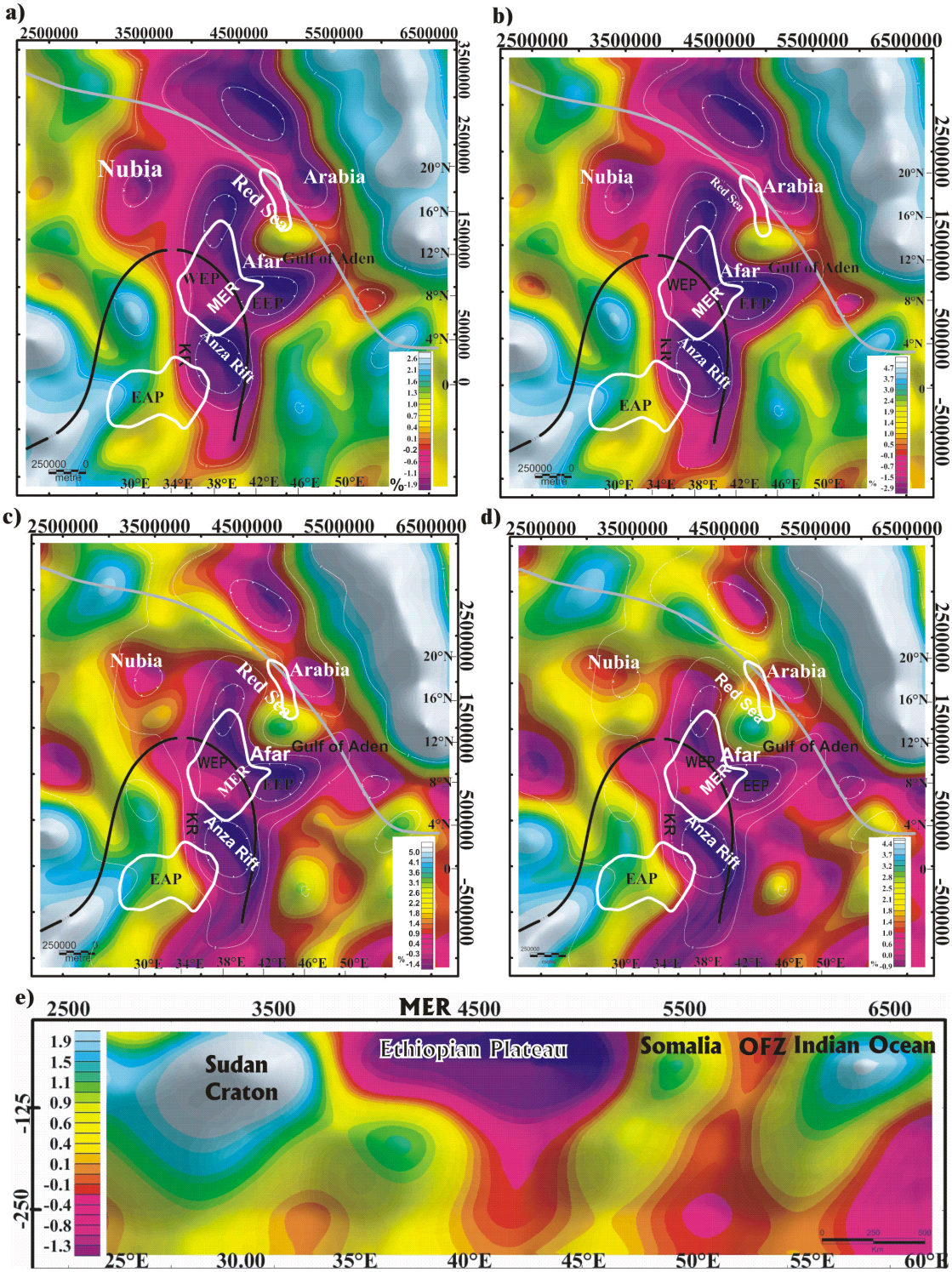

Figure 3.1 Global shear wave tomography using data from Jeron Ritsema (pers. comm.). Colour scale represents percentage velocity differences from reference model (PREM). The depth slices are at: a) 40 km, b) 70 km, c) 120 km and d) 150 km. The 1km topography contour (white line) outlines the plateau and 500 m dynamic topography contour (black line) and zero contour grey lines are also shown. e) A cross-section to a depth of 300km along 7°N intersecting the Sudan craton (Nubia plate), MER (Ethiopian plateau), Somalia plate and ending in the Indian Ocean (OFZ), see text. EAP: East African Plateau, EEP: Eastern Ethiopian Plateau, KR: Kenya rift, MER: Main Ethiopian Rift, WEP: Western Ethiopian Plateau.

The part of the data set for the East African region (Jeron Ritsema, pers. comm.) was used to prepare representative sections and depth slice maps overlain by tectonic features (Fig. 3.1 a-d). These figures assist the interpretation of the deeper lithosphere of East Africa that corresponds to the fast and slow velocity patterns. The depth slices between 40 km and 150 km show a distinct slow velocity anomaly that covers most of the Nubia-Somalia plateau and rift system. Anomalous slow velocities are particularly clear in Turkana and below Afar, where they are probably related to plume heads or to channelled upwelling mantle.

At greater depth, the anomaly appears to be limited by the 0 contour of the dynamic topography in the northeast, while it coincides with the maximum contour (600m) to the southwest (see chapter 6 for dynamic topography models). These two extremes could be related to the downwelling (at the start of fast velocity) and upwelling of the mantle currents/asthenosphere respectively (see Fig. 3.1). Figure 3.1e shows an example cross-section across 7°N latitude that intersects the Sudan craton, Ethiopian plateau, MER, Somalia plate and ending at about Own fracture zone (OFZ) in the Indian Ocean. To the west and east of the MER, the Nubia plate and Somalia plate are marked by fast velocity that may indicate intact mantle lithosphere (Fig. 3.1e). In particular, the cross-section highlights a plume type slow velocity anomaly under the Ethiopian plateau and the Main Ethiopian Rift (MER). The anomaly is consistently strong to a depth of 300 km. At the east end of the section (beyond OFZ), the start of a slow velocity anomaly is part of the Mid Oceanic Ridge System that joins the Gulf of Aden ridge system to the north and the Carlsberg ridge to the south. The depth contour plots of the shear wave velocity structures are digitised for the whole area and integrated into the 3D structure using the 3D functionality of IGMAS (see Chapter 6).

3.3 Density Determination

3.3.1 Velocity to density conversions

There are several conversion methods of velocity to density that utilize the inter-dependent relationships between density and seismic velocities. The widely practiced method is the linear approximation to the curve of Nafe and Drake (1957). Uncertainties in this approximation are on the order of $\pm$ 20 Mg/m^3 (Barton, 1986).

In this study, density and elastic parameter calculations are made in two ways:

1) using analytical relationships (Sobolev and Babyeko, 1994; see below) and the temperature and pressure calculated at specific depth for the geotherms described above and the seismic velocities of the lower crust as reported by Berckhemer (1975), KRISP (

1991) and Keller et al. (2004). Results of these velocity conversions are summarized in Table 1.

2) using the bulk chemical compositions of selected xenoliths, lavas and samples across Turkana, MER, Afar and Ethiopian Plateau, that may represent the lower crustal compositions of the lithosphere and the program code developed by Sobolev (pers. comm.).

The Sobolev and Babyeko (1994) approach is applied in many studies (e.g. Döring, 1998; Ebbing, 2002). The approach takes into account insitu temperature and pressure and velocities are converted into in situ densities using the following three steps:

1) $V_{p,0} = V_{p,insitu} - \frac{\partial Vp}{\partial P} P - \frac{\partial Vp}{\partial T} (T-25°C)$

where $V_{p,0}$ = velocity under normal pressure and temperature conditions (T_0=25°C, Po=0.1MPa) and $V_{p,\ insitu}$= measured velocity (e.g. from seismic experiments),

$\frac{\partial Vp}{\partial P} = 0.12$ km/s GPa and $\frac{\partial Vp}{\partial T} = -0.00045$ km/s °C

2. Using the $V_{p,\ 0\ values}$, densities are calculated from the following relations.

$\rho_0 = 0.446\ V_{p,\ 0} - 0.074$ for a range of 6.05 km/s $\leq V_{p,0} \leq$ 6.695km/s

$\rho_0 = 0.487\ V_{p,\ 0} - 0.359$ for a range of 6.95km/s $\leq V_{p,0} \leq$ 7.80km/s

3. This step gives the insitu densities and is calculated using the following relations:

$$\rho_{insitu} = \rho_0 + \frac{\partial \rho}{\partial P} P + \frac{\partial \rho}{\partial T} (T-T0) \quad with \quad \frac{\partial \rho}{\partial P} = 0.05 Mgm^{-3}/GPa, \quad \frac{\partial \rho}{\partial T} = -0.00009 Mg\ m^{-3}/°C$$

Table 1 shows the densities determined using the above relations for velocities from the EARS. The estimation of P and T using the approximate geotherms calculated from the scarce heat flow data in EARS reduces additional errors into the calculations. Other uncertainties inherent in the above relations are the range of values for the constants as indicated above (first step) and the average relations in the second step corresponding to felsic and mafic rocks.

Table 1

Density calculated using the method of Sobolev and Babyeko (1994): Vp= average velocity, Po= Pressure in GPa, P= insitu pressure in GPa, D= depth in km, T= temperature, ρ=density

Main Ethiopian Rift (EAGLE profile along the rift), velocity data from Keller et al. (2004)					
Vp	Po	P	D	T	ρ
7.6	1.1	1.2	40	573	3.28
7.6	0.96	1.06	35	521	3.28
7.6	0.755	0.855	27	440	3.29

Continued from Table 1					
7.55	0.598	0.698	37	546	3.26
7.5	0.77	0.87	28	446	3.24
7.5	0.71	0.81	26	424	3.25
7.2	1.1	1.2	40.5	573	3.08
6.65	0.55	0.65	20	355	2.85
6.4	0.07	0.17	2.25	134	2.77
6.625	0.41	0.51	15	292	2.85
6.6	0.26	0.36	9	219	2.85
6.45	0.014	0.114	0.42	40	2.80
6.75	0.16	0.26	6	153	2.92
6.85	0.18	0.28	6.5	162	2.97
6.45	0.08	0.18	3.1	94	2.79
6.85	0.22	0.32	8	188	2.96
6.42	0.08	0.18	3.5	93.32	2.78
Turkana North to Baringo South, Velocity data KRISP 1991					
6.275	0.27	0.37	10	220	2.71
6.4	0.49	0.59	18	330	2.75
7.4	0.57	0.67	21	362	3.21
7.75	1.1	1.2	40	572	3.35
7.2	0.57	0.67	21	362	3.11
6.4	0.3	0.4	11	220	2.76
6.5	0.49	0.59	18	330	2.80
6.75	0.6	0.7	22	379	2.90
7.6	0.62	0.72	23	390	3.30
7.7	1.1	1.2	40	572	3.33
6.4	0.35	0.45	13	264	2.75
6.65	0.64	0.74	23	390	2.86
7.225	0.82	0.92	30	390	3.11
7.65	1.1	1.2	40	572	3.31
Ethiopian rift and plateau based on Afar-Ethiopia experiment, velocity data from Berckhemer et al.(1975). Geotherm is similar to the above except for the plateau area.					
6.3	0.22	0.32	8	188	2.72
7.6	1.04	1.14	38	552	3.28
6.9	0.49	0.59	18	330	2.97
7.5	0.99	1.09	36	531	3.24
6.3	0.16	0.26	6	153	2.72
6.9	0.49	0.59	18	330	2.97
7.6	0.97	1.07	35	520	3.29
6.35	0.22	0.32	8	188	2.74
6.9	0.49	0.59	18	330	2.97
7.65	0.77	0.87	28	446	3.32
6.3	0.27	0.37	10	219	2.71
6.9	0.79	0.89	29	456	2.96
Western flank Didesa (Ethiopia) Geotherm 45 is used, Velocity from Berckhemer et al. (1975)					
6.3	0.22	0.32	8	133	2.72
6.9	0.63	0.73	23	300	2.98

3.3.2 Measured densities

Densities of surface samples and from geothermal bore holes in the Main Ethiopian Rift measured by the Geological Survey of Ethiopia, along with representative density measurements from the Precambrian rocks of western Ethiopia, are presented in this section. The density assessment at crustal and lithospheric scales is not only important for setting the initial densities in the three dimensional model, but also provides some insights into lithospheric processes and interpretations.

Density measurements in the Northern Main Ethiopian Rift (NMER)

Some 800 density measurements made at the petrophysical laboratory of GSE were acquired for this study and the following summary has been made based on these data. The rock units measured represent the surface exposures in NMER and are mainly pyroclastic flows, tuffs, ignimbrites, basalt flows, limestone, pumice, marble and granitic gneiss. Doubtful measurements from only a few samples (less than two) are removed in order to allow for reasonable mean and average values to be determined. Figure 3.2 is produced using these measurements. The minimum density is 1.21 Mg/m^3 for pumice and tuffs, the maximum 3.06 Mg/m^3 (based on two samples) for basaltic flows, and the mean value 2.23 Mg/m^3 for the NMER. The detailed statistics of the various groups of rocks are summarized in Table 2.

Table 2.
Summary of density measurements in NMER (Mg/m^3)

Rock type	# samples	Min	Max	Mean	SD
Basalt	277	1.54	3.06	2.31	0.403
Granite	9	2.31	2.83	2.57	0.162
Granite gneiss	10	2.33	2.97	2.77	0.185
Ignimbrite	137	1.70	2.97	2.28	0.258
Limestone	31	1.44	2.69	2.35	0.468
Marble	8	2.64	2.98	2.72	0.125
Obsidian	27	1.90	2.49	2.35	0.118
Pumice	12	1.11	2.40	1.81	0.449
Pyroclastic	38	1.99	2.87	2.38	0.192
Tuff	172	1.14	2.70	2.03	0.378

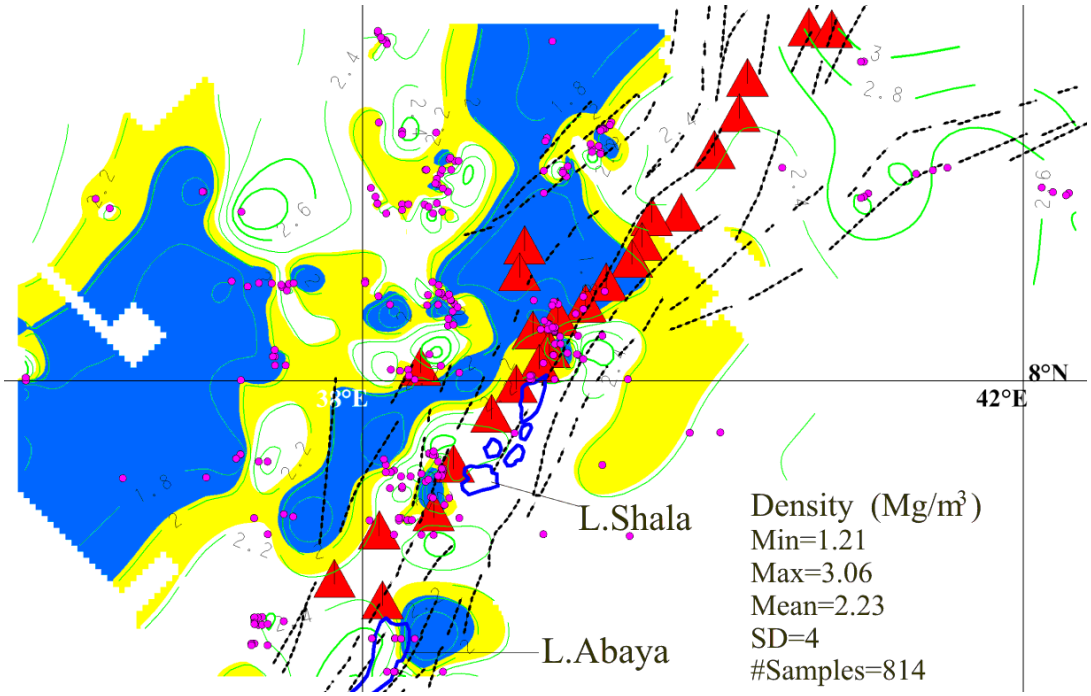

Figure 3.2 Measured densities (Mg/m^3) using samples from around the NMER: Blue colour is for less than 2 and yellow less than 2.2 (tuffs, pumice, and pyroclastic flows). Volcanoes (red triangles), sample locations (pink circles) and faults (black dotted) lines are shown.

Bore hole density measurements from geothermal boreholes in the MER were also made by the Geological Survey of Ethiopia. The compilation of borehole measurements from Belaineh (1983) shows similar lithologies to the surface measurements at a maximum depth of about 2.2 km.

Density measurements from western Ethiopian plateau

Density/susceptibility measurements of about 100 samples collected from Neoproterozic suits of western Ethiopia that may represent basement units were made as part of a detailed and integrated geophysical investigation of the Egambo and Baruda prospects (Woldetinsae et al., 2000). The density measurements are particularly useful for the 3D modelling. Table 3 shows the measurements.

Table 3
Averaged density/susceptibility from the Neoproterozoic rocks of western Ethiopia

Rock type	No. samples	Density (Mg/m^3)	Susceptibilityx10^{-6}cgs unit
Quartz/quartzite	3	2.45	0
Breccia	14	2.55	65
Metasediment	4	2.29	100
Graphite schist	4	2.36	148
Sericite schist	11	2.38	186
Ultrabasic	3	2.62	203
Serpentinized rock	5	2.79	243
Chlorite schist	17	2.58	432
chlorite	6	2.70	631

Continued from Table 3			
Sericite chlorite schist	2	2.58	812
Magnetite bearing (sulphide rich rock)	2	2.70	1527
Talc schist	4	2.51	2027
Talc chlorite schist	1	2.56	2080
Sericite schist (garnet bearing)	1	2.31	37724
Talc sericite schist	1	2.09	55443
Average density for the area		2.47	
Meta-sediments and schists		2.1-2.4	
Ultrabasics, Serpentinite, Chlorite		2.5-2.8	

Alternatively, density calculations (not presented here) using the regional bulk chemical compositions from Tadesse and Allen (2004) and Sobolev code (pers. comm.) are made to estimate densities underlying the metamorphic basement of western Ethiopia. Analysis of these calculations does not particularly change the regional density model. Furthermore, the geotherm used for the calculation is based on regional approximation and makes it less reliable. Tadesse and Allen (2004) report that rocks from this area represent an ophiolitic terrane of crustal origin and their samples are partly tholleitic, but mostly are subalkaline and basaltic andesitic composition.

Density information from Eastern Sudan

The density information used to model the Eastern Sudan (sediments) is taken from the compilation work of Ibrahim et al., (1996) as indicated in (Table 4).

Table 4
Composite density log measurements (after Ibrahim et al. (1996).

Layer density (Mg/m^3)	unit	Depth range (km)
2.25	L. Cenozoic	0-0.7
2.35	Paleogene	0.7-2
2.55	L. Cretaceous	2-2.9
2.65	E. Cretaceous to L. Jurassic	2.9-3.5

3.3.3 Density calculations using chemical compositions from MER, Turkana and southern rifts

The calculations here are based on data from Furman et al. (2004), Furman (pers. comm.), Chernet and Hart (1999), Stewart and Rogers (1996), Rogers et al. (2000) and Bedini et al. (1997). Some of the results are summarized in Figures 3.4, 3.5, 3.6 and Table 5. It is not relevant to discuss all the density calculations made from this large database of chemical compositions. However, some important highlights of the results are noted in the following. The sample locations in the areas discussed in Figures 3.4, 3.5, and 3.6 are indicated in Fig. 3.3.

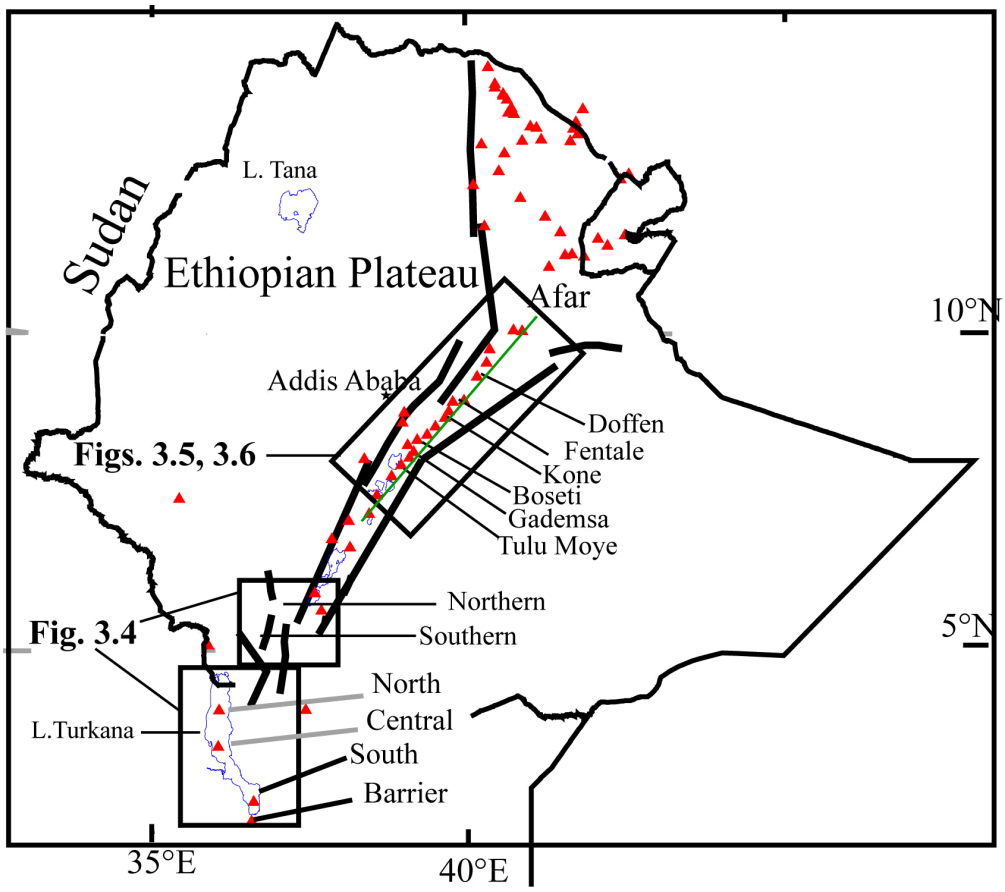

Figure 3.3 Locations of samples are used for density calculation using bulk chemical compositions. The locations for Figures 3.4, 3.5 and 3.6 are indicated. The green line is the approximate location for the EAGLE experiment (axial line in the Main Ethiopian Rift, see Fig 3.4a). Red triangles are volcanoes.

Figure 3.4 shows the calculations made in the Turkana area using the lava samples from Furman et al. (2004) to investigate north-south axial variations in density beneath the lavas. There are no distinct systematic variations in elastic parameters from north to south and all lavas show more or less similar trends. The upper panels of Figure 3.4 show the bulk chemical compositions from Stewart and Rogers (1996), mainly to see if there are any age-related variations in density and elastic parameters corresponding to the various volcanic episodes (pre-rift, syn-rift and post-rift). In the southern Ethiopian rift, rift trends are diffuse in a broad area and are often associated with sedimentary basins. The locations 'southern' and 'northern' are relative sample positions within Southern Ethiopia (see Figs. 3.3, 3.4) according to Stewart and Rogers (1996). There is no uniform correlation between all the various age groups and calculated densities or elastic parameters. However, there are distinct geochemical differences between the southern and northern group lavas that are associated with two eruption episodes: 45-35 Ma for Amaro and Gamo pre-rift flood basalts (transitional tholeiites) and 19-11 Ma syn-rift Getrakelle basalts more of alkaline compositions, approximately coincident with crustal extension, basin subsidence and flank uplift (Stewart and Rogers, 1996).

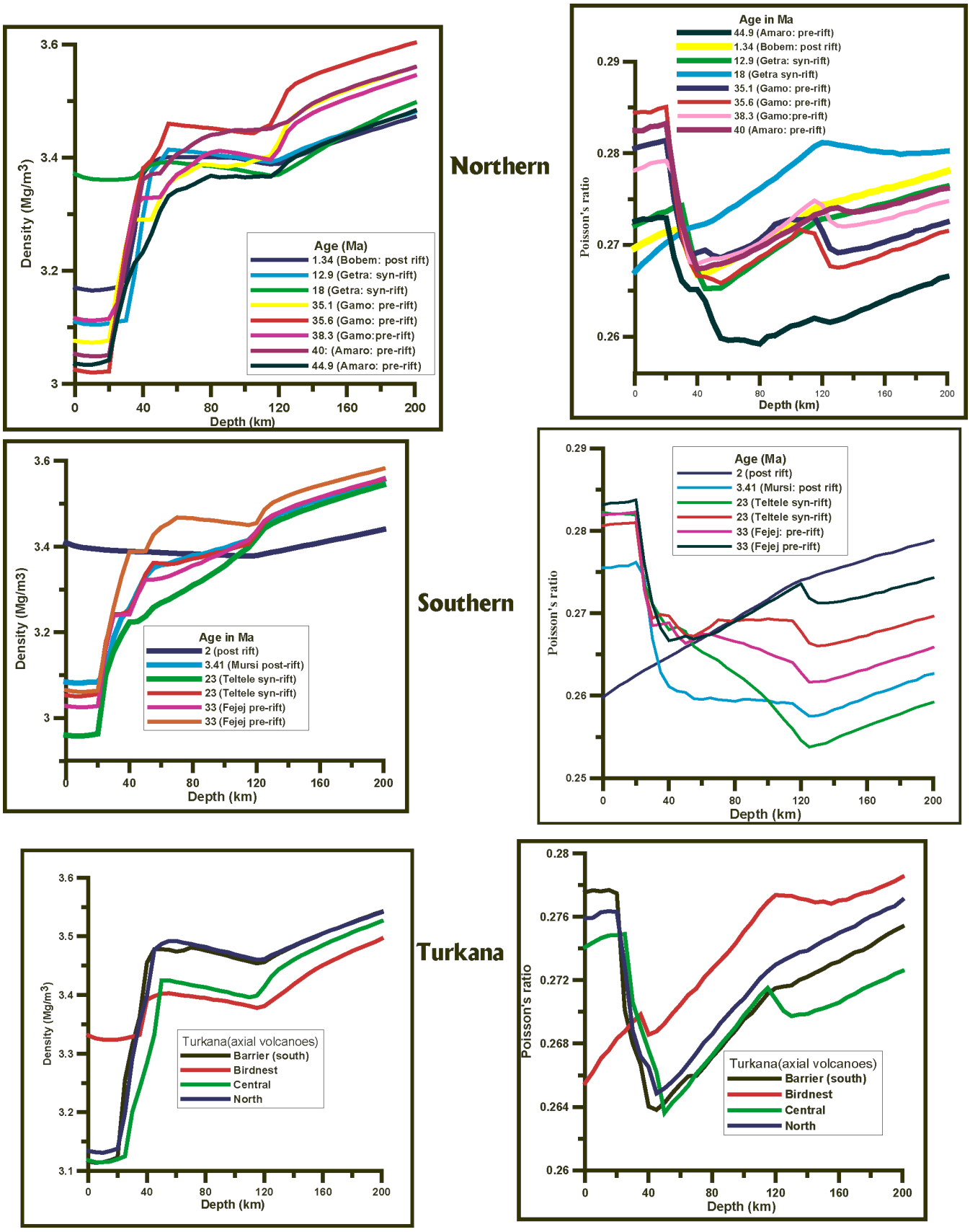

Figure 3.4 Density and Poisson's ratio calculated from the chemical composition data in the southern Ethiopian rift and Turkana area. Southern and northern indicate the relative positions of the samples in the southern Ethiopian rift. The estimates are also made to highlight some variations in density with age.

The density and elastic parameters calculations can be compared with the seismic velocity model of the NMER from EAGLE (see Fig. 3.5). The low velocity zone (LVZ) and corresponding high-density region lie under the most central axial volcanoes of Boseti, Kone, and Fentale closer to southern Afar. The anomalous region tapers off near the volcanoes, which are closer to the border faults (e.g. Doffen) and the southern end of the NMER (e.g. Tulu Moye and Gedemesa) (Figs. 3.5a, b and c).

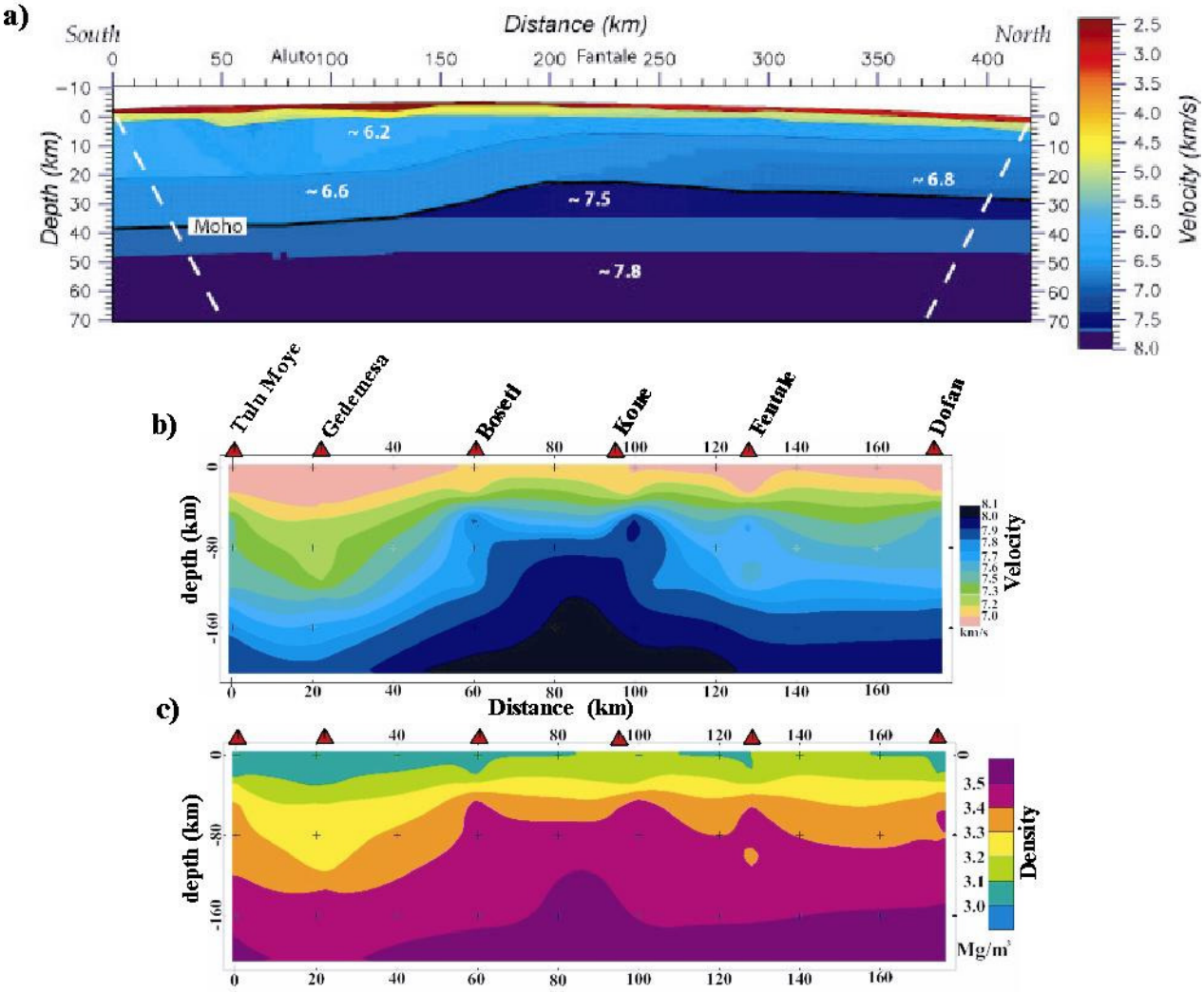

Figure 3.5 Measured and derived velocity and density models in the Main Ethiopian Rift.

a) Seismic velocity model along the Main Ethiopian Rift from EAGLE (Keller et al. 2004), see the approximate location in Figure 3.3.

b) Velocity model derived during this work using chemical bulk compositions of the axial volcanoes (Tulu Moye, Gedemesa, Boseti, Kone, Fentale and Doffen). The chemical composition data are acquired from T. Furman (pers. comm.) c) The density model corresponding to b calculated using the program code from Sobolev (pers. comm.). The axial volcanoes form approximately a straight line in the MER and roughly correspond to the location of the EAGLE axial experiment. The result shows some broad correlations from an independent approach (see text).

It has been observed that the current locus of strain is towards the centre of the MER (e.g. Bilham et al., 1999), shift away from the border faults (Ebinger and Casey, 2001) and to the south decreases or deeply seated. The independent velocity and density calculations generally correlate to the recent observed seismic velocity section by Keller et al. (2004) (Figs. 3.5a, b, and c.

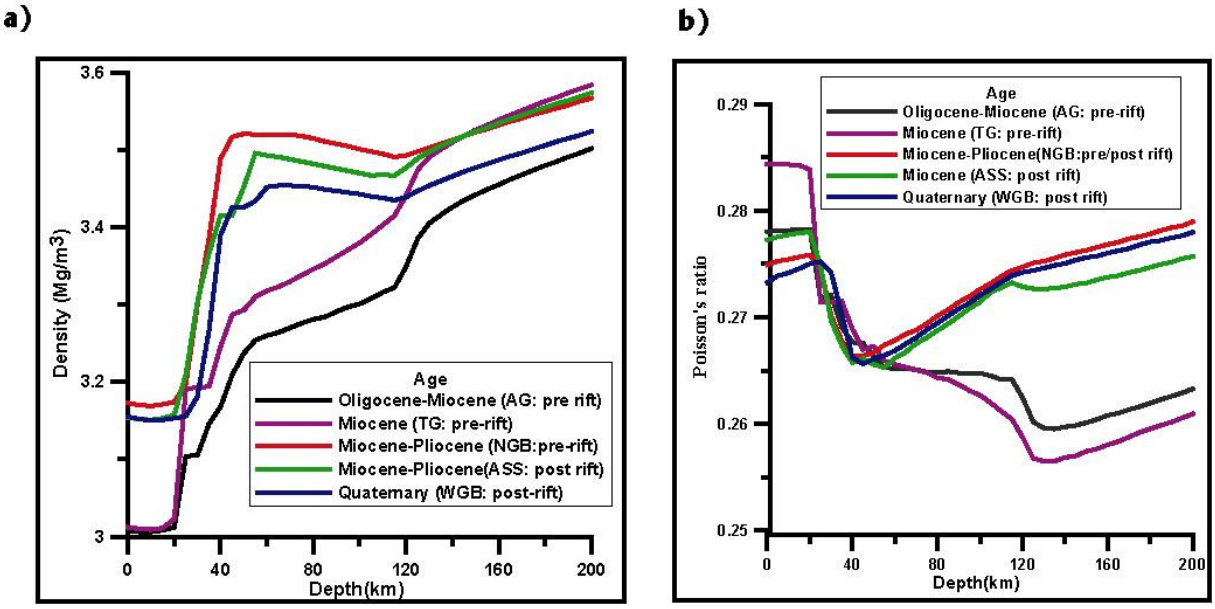

Figure 3.6 Density calculations made in this study using chemical compositions from Chernet and Hart, 1999 in the northern Main Ethiopian rift and southern Afar transition region. (a) density and (b) corresponding Poisson's ratio. The Figure shows significant differences of density and Poisson ratio highlighting bimodality of volcanism (crustal and lithospheric origins see text). AG: Alaji Group plateau basalts, TG: Tarmaber Group (basalts), NGB: Nazaret Group, ASS: Afar rift floor basalts, WGB: Wonj Group young rift floor basalts (see further petrology and geochemistry in Chernet and Hart, (1999).

Density variations with respect to age show two distinct patterns (Fig. 3.6) and these variations are much clearer than shown by the earlier analysis in Turkana and the southern rift systems (Fig. 3.4). This may be related to the good quality of chemical composition data from the NMER. The pre-rift lavas have a relative low density and low Poisson's ratio, whereas the post-rift lavas have high density and high Poisson's ratio (see Fig. 3.6a, b). The pre-rift lavas (Oligocene-Miocene) are the result of silica rich rhyolitic volcanism and, as a result have reduced density. In contrast, the post-rift lavas are from high-density basaltic volcanism of lower silica content. The pre-rift lavas are more crustal in character and the post-rift lavas are more of lithospheric origin. The distinct variations in elastic parameters exhibited by the pre-rift and post-rift lavas are most obvious between 20 and 40 km depth where lower crust has been modified by the mantle material. This result is also consistent with the commonly observed bimodal volcanism for continental rifts. Furthermore, the difference also implies that the

densities are laterally different in the rift and away from the rift zones or plateau areas. Therefore, this suggests that different densities have to be used under the rifted zones and adjacent plateau.

Table 5

Elastic parameters calculated for Doffen axial volcano in the NMER using bulk chemical composition data from T. Furman (pers. comm.)

Depth(km)	Density	Vp	Vs
5	3.08	6.95	3.86
10	3.09	6.95	3.85
20	3.09	6.95	3.85
25	3.15	7.05	3.93
30	3.25	7.24	4.07

The following densities (Mg/m^3) are allocated for the starting model in chapter 6.

Precambrian exposure in western Ethiopia: 2.65 (average value for most metamorphic rocks other than the meatsediments);

Most sediments in Eastern Sudan using average density to a depth of 3.5 km 2.45-2.5;

Upper crystalline basement (Ethiopian Plateau): 2.70-2.72, (see Table 1);

Lower crystalline basement: 2.75 outside rift and 2.8-2.82 within rift (see Table 4);

Lower crust: 2.90 outside rift and 2.92 inside rift;

Tertiary volcanics (Ethiopian Plateau): 2.53-2.67;

Rift sediments and infill variable in MER and Turkana: 2.3-2.5;

Anomalous upper mantle: 3.15 for Afar, 3.0 in MER and 3.1 in Turkana (see also Table 5);

Mantle density: 3.26 for east and west parts of mantle lithosphere and 3.20 under the rift.

4 Potential field database

In this chapter, the potential field data (the aeromagnetic data coverage in Ethiopia and the gravity data that covers the East African region) are presented. In particular, the gravity data is reassessed, reprocessed, qualitatively interpreted and dealt with extensively because it is the principal data used in the three dimensional modelling. As described before, the aeromagnetic data coverage in this region does not allow a regional compilation. Therefore, in the following section the data coverage is only briefly mentioned.

4.1 Aeromagnetic data coverage

Extensive aeromagnetic surveys in economically interesting blocks of Ethiopia (e.g. Precambrian basement exposures in western, southern and northern Ethiopia; sedimentary basins e.g. Gambela, Ogaden and in parts of Afar) have been made during the last 30-40 years. Likewise, surveys have been conducted in the Sudan, Kenya, and Somalia and coastal parts of Eritrea. However, the aeromagnetic data coverage in these regions is not sufficient to prepare a regional compilation of the type made for the gravity data set (section 4.2).

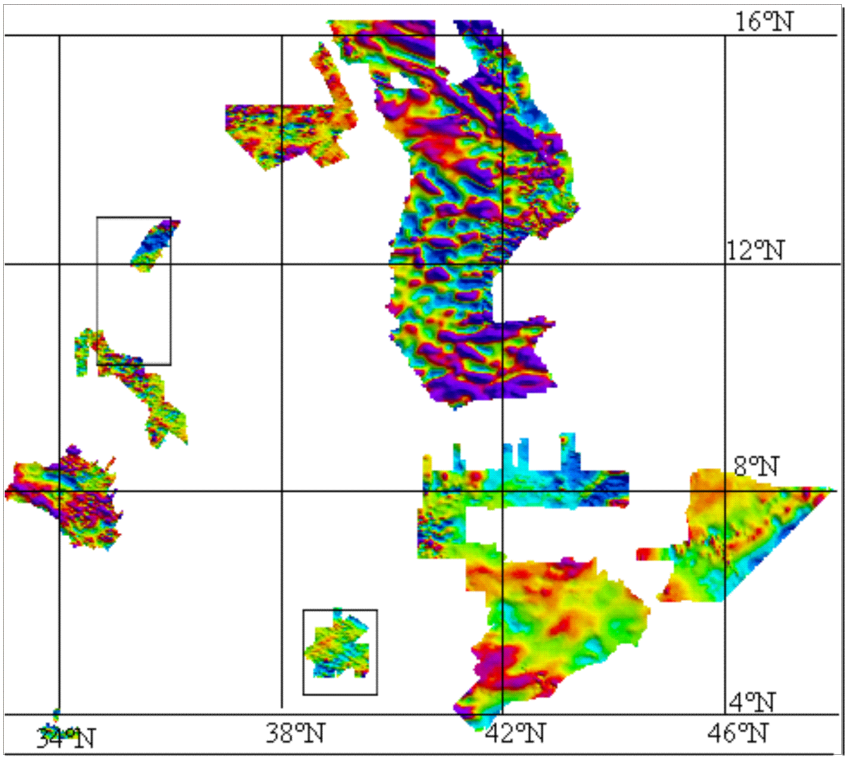

Figure 4. Magnetic data coverage in Ethiopia and Eritrea (modified from AMMP, see text), the rectangular blocks show the approximate location of recent aeromagnetic surveys in Ethiopia (see text).

On a continental scale, the African Magnetic Mapping Project (AMMP) and a new initiative of Eastern African Mineral Resources (ESAMRDC/GEODESA) made an extensive inventory and database of existing aeromagnetic and gravity data sets. Figure 4 shows the distribution of the aeromagnetic data in Ethiopia and Eritrea. AMMP was very successful in homogenizing the aeromagnetic data to a certain level (see Fig. 4). The part of the aeromagnetic data re-adjusted for areas in Ethiopia by AMMP has recently been updated with new integrated aeromagnetic data acquired in southern Ethiopia (UNDP, 1994) and southwestern Ethiopia (Ethio-Nor project, 1997-2001, GSE pers. comm.). The objective of this section is mainly to show the distribution of the database. Furthermore, the aeromagnetic surveys being conducted either closer to the rift margins of Ethiopia or within the rifts (e.g. Afar) and Neoproterozoic exposures (e.g. Western Ethiopia) and basins adjacent to the rift and plateau are useful for interpretation. However, in this work only the gravity data are used for regional analysis and three-dimensional modelling because it is not possible to treat both data sets at the same regional scale.

4.2 Gravity database

Our knowledge of the gravity field of this region is a result of many gravity-related campaigns and small scale surveys initiated and executed over the last 100 years (e.g., Willis, 1936; Bullard, 1936; Girdler et al., 1969; Makris et al., 1969, 1972, 1975; Baker and Wohlenberg, 1971; Searle and Gouin, 1972; Purcell, 1986; Makris and Ginzburg, 1987; Ebinger et al., 1989; Alemu, 1992; Hay et al., 1995; Negash and Ayele, 1995; Wondirad, 2000; Uluma and Zewge, 2001). A compilation of all available gravity data between the equator and 20°N (Fig. 4.1) has been made. Data are scarce in some parts and totally absent in others. Data from oil companies and some government organizations are confidential and inaccessible. Therefore, adding additional data sets remains a difficult task.

4.2.1 Source of data and coverage

Over 45000 land and sea gravity data points generated by different companies, research institutions and archived in international organizations and geological survey data bases have been compiled. Preliminary works covering the Afar region of Ethiopia and Djibouti, the western escarpment and the highlands of Ethiopia were made in the early 70s (Makris, 1972). The earliest gravity observations in Ethiopia are documented by Pacella (1948), and later measurements by the University of Addis Ababa research group are archived at the Geophysical

observatory of Addis Ababa (Mohr and Gouin, 1967; Searle and Gouin, 1972). In the southern rift and Afar area, Ebinger (1994) and Ebinger and Hayward (1996) have collected more gravity data. The Geological Survey of Ethiopia (GSE) has made a substantial contribution under various research projects (e.g. SAREC/ESTC 1988-1994 and ETHIO-NOR programs) and has continued to conduct gravity campaigns despite limited resources. Other data sets covering the East African rift system, the Red Sea, Indian Ocean, and coastal regions of Eritrea and Saudi Arabia were sourced from the Bureau Gravimetric International (BGI) and Eastern Sudan from GETECH/Sudan Geological Authority. The distribution of these data is presented in Figure 4.1.

4.2.2 Data evaluation, reprocessing and correction

The existing data sets were tied either to the IGSN71 or Potsdam systems and, in some cases, the theoretical gravity was computed using the 1930 formula (e.g., Makris, 1972). Some datasets document to which system the gravity data are tied, but in the absence of such information, free-air anomalies were used to trace the formula. Gravity data sets from Ethiopia were referenced to the Potsdam datum (e.g. M. Zewuge, pers. comm., GSE). The comparison of IGSN71 and Potsdam base stations in Ethiopia shows a difference of about 14×10^{-5} m/s^2 for exactly similar base stations (e.g. Addis Ababa and Harar). Differences vary between 13 and 17 $\times 10^{-5}$m/s^2 for closely located stations (see Table 6). Hence, a gravity correction of -14×10^{-5}m/s^2 was applied to the observations to bring them to the IGSN71 datum. Currently, many of the IGSN71 base stations in Ethiopia are not functional (for many reasons). Thus, gravity network adjustment is necessary to renew the abandoned stations and to establish new ones for successive gravity densification. Data spacing along roads ranges between one and six kilometres in Ethiopia. Data are more detailed and have a uniform coverage in Eastern Sudan. The standard gravity reductions are applied using density ρ=2.67 Mg/m^3 and the 1967 International Gravity Formula (IGF) as indicated in eq. 1.

$$\Delta g_B = g_{meas} - [\gamma - \delta g_F + \delta g_B - \delta g_T] \qquad 4.1$$

where

Δg_B = Bouguer anomaly

g_{meas} = measured gravity

γ = the normal gravity calculated using the 1967 IGF (eq. 4.2)

δg_F = the free air correction (see eq. 4.3 below)

δg_B = the Bouguer correction estimated using an infinite Bouguer slab (eq. 4.4)

δg_T = topographic correction (see below).

The standard gravity survey reductions based on the IGSN71 for absolute gravity values and the1967 IGF is given by:

$$\gamma(1967) = 9.78031846(1+0.0053024\sin^2\phi - 0.0000058\sin^2 2\phi) \quad 4.2$$

where ϕ *is the geodetic latitude.*

The values of the constants that form the IGF are constantly improved using new data from Earth-observing satellites. Currently, the 1967 IGF is universally accepted. Some of the data in this region apply the old 1930 IGF, where a gravity difference ranging from +3.2 $x10^{-5}m/s^2$ (at the equator) and -10.4 $x10^{-5}m/s^2$ (at the pole) is expected. More recently a much improved IGF 'GRS1980' has been derived. The differences between the various IGFs and more details of the constants are discussed in Featherston and Dentith (1997) and Li and Götze (2001). The differences between IGF 1967 and 1980 are small (e.g. Li and Götze, 2001), therefore, in such a large-scale gravity data adjustment the 1980 IGF is not used.

The purpose of the free-air and Bouguer corrections is to adjust normal gravity on the reference ellipsoid (γ) to the level of the observation point.

The free air correction in eq. 4.1 is given by:

$\delta g_F = [\partial\gamma/\partial h] * H_s \approx -0.3086 * H_s$, where $\partial\gamma/\partial h$ approximates the vertical gradient of the normal gravity (h=height above reference ellipsoid and H_s= elevation in meters above the geoid) (4.3)

The Bouguer correction accounts for rock between the ellipsoid and measurement point by using an infinite Bouguer slab and is given by:

$\delta g_{B=} 2\pi G\rho H_s$, where G= gravitational constant ($6.67x10^{-11}$ m^3 kg^{-1} s^{-2}).

The terrain corrections are calculated using the Digital Elevation Model (DEM) GTOPO30. The statistics show that for ~ 67 % of the data the terrain correction is 0-0.419 $x10^{-5}$ m/s^2, for 23.7%, 0.419-1.88 $x10^{-5}$ m/s^2, 5.3 %, 1.88-3.356 $x10^{-5}$ m/s^2, 2%, 3.356-4.82 and less than 1% greater than 6.29 $x10^{-5}m/s^2$.

In cases where only free-air anomalies (FA) were available, calculations have been made using the following steps.

- Known absolute gravity values are checked from literature and BGI data,
- theoretical gravity is calculated using the 1967 formula,
- absolute gravity values are calculated using the supplied free air and elevation data,
- absolute gravity data points are tied to IGSN71,
- Bouguer anomalies are recalculated.

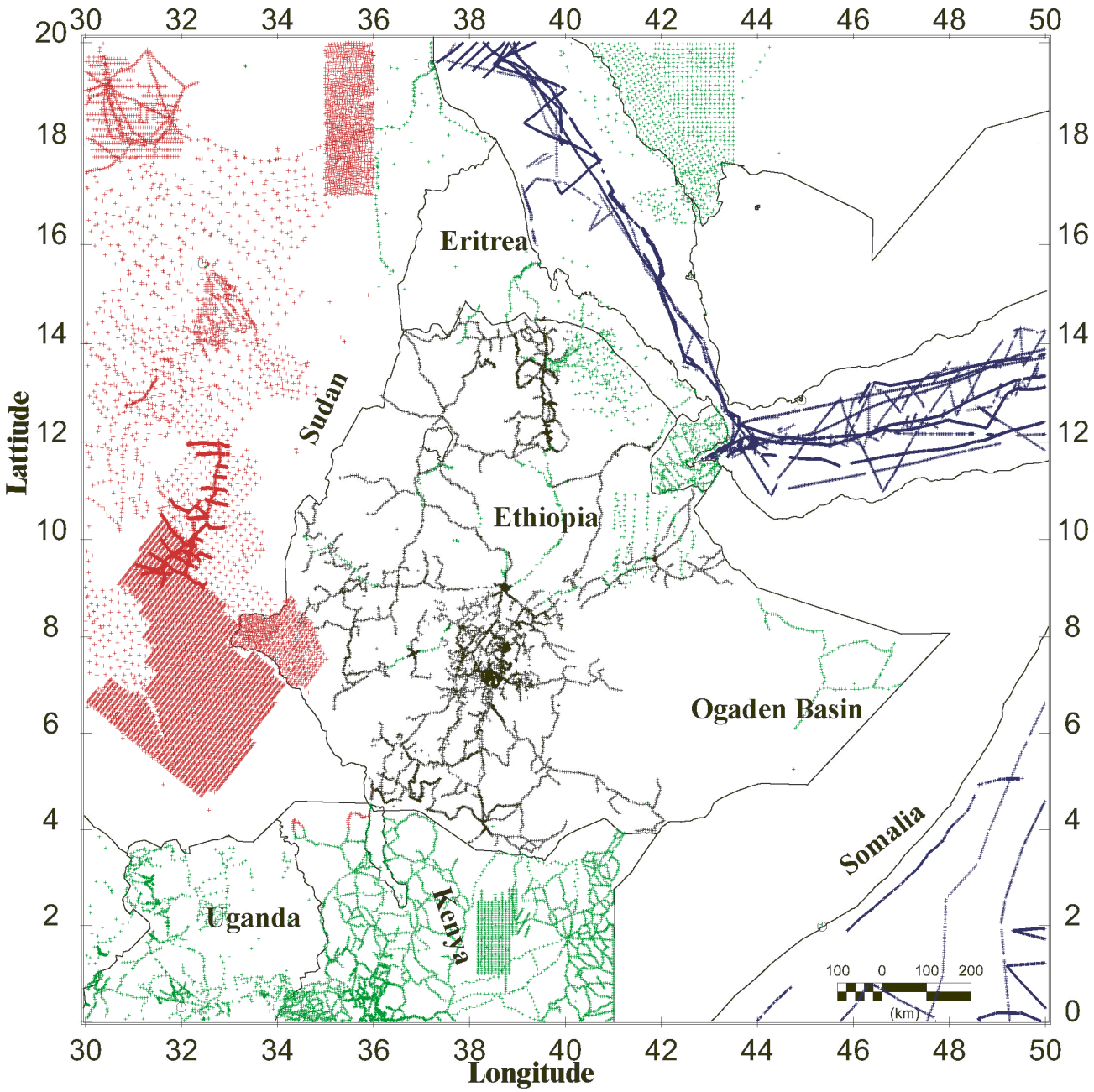

Figure 4.1 Gravity stations acquired from geological survey of Ethiopia (black); BGI (land: green, sea: blue); GETECH and Sudan geological authority (red). Data are re-evaluated, re-processed and adjusted using the procedures described in the text. Important data gaps include: Sudan/Ethiopia border, Uganda, Kenya, Ethiopia and Sudan common border region (4°N-6°N), Ogaden basin of Ethiopia and most parts of Eritrea.

Table 6
Comparisons of IGSN71 and Potsdam base stations in Ethiopia. BGI stations are from the BGI database and Potsdam stations from the literature and Geological Survey of Ethiopia (GSE). Complete IGSN71 stations are available at (http:/bgi.cnes.fr.8110/cgi-bin/cre_carte_refe. (*X=Longitude, Y=Latitude and Z= height).

Location	X, Y, Z (X & Y in decimal degrees, Z in meters)*	g_{obs} 10^{-5} m/s^2	Datum	Source	Gacc 10^{-5} m/s^2	
Addis Ababa	38.8, 8.98, 2362	977466.91	IGSN71	BGI	0.1	No documented Ref.(Makris et al., 1969). The name of the site is the same (diff. about 14x10^{-5}m/s^2).
Addis Ababa		977481.75	Potsdam		0.1	
Axum	38.7178, 14.1299, 2164	977777.4	not available	GSE	not available	Stations are not the same but are close. Diff. is about 17x10^{-5}m/s^2.
Axum	38.7167,14.1167, 2145	977760.96	IGSN71	BGI	0.3	
Harar	42.1169, 9.30,1850	977632.16	IGSN71	BGI	0.3	Difference is about 14 x10^{-5}m/s^2.
Harar	42.1216, 9.3109,1850	977645.8	Potsdam	GSE	not available	
Miesso	40.750, 9.2167,1314	977762.16	IGSN71	BGI	not available	Difference approx. 13.8 x10^{-5}m/s^2.
Miesso	40.7549,9.2331, 1314	977775.9	Potsdam	GSE	not available	

Analysis and data evaluation and error checking were made using the interactive Java program ` DbGrav´ (author: S. Schmidt). This program allows the identification of observations that show a misfit with the general trend in a particular data set. Similar comparisons are also made with different data sets (see Fig. 4.2). In the case of total misfit, the best solution is to re-measure the data, but this was not practical in this work (see Fig. 4.2). In most cases, when the differences with adjacent observation point reach more than (20-40 x10^{-5}m/s^2), such data is excluded from the present compilation. It was also found to be useful first to check errors in horizontal and vertical positioning, elevation and consider also to the local geology. Systematic errors mainly arising from gravity reference stations are very difficult to rectify since the observations have to be reoccupied, whereas errors due to reference ellipsoids could be identified by comparing surveys. Errors from wrong calibration of instruments drift and tide corrections are not recoverable unless date of observation and instrument type are documented. Since such information is lacking in many of the gravity surveys in this area (particularly Ethiopia), an intensive control and check of the Ethiopian data was conducted. Then, the error-reduced data for each survey was merged with BGI data from the Turkana area, Eastern Sudan

and offshore data sets. Available error estimates resulting from observation errors and errors in elevation, position and terrain correction are summarized in table 7.

Table 7
Estimated errors from the different surveys

Survey	Error $x10^{-5} m/s^2$	Reference	Remark
Main Ethiopian Rift (MER)	±0.3 in the basin ±1 over the plateau.	Mahatsente (1998)	
Southern Ethiopia Rift	± 0.2 in the basin, ±1.20 on the plateau	Ebinger (1994)	
Afar	±0.36 (Bouguer) for 2.67 Mg/m^3	Ebinger and Hayward (1996)	Less than 100m position error)
South-eastern plateau and low lands of Ethiopia.	±1.967 (elevation) ±0.059 in positioning	Wondirad (2000)	±10m elevation error ±300m positioning error
Central rift valley (Ethiopia)	±2l	Searle and Gouin, (1972)	±1km error on station location.
MER	±2.9	Alemu (1992)	General accuracy
Afar	±5	Makris et al. (1969)	Accuracy after topographic correction.

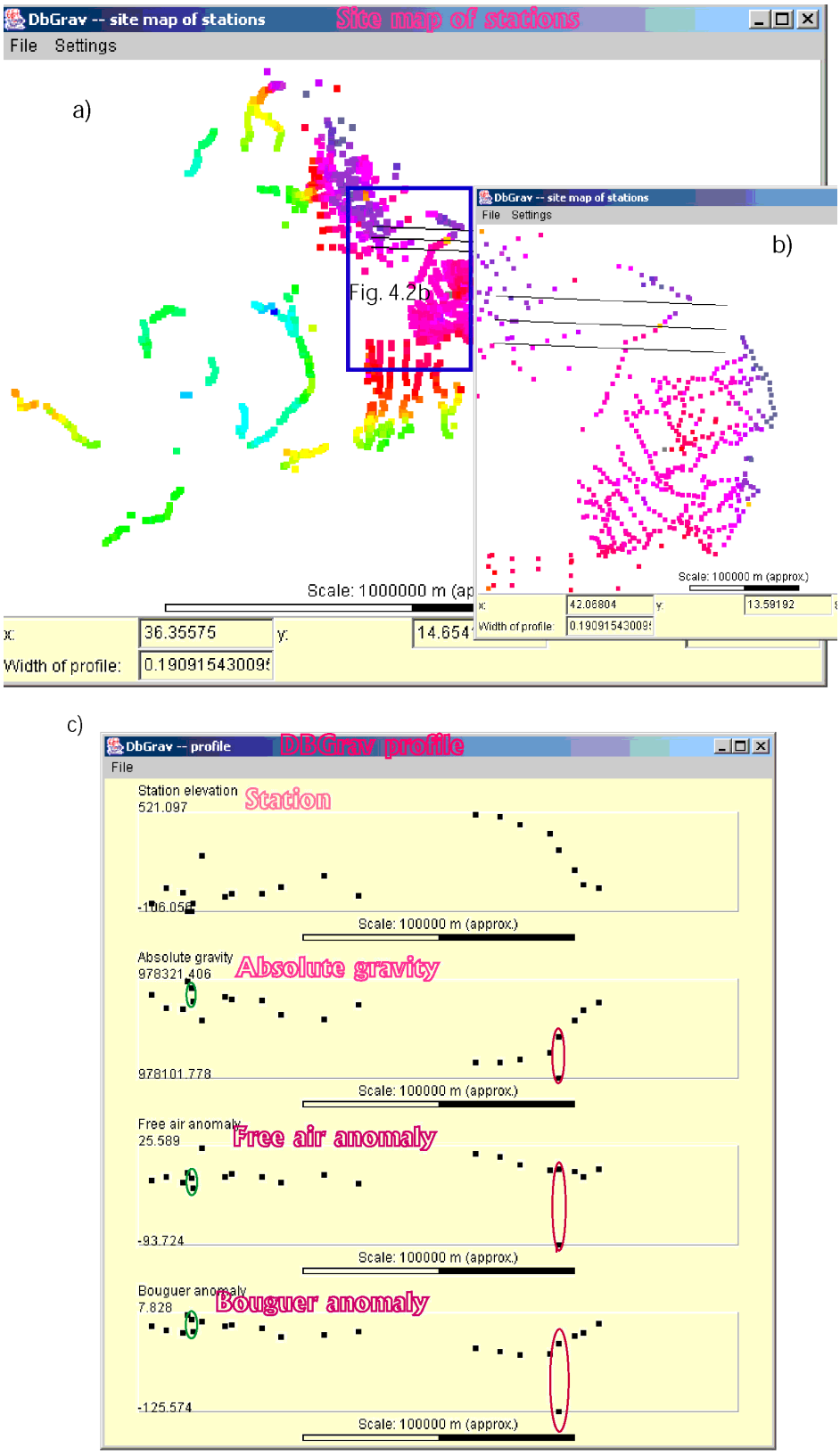

Figure 4.2 Data validation and adjustment using DBGRAV software an example using the part of a gravity database from BGI and GSE in the Afar area (a) and enlarged view (b). Two examples with different values at the same point identified using an arbitrary profile (c). Similar problems are common in other data sets as well. In the case of the data circled red, it is easier to reject the data that is not conformable to the general trend. Determining erroneous values for the example marked green is more difficult.

In most parts of Ethiopia, elevations were determined using altimeters (GSE pers. comm.). The errors in such measurements may reach ± 20m (Wondirad, 2000, and Table 7) and in the MER ±10m (Alemu, 1992) and are the major source of error in gravity observations. The newly compiled and reprocessed database is not an error-free gravity database, but an error reduced one with more consistent processing and reduction procedures than any of the previous compilations. However, there are still uncertainties, particularly with the data sets in the northwest highlands of Ethiopia and western Ethiopia near the Sudan/Ethiopia border. Although some data from these regions are part of the regional database, they are not used in the three-dimensional modelling because it is very difficult to reconcile them with the rest of the observations and model.

The total sum of mean square errors (σ_B) in the Bouguer gravity values is composed of the sum of errors in the gravity observation (σ_g); vertical positioning (σ_h); horizontal positioning (σ_p) and terrain correction (σ_T).

$$\sigma_B^2 = \sigma_g^2 + \sigma_h^2 + \sigma_p^2 + \sigma_T^2$$

The errors in observation (σ_g) are variable and depend on the type of data set and are in most cases minimal. The errors in elevation (σ_h) could be estimated by using the combined Bouguer slab and free air correction (~0.1967×10^{-5} m/s^2/m) and may reach $\pm 2.95 \times 10^{-5}$ m/s^2 for average elevation error of ±15m. Therefore, a conservative estimate of error in the whole database is $1.5\text{-}4.5 \times 10^{-5}$ m/s^2, with maximum errors over the plateau areas. Using the data in the Main Ethiopian Rift alone Mahatsente (1999) estimates a combined error of $\pm 0.3 \times 10^{-5}$m/s^2 in the basin and $\pm 1 \times 10^{-5}$m/s^2 on the plateaus. On a relative large section of the MER, Alemu (1992) estimates an accuracy of the Bouguer anomaly on the order of $\pm 2.5 \times 10^{-5}$m/s^2. The fit between the observed and calculated Bouguer gravity has a standard deviation of about 16×10^{-5}m/s^2 (see Chapter 6). If we take the square root of the standard deviation, then a misfit of $\pm 4 \times 10^{-5}$m/s^2 is similar to the total error in the Bouguer gravity database estimated above.

In the absence of sufficient reliable IGSN71 base stations, the approach followed to homogenize existing gravity data sets is at least useful for regional analysis and as a basis for future network improvement.

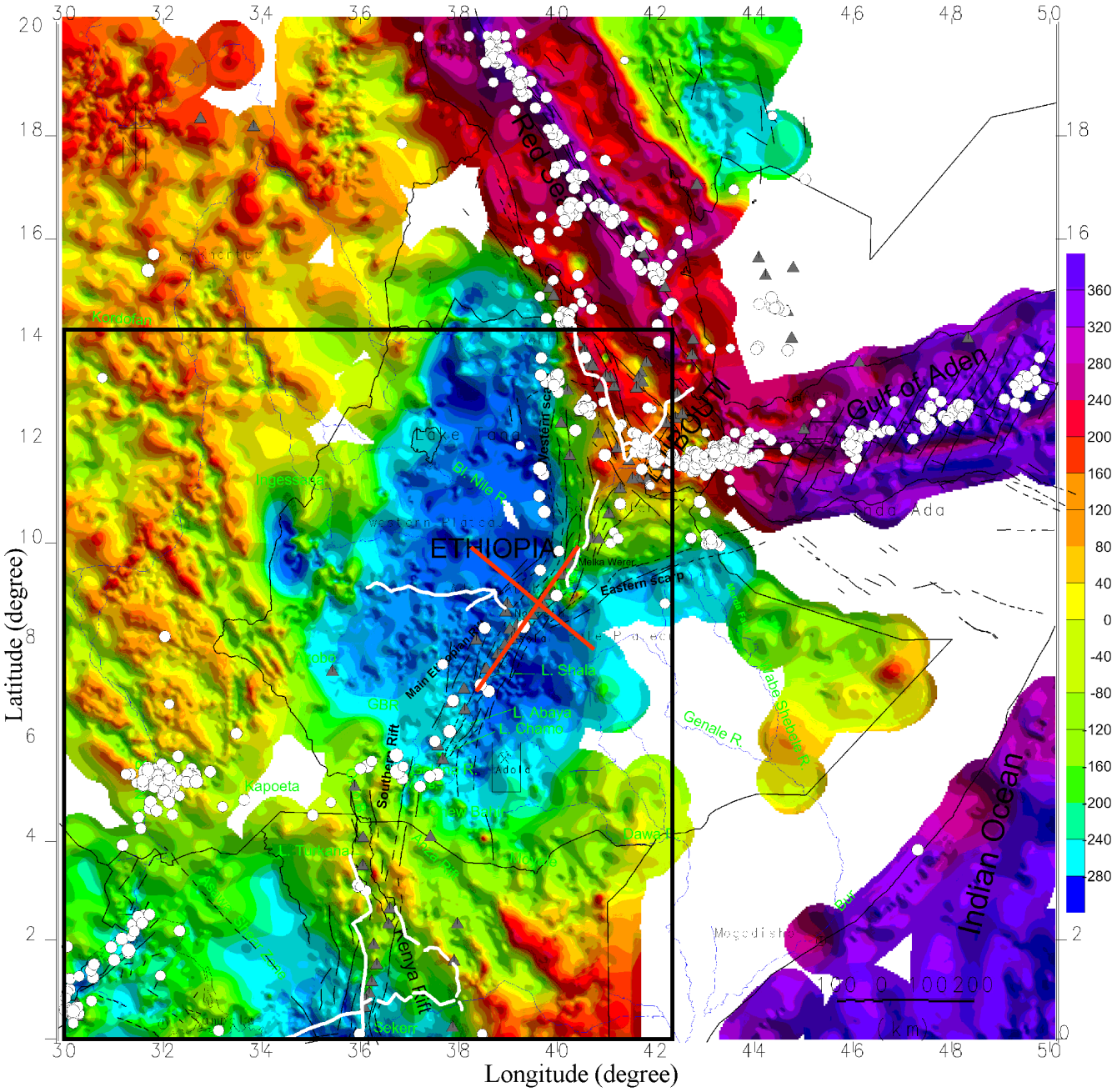

Figure 4.3 Bouguer anomaly (x10^{-5} m/s^2) map prepared using the gravity stations of Fig. 4.1. Positive Bouguer anomalies are evident along the fracture systems of the Gulf of Aden, Indian Ocean and Red Sea axial zone. Relative positive anomalies are depicted in the Afar depression of Ethiopia, the Anza cross-rift structure and Eastern Sudan. The main Ethiopian rift and plateau, the Kenyan and Arabia plateaus are indicated by strong negative anomalies. The negative correlation of topography and gravity anomalies indicates the existence of isostatic anomalies (later modelled and subtracted). White thick lines are seismic refraction experiments in Ethiopia (Berckhemer et al. 1970) and Kenya (KRISP). The new EAGLE experiments are indicated by red line (approximate) and the black box is outlines the 3D modelling area.

4.2.3 Gravity data gaps and alternative solutions

Gravity data coverage for this region (Fig. 4.1) shows some gaps in western Ethiopia along the border with Sudan and an important region between Northern Uganda, southeastern Sudan and southwestern Ethiopia. This area is very important for the understanding of the northern extension of the Western Rift System and its interaction with the NW and NE trending Anza rift and Tertiary rifts in Sudan and Ethiopia. It is a region of high seismicity, and the extension of the western rift system may reach 350 km north of Lake Albert (Girdler and McConnel, 1994). Additional data gaps exist in the western plateau of Ethiopia, northern Ethiopia and Eritrea, the Eastern plateau and southeast Ethiopia, the southern border of Ethiopia with Kenya and Somalia, and extensive region of the Ogaden basin (Eastern Ethiopia). When combined with existing data, new data from these regions would help to answer many of the pending scientific questions and also for the economic growth of the countries in question.

A possible option is an aero-gravity survey covering the remote and inaccessible regions in a much-reduced time. It is proposed that an aero-gravity survey should cover the large tract of land (the western Gondawana margin or suture zone) between 14°N-4°N and 34°E-38°E, with an option of extension to the south and north (see Fig. 4.1). It is a region that approximately covers the large section of the Nile basin, and making it very useful for interdisciplinary geoscientific research.

Merging Satellite gravity data (GRACE)

The Gravity Recovery and Climate Experiment (GRACE) mission recently calculated and released a new global gravity field model called EIGEN-GRACE02S (Reigber et al., 2004). GRACE is a dedicated satellite mission with the objective to map the global gravity field (see further information: http://op.gfz-potsdam.de/grace/results/grav/g002_eigen-grace2s.html). The gravity anomalies from the EIGEN-GRACE02S are computed using the program 'harmonics' from Will Featherstone and John Kirby at Curtain university of Technology (Hackney et al., 2004). The program uses spherical harmonic coefficients of a given global geopotential model to compute the anomalies. The anomalies are calculated at the ellipsoid (i.e. a downward continuation from the satellite height is already incorporated). Therefore, the application of downward continuation or other similar methods before incorporating terrestrial gravity data is not necessary. The model gives free-air anomalies, but a simple Bouguer correction assuming an infinite slab and density of 2.67Mg/m^3 on shore and 1.67 Mg/m^3 offshore is applied to produce the Bouguer anomalies (Hackney pers. comm.). This approach is consistent with corrections applied during the terrestrial gravity data validation.

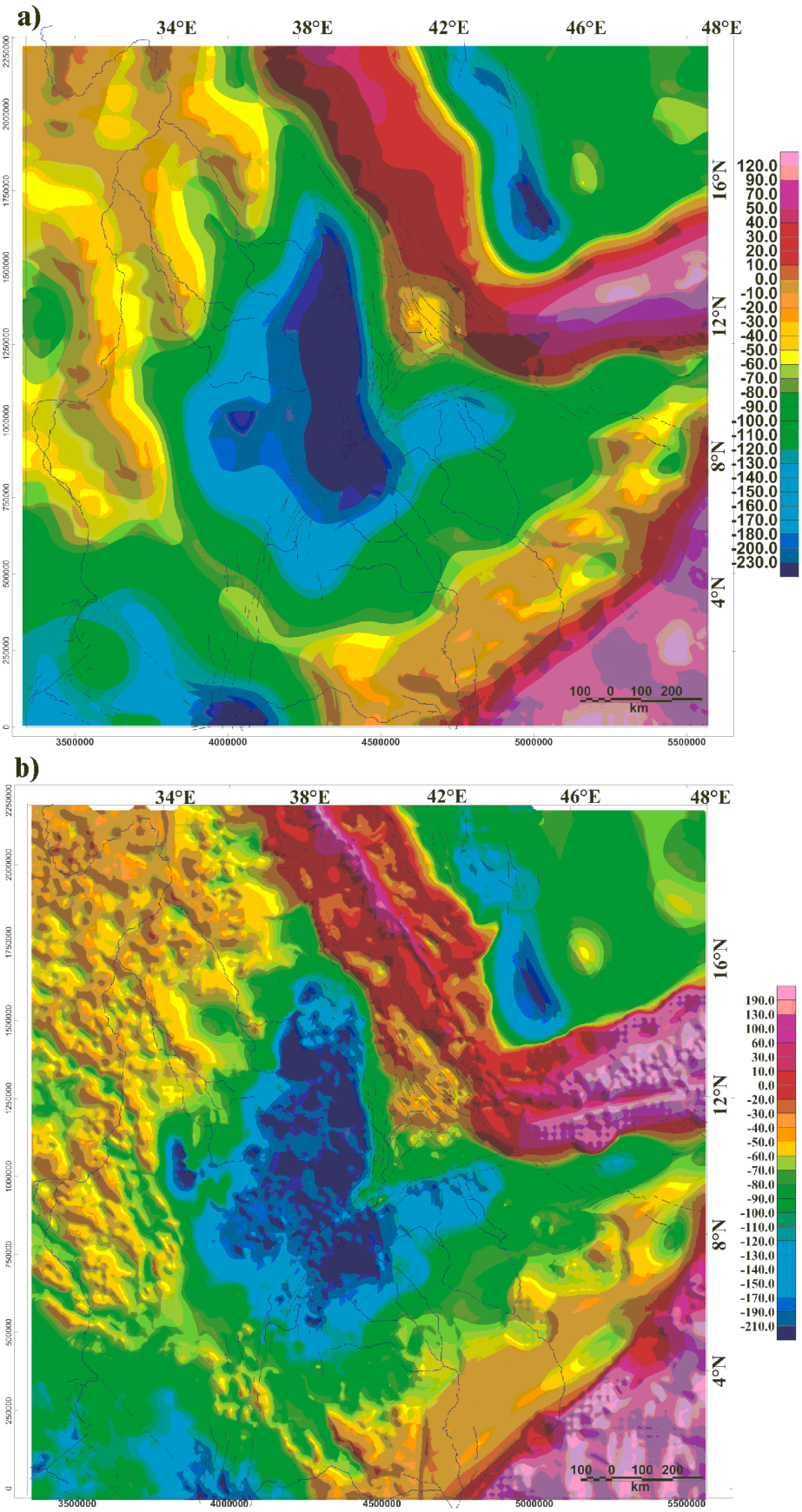

Figure 4.4 a: Bouguer gravity (x10^{-5} m/s^2) calculated using the new EIGEN-GRACE02S global geopotential model (nmin=2 and nmax=120). b: The Bouguer gravity from (a) is merged with land data and smoothed using a convolution filter. Fault patterns (faint black lines) and major drainage (thin blue lines) are overlain for reference.

The potential of the new GRACE satellite gravity data to map large-scale hidden structures in the East African Orogen (EAO) is demonstrated by combining the EIGEN-GRACE02S model with terrestrial data. The Bouguer gravity data calculated for a minimum spatial wavelength of 300 km (complete to degree and order 120, Hackney pers. comm.) for the part of the study area are shown in Figure 4.4a.

The gravity database (Fig. 4.1) compiled north of Equator and south of 20°N in this region and the Eastern Sudan gravity data (GETECH and the Sudan Geological Authority) is merged with satellite gravity data to produce the regional Bouguer gravity map of the region shown in Figure 4.4b. The merged data is produced by simply combining and gridding the data using a grid cell size of 4 km. The resulting data is subjected to a convolution filter of 3x3 in order to remove uneven sampling and high frequency spikes due to the gridding and merging process.

The combined Bouguer anomaly map displays the Bouguer gravity field of the entire area in this region. It renders a picture of the interplay of the three plates (Nubia-Arabia-Somalia) at the triple junction of the Rifts (Red Sea-Gulf of Aden-the Main Ethiopian Rift) in Afar.

A structure parallel to the Red Sea that is a part of the structure of Anza-Turkana-Central African Rift system (CARS) extending from the Kenya embayment (the southern end of Anza Rift, Indian Ocean) to the Mesozoic CARS and terminated by the Central African Shear Zone (CASZ), is clearly evident (see also Fig. 2.1). The plateau uplifts of the Yemen-Saudi Arabia region (Arabian plate), Ethiopian and East African plateau are marked by a pronounced negative Bouguer anomaly separated by the parallel rift margins of the Red Sea and Anza-Turkana trend.

The GRACE02S model is inadequate and better results might be possible in the future as models are improved. Furthermore, the GOCE (Gravity Field and Steady State Ocean Circulation Explorer) mission, that will measure the Earth's gravity field with more accuracy should also provide better models.

4.2.4 Free air anomaly and Bouguer gravity

The free-air anomaly map (figure not presented) reflects the following major features. Large sections of the highlands of Ethiopia are characterized by positive free-air anomaly that delineates the boundaries of the rift margins. These correspond to the Cenozoic transitional to sub alkaline flood basalts (see Davidson and Rex, 1980; WoldeGabriel et al., 1990). Negative free-air anomalies are depicted in all topographically depressed zones of Sudan and Ethiopia, the southern lowlands, Ogaden basin and basins north of Lake Turkana. The free-air anomaly variations in different parts of the area indicate isostatic imbalance and the dynamics of these

regions. Removing the topographic effect produce a broad negative Bouguer anomaly centred about the latitude of Addis Ababa (Fig. 4.3).

Bouguer anomalies (Fig. 4.3) are discernible in continental areas, the Afar depression of Ethiopia, Anza rift of Kenya and in oceanic areas. The new data compilation presented here confirms the long-wavelength negative Bouguer anomaly feature which covers the entire plateau region, the Main Ethiopian Rift (MER) and East African plateau (see also Ebinger et al., 1989), and the Arabian shield to the north (e.g., Gettings, et al., 1986; Makris et al., 1991). Strong positive Bouguer anomalies are depicted over the Red Sea rift, Gulf of Aden and in the Indian Ocean of Somalia (Fig. 4.3). Relative positive Bouguer anomalies are evident in the Afar depression, in the western lowlands of Ethiopia and Eritrea, and to the south of the Ethiopia-Kenya border.

A closer inspection reveals some variations in the gross pattern of Bouguer anomalies. Within the Red Sea, the Bouguer anomaly decreases away from the axial zone in both directions. Bouguer anomalies with reduced amplitudes are evident along the eastern side of Red Sea, parallel to the coastline of Saudi Arabia and along the coast of Eritrea (near Zula). These anomalies are related to sedimentary basins. The main continental rifts, including the western rift system, are characterized by negative Bouguer anomalies, though the trend of the rifts is not clearly outlined. The area situated between the southern rift system of Ethiopia and the northern part of the Kenyan rift has a remarkable similarity to the Afar depression of Ethiopia. Some of the major similarities are: the relative positive Bouguer anomaly and topographic depression (see also Ebinger and Ibrahim, 1994); evidence of crustal thinning (~20 km) and significant extension (e.g. Prodehl et al., 1997); and overlap of three rift systems (e.g., Ebinger and Ibrahim, 1994). To the north in Afar, a broad accommodation zone (e.g. Tesfaye et al., 2003) and connects the different arms of the triple rift and links the Main Ethiopian Rift, while to the south broad extensional zones (e.g. Ebinger et al., 2000) link the main Ethiopian Rift to the Kenyan Rift. Despite this, most gravity and related investigations suggest that the entire rift system is linked, but this is not directly evident in the newly compiled Bouguer anomaly map (Fig. 4.3). Therefore, in Chapter 5 an attempt is made to highlight the linkage of the entire rift system using isostatic residual maps that enhance signatures from the upper crust.

4.2.5 Curvature of Bouguer gravity

Enhancing potential field data is one of the first procedures applied in order to identify subtle features and to aid visual interpretation. Enhancement can be made in many different ways, such as for example, using digital filters (by Fourier transform); smoothing using

averages, fitting and then subtracting polynomial functions of various orders, isostatic models (regional and local) and curvature attributes. The isostatic models will be dealt in more detail in a separate chapter. Here, only the curvature attributes are considered.

One of the numerical methods applied in the oil industry, medicine and optimetry, is the calculation of curvature attributes (Roberts, 2001). It is applied here to enhance gravity lineaments. The attributes are generated using the computer code by S. Schmidt (pers. comm.). The curvature K, of a field describes the deviation of a curve, bent at a point P from a straight line (Roberts, 2001, Fig. 4.5). It is defined mathematically using the equation 4.4:

$$K=d\omega/dS=2\pi/2\pi R=1/R \qquad 4.4$$

where, $d\omega$ is the angle subtended by the osculating circle at the point of observation (P), dS is the corresponding elemental arc length and R is the radius of curvature (Fig. 4.5).

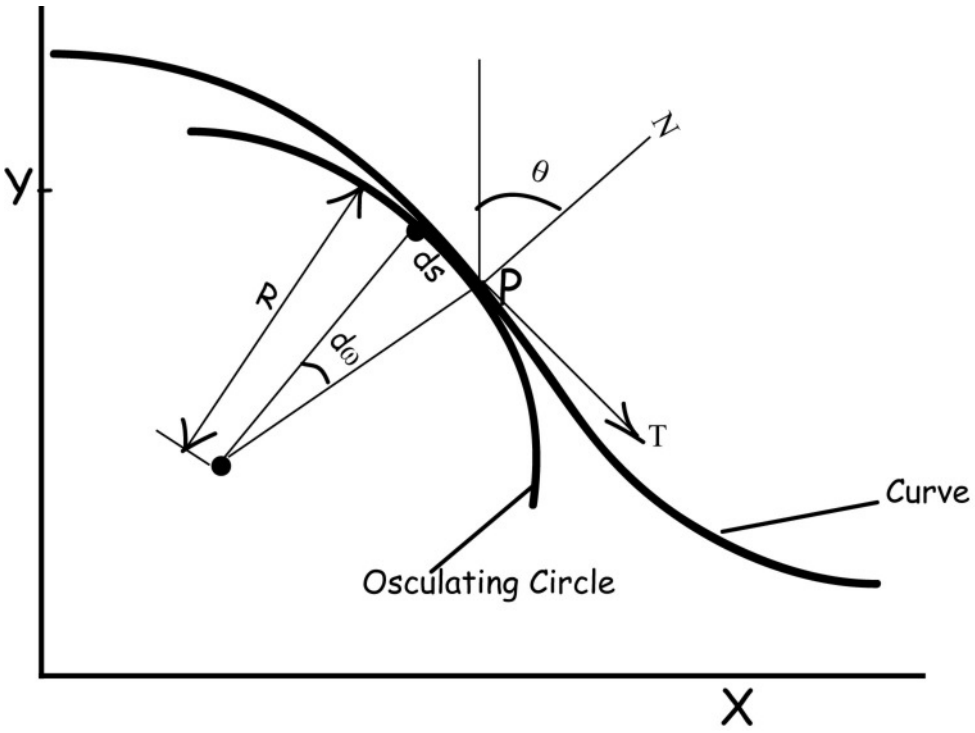

Figure 4.5 Definition of curvature for a particular point 'P' on a curve (after Roberts, 2001).

The curvature attribute could be also equally expressed using second derivative functions (eq. 4.5), from which the various curvature attributes (e.g. dip, minimum curvature, shape index etc.) are derived:

$$K= d^2y/dx^2/(1+(dy/dx)^2)^{3/2} \qquad 4.5$$

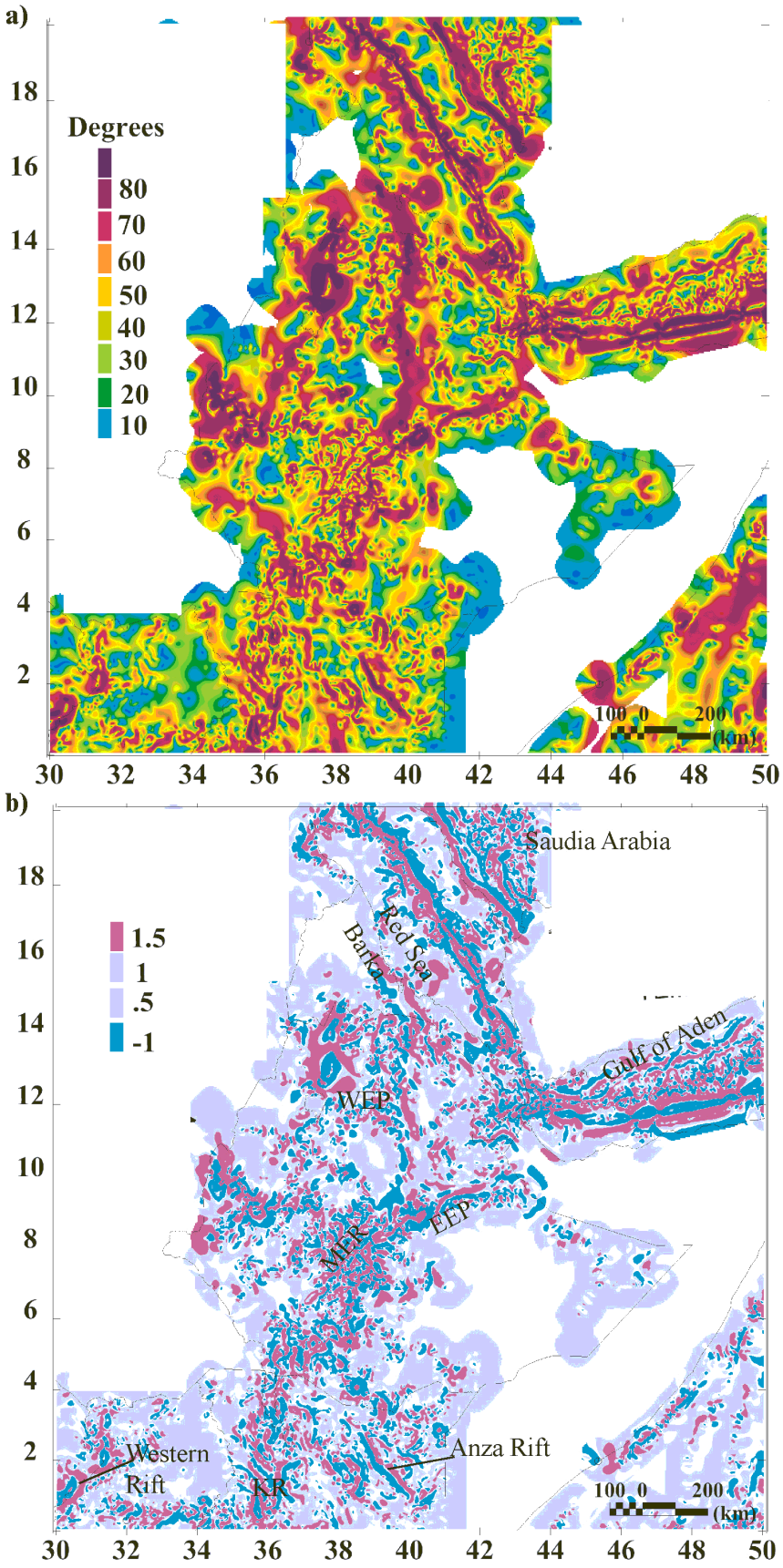

Figure 4.6 Curvature attributes applied to Bouguer gravity anomaly. (a) dip angle (b) dip curvature. EEP: Eastern Ethiopian Plateau, KR: Kenya Rift, MER: Main Ethiopian Rift and WEP: Western Ethiopian Plateau.

In this case, dip angle and dip curvature attributes applied to a part of the Bouguer gravity anomaly are found to give good results. Figure 4.6 shows the result of applying this method. The maximum dip angle values (Fig. 4.6a) follow the western (WEP) and eastern (EEP) escarpment of the rift along the MER and Kenyan Rift (KR) and outline the rift margins or border faults. The Red Sea and Gulf of Aden spreading zone and the boundaries of the fault along the western rift are clearly outlined. To the west, overlying the western Precambrian domain, a gravity lineament is outlined which probably merges with the Barka (Red Sea) lineament in Eritrea (Fig. 4.6a, see Fig. 1.1 for additional locations).

The dip curvature attribute (Fig. 4.6b) revealed additional information. Moderate values are suppressed and only low and high values presented in contrasting colours. A problem associated with using this attribute may be indicated by the juxtaposition of positive (red) up-thrown and negative (blue) down-thrown curvatures, as indicated in Roberts, (2001). Therefore, in the Red Sea area and Gulf of Aden, the ridge is apparently down-thrown to the northeast. Similarly, the gravity lineament along the eastern Red Sea uplift (Saudi Arabian coast) shows a down-thrown side to the northeast. There are offsets on the northern extreme of the Red Sea and in many parts of the Gulf of Aden. These are the effects of the transform faults identified from earthquake epicentres and magnetic surveys (Fairhead and Girdler, 1970; Allan, 1970). Similar patterns are also depicted on the eastern escarpment (EEP) that marks the boundary between the Somalian plate and Afar, which displays a down-thrown side to the southeast.

In the MER southern section, the left lateral shift of the fault system is clearly manifested at about 5°N latitude. The Anza rift, Kenyan rift system and western rift exhibit a westerly down-thrown side. To the north in Saudi Arabia, the Najid fault systems are outlined as NW-SE trending lineaments, and are similar to the structures interpreted from gravity data by Gettings et al. (1986). Due to the scarce data density the response is particularly flat in the Afar area and along the western escarpment.

4.2.6 Geoid

The geoid map from the EGM96 model extracted for this region shows a clear distinction between the western plateau region and the rift margins (Fig. 4.7). High geoid (above 4 m) coincides with the high topography of the Ethiopian plateau (WEP) and the Sudan craton (Nubia), and the minimum is about –55 m in the Indian Ocean. In spite of the reduced amplitude, a relative increasing trend in the Kenyan plateau region (Fig. 4.7) is also exhibited. The Afar of Ethiopia and broadly rift regions of southern Ethiopia are marked by distinct trends in the geoid anomaly. Unlike the general assumption of the geoid high and hot spot correlation,

the Afar hot spot (location 42°E, 12.47N) does not show a geoid high. The goid is equally elevated along the axial line of the Main Ethiopian Rift and most regions of the MER are represented by lower geoid (pronounced negative geoid heights) than the plateau areas. The general trend shows the change in geoid along the rift structures. Closures of relative positive Geoid are depicted along the Barka lineament and northwestern plateau of Ethiopia (Fig. 4.7).

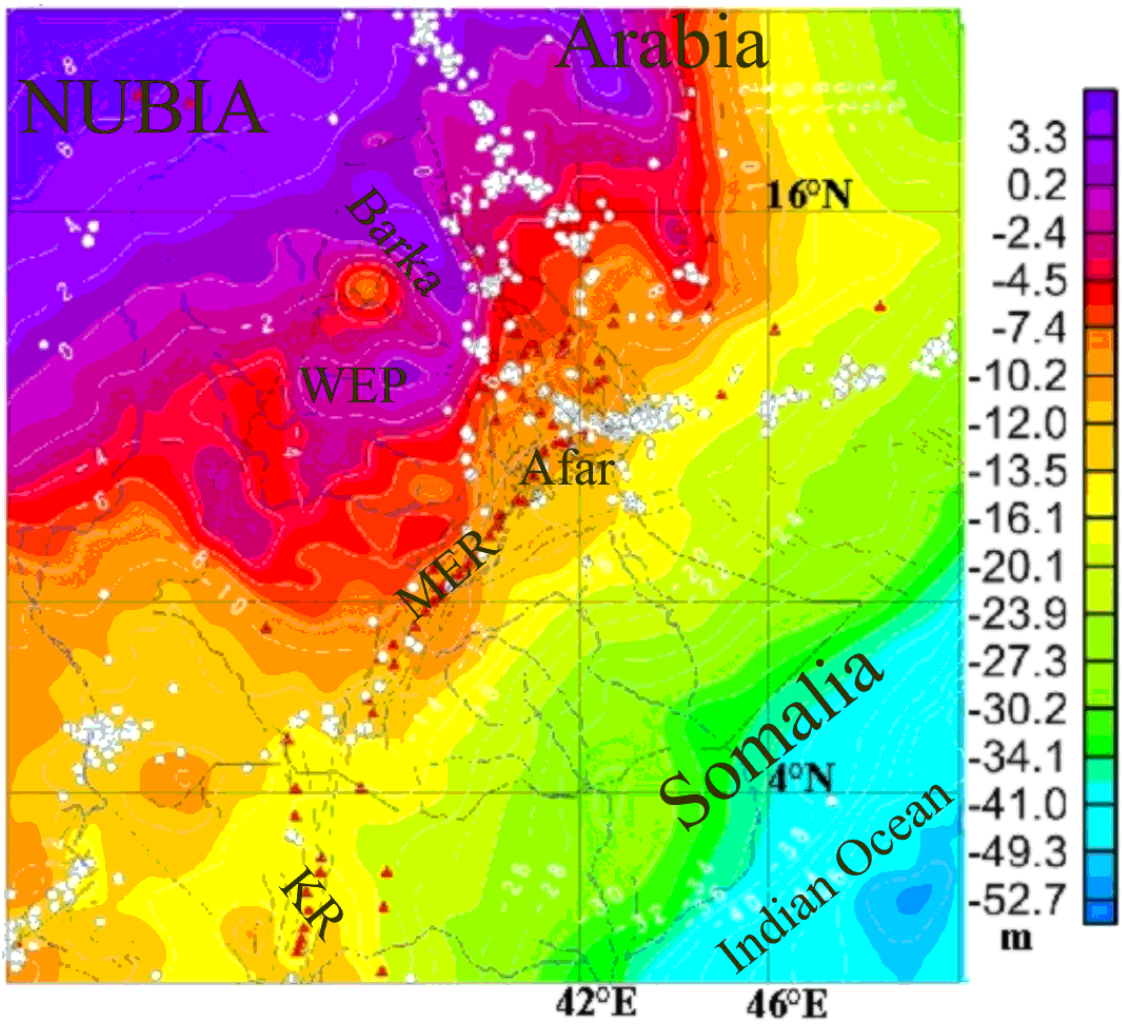

Figure 4.7. Geoid from the EGM96 model.

In summary, it is shown in this chapter that the acquired 15000 gravity data values authorized by Sudan Geological authority and supplied by GETECH, are directly combined to produce a regional Bouguer anomaly map. Though inclusion of the eastern Sudan data helps to fill wide data gaps, data gaps still exist in many parts (e.g. most plateau regions of Ethiopia, large parts of the Somalia plate, most parts of Eritrea, regions bordering Eastern Sudan and Ethiopia, areas between northern Kenya and southern Ethiopia). The potential of GRACE is demonstrated in an attempt to fill data gaps and to provide a regional Bouguer gravity field of the region. The merger process has been conducted following a simple procedure and the

resulting Bouguer anomaly map for the Afro-Arabian plate is at least useful to investigate first-order structures. The compiled Bouguer anomaly map shows broad negative anomalies over the main Ethiopian rift, plateau regions and Eastern and western rift systems, relative positive anomalies in the eastern Sudan craton bounding the various extensional basins and Precambrian basement, and positive anomalies in the Red Sea Rift and Gulf of Aden. In the next chapter, the land data are used to study the isostatic state of the region.

5 Isostasy and isostatic state of the area

The history of isostatic observation in Africa dates back as early as 1900 when pendulum measurements were made by Ernst Kohlschütter. Some analyses of these measurements were made (Kernekel, 1922; Willis, 1936) and gravity measurements were also made in East Africa (Bullard, 1936). In the early 70s Fairhead (1976) applied an Airy isostasy model to the eastern rift (southern Kenya). Isostatic maps (Airy compensation model) were prepared in the northern part of Ethiopia by Makris et al. (1975) and in the Main Ethiopian rift by Alemu (1992) prepared isostatic maps. Very few studies deal with regional interpretation of isostatic maps in East Africa, whereas isostatic maps computed using different models in a large area are common elsewhere. In the conterminous United States, Simpson et al. (1986) used isostatic residual maps (Airy model) to categorize anomalies by geological correlation rather than for the usual interpretations of under compensation/over compensation.

5.1 Methods, analysis and models

The Bouguer anomaly map (Fig. 4.3) depicts broad positive anomalies over oceans and depressions, and strong negative anomalies over continental areas. The recognition of this inverse correlation of negative Bouguer anomalies with topography led to the concept of isostasy (e.g. Banks et al., 1977; Watts, 2001). The topographic loads and loads produced by density inhomogeneities in the underlying crust are supported isostatically, but the standard gravity corrections do not account for the gravitational attractions of the compensating masses. Both Airy (local) and Vening-Meinesz (regional) isostatic models are applied to approximate the gravity field of the compensating masses (isostatic regional). A local Airy model does not consider the lithospheric strength, whereas the regional Vening-Meinesz (VM) compensation model considers the mechanical strength of the lithosphere and distributes compensation laterally over an area limited by the VM regionality, R (Heiskanen and Vening Meinsez, 1958). Isostatic regional fields are computed here using a two-minute merged topography and bathymetric data set (Smith and Sandwell, 1997) that covers the area shown in Figure 1 and an extra 300 km to avoid edge effects.

In addition to topographic data, the models need prior assumptions of the density contrast between upper mantle and crust ($\Delta\rho$), average density of the topographic load (ρ), normal crustal thickness and flexural rigidity (D), which is directly proportional to effective elastic thickness (T_e) (e.g. Burov and Diament, 1995; Watts, 2001):

$$D = \frac{E\,Te^{3}}{12(1-\sigma^{2})} \qquad with\ \sigma = \frac{[Vp/Vs] - 2}{2([Vp/Vs]-1)}$$

where E= Young's modulus and σ = Poisson's ratio, V_p, V_s= average P-wave and S-wave velocities (e.g. Turcotte and Shubert, 2002).

More on elastic thickness/rigidity is discussed in chapter 6, but here some tests using a range of flexural rigidities (low to high) and comparison to the resulting models with the approximate boundaries of the basement rocks and major faults from the tectonic map of Africa (CGMW, 1968) have been made. The T_e used here is biased towards the average elastic thickness of active regions (rifts), closer to the average values determined for the MER, Afar and southern rifts (Ebinger and Hayward, 1996). On the other hand, while considering the dynamic topography a different T_e for the entire region is used in order to account for the rigidity of the cratons (e.g. Sudan craton).

Other isostatic model parameters (normal crustal thickness, density contrast from velocities) are inferred from available seismic refraction investigation (e.g. Berckhemer, 1975), previous isostatic (e.g. Alemu, 1992) and related studies, but varied in a more general case. It is difficult to determine the most applicable compensation model and model parameters for a given area. Therefore, a number of different parameters were tested using: normal crustal thickness of 25, 30, 35 and 40 km; Δρ of 0.3, 0.35, 0.4 and 0.45 Mg/m^3; and rigidity D, from 1x10^{20} Nm to 1x 10^{25} Nm. Even though the variations in both model parameters and type of compensation models are small, quick visual correlations have been made for every isostatic model in order to choose which model best displays the geological and geodynamic situation. The models finally selected have the following parameters:
(1) Airy model (local isostasy/zero flexure): Crust/mantle density contrast Δρ=0.45 Mg/m^3, mantle density=3.1 Mg/m ^{3}, normal crustal thickness=35 km; (2) Vening-Meinesz model: D=1x10^{22} Nm, with approximate effective elastic thickness, T_e=10 km. Topographic density ρ= 2.67 Mg/m ^{3} and water density ρ_w = 1.03 Mg/m ^{3}.

The isostatic model calculations are made using a program based on Parker's algorithm (Parker, 1972). A number of isostatic models derived by changing the model parameters show that it is very difficult to determine the type of compensation since it is complex and isostatic models tend to be similar (e.g. McNutt, 1980; Heiskanen and Meinesz, 1958). Based on this and the test using a number of model parameters, large differences in the isostatic anomalies are not evident with small variations of model parameters and also between the types of compensation models (i.e. local vs. regional). The following discussions of isostatic anomalies are only based on the Vening-Meinesz model.

5.2 Dynamic topography and dynamic compensation

The observed topography of the earth is the result of the isostatic and non-isostatic compensation of deep masses. There are two forms of mechanism: isostatic (static) and non-isostatic (dynamic). The variation/irregularities of the observed topography are due to the density inhomogeneities (anomalous mass distributions) indicated in gravity anomalies. In turn, these are the outcome of the tectonic processes both at crustal and upper mantle levels. Theoretically, in a completely compensated environment, ideally a near-zero isostatic anomaly is expected, or the free-air gravity anomalies are zero and the topography and the long wavelength gravity anomaly are inversely correlated. The differences from the normal observation mainly stem from the tectonic and geologic processes and also show the presence of local uncompensated geological bodies supported mainly by the rigidity of the upper crust.

Customarily, we use the observed topography to calculate an isostatic anomaly that approximately corresponds to the long-wavelength topography. Then, we remove the long wavelength isostatic anomaly (which isostatically supports the topography) in order to highlight the upper crustal density distributions. In effect, the resulting anomaly (isostatic) residual is comparable to the residual anomalies calculated by Fourier transform, visual inspection and/or polynomial fitting methods. This is the long-standing problem of regional and residual separation in potential fields, which is variably subjective to the choice of the particular frequency and choice of parameters used for estimating the regional field or long-wavelength anomaly. Both local (Airy) and regional (flexural rigidity) isostatic models are also dependent on the choice of initial assumptions for the controlling parameters (crustal thickness, density contrast at the crust-mantle interface and also the flexural constant).

Compensation is not only static, but there is also dynamic support of the present observed topography. Global estimates of topography show amplitudes of ±1km resulting from sub-lithospheric density contrast (Hager et al., 1985). East Africa, Australia and northern Africa are elevated (Panasyuk and Hager, 2000), indicating the presence of non-isostatic support. Therefore, observed topography is defined as the sum of static (isostatic) and dynamic topography (e.g. Panasyuk and Hager, 2000). The dynamic topography is supported by the stresses generated by the density contrast in the sub-lithospheric mantle (Panasyuk, et al., 1996). Global dynamic topography predicted by Lithgow-Bertelloni and Silver (1998) use two different models of mantle density heterogeneity: 1) based on subduction history (e.g. Lithgow-Bertelloni and Richards, 1995) and, 2) inferred from seismic tomography (e.g. Grand et al., 1997). The dynamic topography models for the part of the East African region (Lithgow-

Bertelloni, pers. comm., and Figs. 5.2, 5.3) were used to remove the contribution of dynamic processes to the observed topography. Then, the remaining topography would be considered corrected for dynamic effects or only due to isostatic compensating masses. It is assumed that both dynamic and isostatic compensation mechanisms are acting and that the combined compensation is more logical than the simple isostatic models. However, uncertainties remain because the dynamic topography models rely on the approximation of initial parameters such as mantle density, viscosity and the global seismic models (see Lithgow-Bertelloni and Silver, 1998). The isostatic models (local and regional) could be improved with the addition of more new data on crustal thickness, density contrast and flexural rigidity. Nevertheless, models are under constant improvement with the inclusion of additional data. The new isostatic residual maps presented here are use the procedures outlined above. In each case, general comparisons have been made. Compensation mechanisms other than the isostatic and dynamic mechanisms may also exist.

5.3 Interpretation of isostatic and "iso-dynamic models"

In the following sections, interpretation of isostatic residual maps by and large refers to the isostatic model in Figures 5, and 5.1. However, the dynamically corrected isostatic residual maps (Figs. 5.2, 5.3) are also used when necessary. Aside from this, the isostatic models with or without dynamic corrections are also compared. The major reasons for incorporating dynamic models are:

1) large negative Bouguer anomalies spanning over the East African plateaux, which could be explained by combining both isostatic and dynamic compensations (e.g. Ebinger et al., 1989);

2) assumptions that invoke asthenospheric upwelling, a low-density structure that dynamically supports the excess topography (e.g. Lithgow-Bertelloni and Silver, 1998) and low velocity (see also shear wave anomaly) consistently observed under the plateau regions of Ethiopia, Kenya and the East African Rift (Ritsema and Van Heijst, 2000). The differences are also evident in the 3D model (Chapter 6) and elastic thickness estimates.

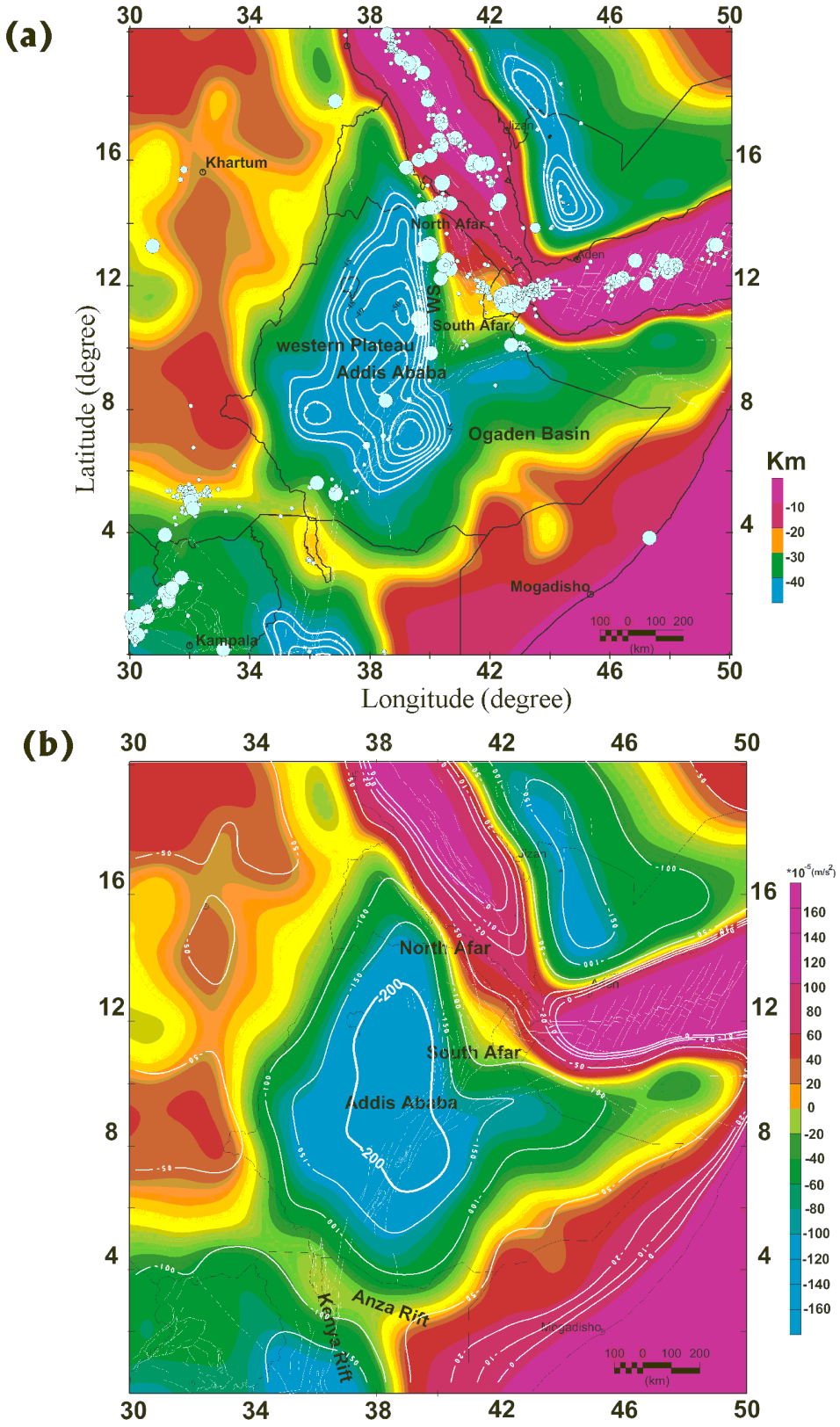

Figure 5 Isostatic regional fields: (a) Vening-Meinesz (VM) modelled Moho: depths greater than 45 km are evident in continental areas (blue colour and white contour lines are deeper than 45 km) thin crust (yellow to red) less than 20 km exists in Afar and oceanic areas. Earthquake epicentres are superimposed according to depth, relatively deeply focused earthquakes (large circles) exist along the western scarp (WS) and near the triple junction. (b) isostatic regional gravity field using VM model for $D=10^{22}$ Nm. Contours (white lines) are only negative anomalies. The broad negative anomaly centred at the latitude of Addis Ababa suggests that the Ethiopian plateau is partly compensated by thick crust.

The earlier gravity analysis considers an isostatic regional model with flexure ($D=10^{22}$ Nm) in order to emphasize the rift structures and leaves open the part of the contribution from dynamic support. Here the isostatic residual anomalies are produced a) using regional isostatic Vening-Meinesz type (flexural rigidity $D= 10^{23}$ Nm) taking into consideration the relatively rigid adjacent craton (Eastern Sudan), and b) calculating the gravity anomalies from dynamic topography models by Lithgow-Bertelloni and Silver (1998) which applies mantle density heterogeneity based on subduction history (slab) and seismic tomography (Grand). Both gravity contributions are eliminated from the Bouguer anomaly and the isostatic model in (a) to produce isostatic residual anomaly maps (see Figs. 5.2, 5.3). Geologic interpretations based on isostatic residual maps are made in a separate section (see section 5.3.2).

5.3.1 Isostatic regional field

The isostatic Moho and isostatic regional field for the VM model are shown in Figure 5. Although not shown here, the Airy Moho and regional field are very similar. Significant differences are only evident in the area over the Ethiopian plateau, in the southeastern sections where the topography drastically changes (sharp gradient) and over the southern part of the Anza Rift. Maximum depth the VM modelled Moho is about 45-48 km under the plateau regions of Ethiopia and Kenya (Fig. 5a). This depth is approximately equivalent to the estimated depth (~50 km) at which the crust-mantle system tends towards isostatic equilibrium (see also Makris et al., 1975; Alemu, 1992; Ayele et al., 2004). The Moho of the Somalia plate, the Sudan craton, Anza rift and Afar depression is between 30 and 35 km depth, and shallow depths (less than 20 km) are evident in the Red Sea area, Gulf of Aden and Indian Ocean.

The corresponding isostatic regional gravity anomaly shows very broad variations, which are related to the thickening of the crust. These broad negative anomalies may also indicate 'upwelling of the asthenosphere' under the rift systems. Previous gravity studies also proposed that the lithosphere beneath the plateau has been thinned and suggested the presence of low-density asthenosphere as isostatic support (e.g., Fairhead, 1976). In addition to the isostatic compensation, Ebinger et al. (1989) suggested in part dynamic compensation by convective processes in the lithosphere. There is a general consensus that 'asthenospheric upwelling' or 'hot low density material' are important, for the East African plateau area. Evidence is drawn from geological, geochemical, seismic refraction, teleseismic, global seismic tomography and topography analysis and heat flow studies, as mentioned before. All these studies suggest that in one way or the other, contributions from the lower mantle are responsible for the rifting process.

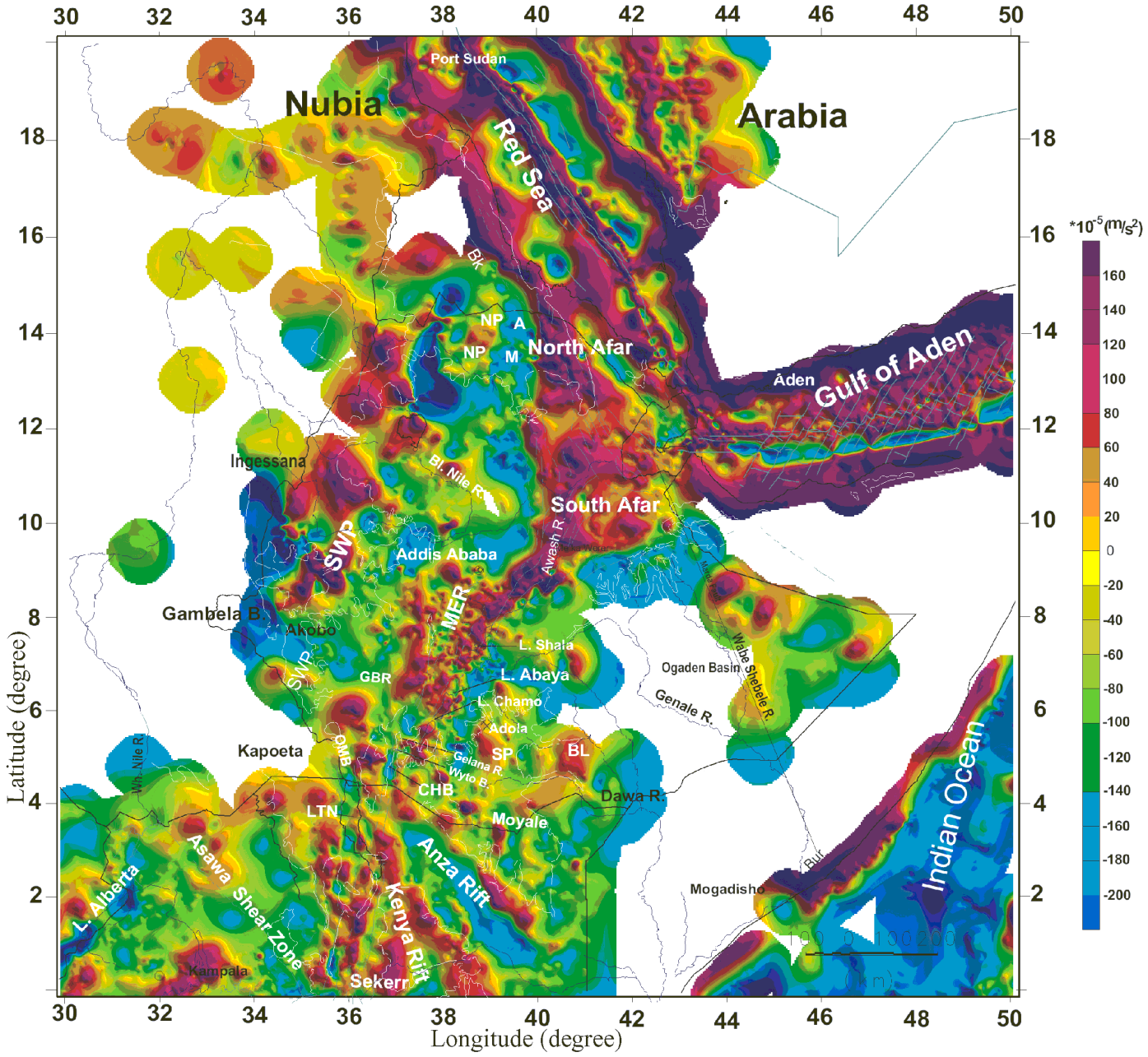

Figure 5.1 Vening-Meinesz (D=10^{22} Nm) modelled residual gravity field produced by subtracting the isostatic regional filed (Fig. 5b) from the Bouguer anomaly (Fig. 4.3). Major rivers (blue thin lines), major faults (black lines) and approximate regions of Precambrian basement rocks (white thin lines) from CGMW (1968) are overlain. The Afro-Arabian Rift and Precambrian structures are characterized by highly positive to relative positive residual anomalies. Strong negative residual anomalies delineate sedimentary basins (e.g. Western Rift, Red Sea area, Gambela basin of Ethiopia, Anza rift and basins in the southern rift system). The isostatic residual anomaly suggests that the entire rift system interconnected and possibly is a zone of intense dyke injection.

However, it is still questionable which compensation models and mechanisms properly explain the tectonic processes in continental rift zones. It is also not possible to argue for a single compensation mechanism (static against dynamic) since compensation may result from a combination of many uplift mechanisms (e.g. Ebinger et al., 1989; Nyblade and Robinson, 1994). Therefore, both isostatic (static) and non-isostatic (dynamic) compensations may be used in combination to forward more reasonable explanations for the broad topographic uplift, associated negative Bouguer anomaly and isostatic regional anomaly.

The 1 km excess elevation of the area (Fig. 2) is part of the 'African superswell' (Nyblade and Robinson, 1994). Thus, the entire African plate may have a similar uplift history in the Mesozoic and Cenozoic (e.g. Partridge and Maud, 1987) that developed significantly in the Cenozoic (e.g. Gurnis et al., 2000). Using a new formulation of dynamic topography and uplift rate, Gurnis et al. (2000) showed the deep mantle flow by removing the contributions of shallow depths (<50 km) and suggested the 'uplift of the African topography by a large-scale buoyant structure'. In addition to the isostatic support indicated by the broad negative anomaly centred around latitude 9°N (see Figs. 2, 5a, b), the presence of dynamic support from great depths (e.g. Ebinger et al., 2000; Gurnis et al., 2000; Ritsema et al., 2000) is suggested.

Both Airy/Vening-Meinesz isostasy models probably are not the perfect models to account for the geodynamic processes. Future residual gravity anomaly maps may incorporate well-constrained dynamic compensation models in addition to isostatic ones. Despite the presence of deep-seated dynamic effects, isostatic residual anomalies obtained by removing the compensating crustal bodies show important correlations with the geology (see the next section).

If it is assumed that the Vening-Meinesz isostatic model is valid, then isostatic residual anomalies would be zero for complete compensation. The positive and negative shift from zero characterizes isostatic under-and over-compensation, respectively (e.g. Götze, et al., 1991). The mean value of the isostatic residual anomaly is about 8 $x10^{-5}m/s^2$. This could indicate: (1) there are upper crustal features not compensated regionally and supported by the strength of the lithosphere or; (2) regional isostatic imbalance. The degree of over-and under-compensation could be also explained by plotting a histogram of the residual field (e.g. Götze et al., 1991; Hackney, 2004).

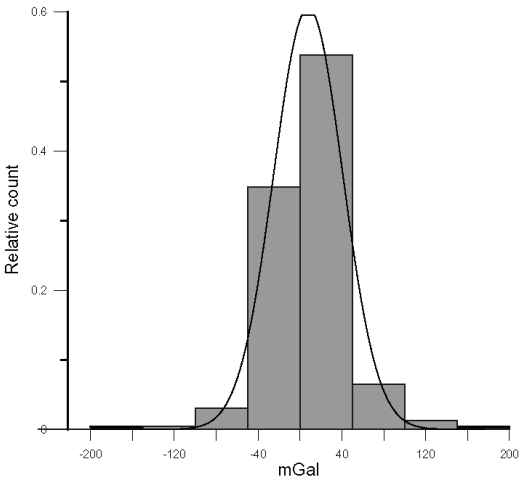

Figure 5.4 Histogram of isostatic residual anomalies displaying a slight positive bias with mean value of $8x10^{-5}$ m/s^2 and standard deviation of $34x10^{-5}$ m/s^2, suggesting under compensation (see text).

The histogram (Fig. 5.4) with small mean positive isostatic residual anomaly shows a slight positive bias and under-compensation could be inferred. The possible implication is that the predicted Moho to compensate the excess topography is thicker than would probably be observed and resulting with a positive isostatic residual anomaly. In summary, the high topography of the Ethiopian plateau is partly compensated by thicker crust and partly by dynamic processes.

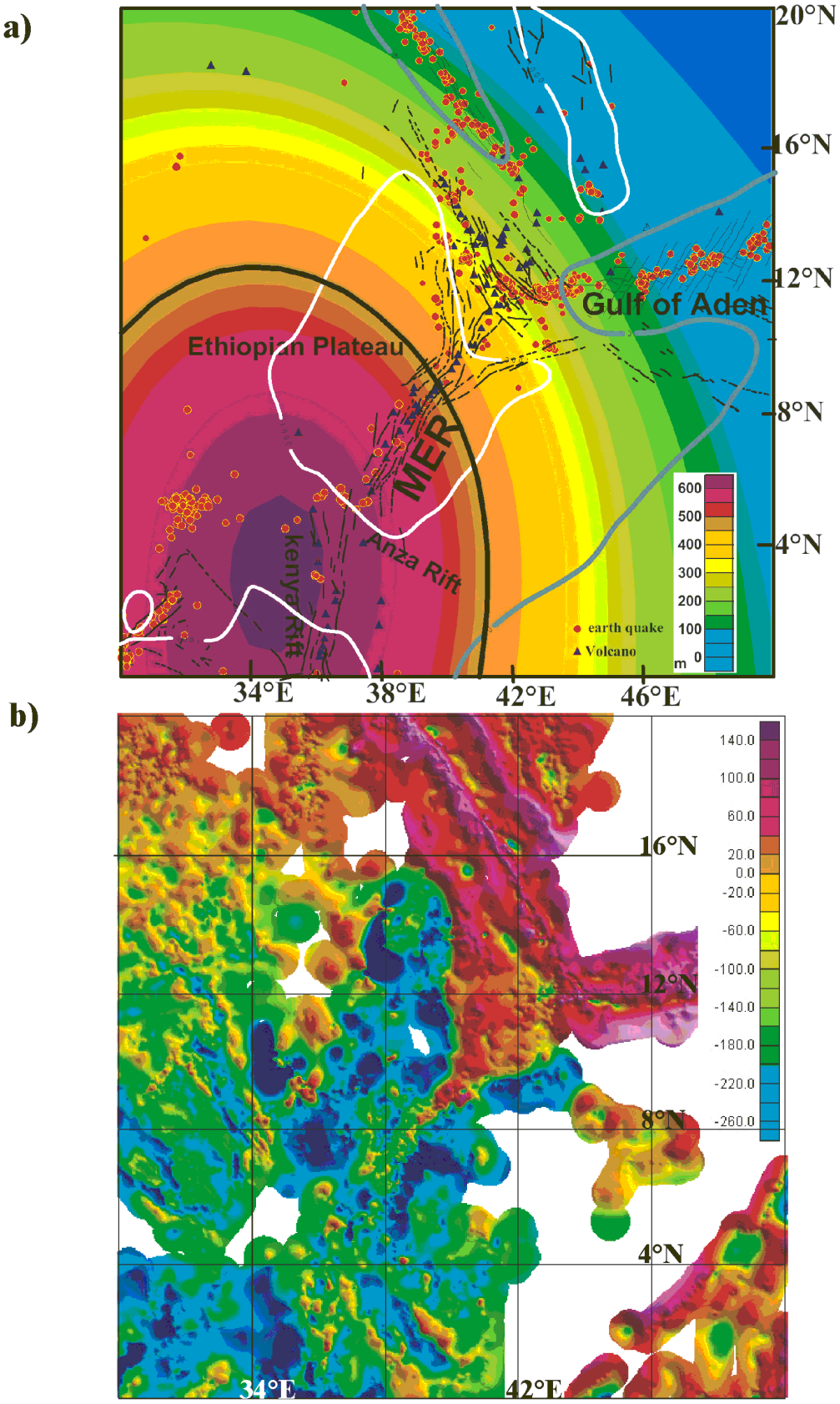

Figure 5.2 a: Dynamic topography of model-Grand (data from Lithgow-Bertelloni pers. comm.). Observed topography is indicated by 1 km contour (thick white line) that marks the Afro-Arabian plateau. The grey contour shows zero elevation and the thick black line is 500 m dynamic topography contour. b: Isostatic residual field modelled from observed topography (Fig. 2a) corrected by dynamic topographic model (a), and D=10^{23} Nm. The results are similar to the isostatic residual field in Figure 5.1 with some variations south of 8°N where dynamic topography is significant.

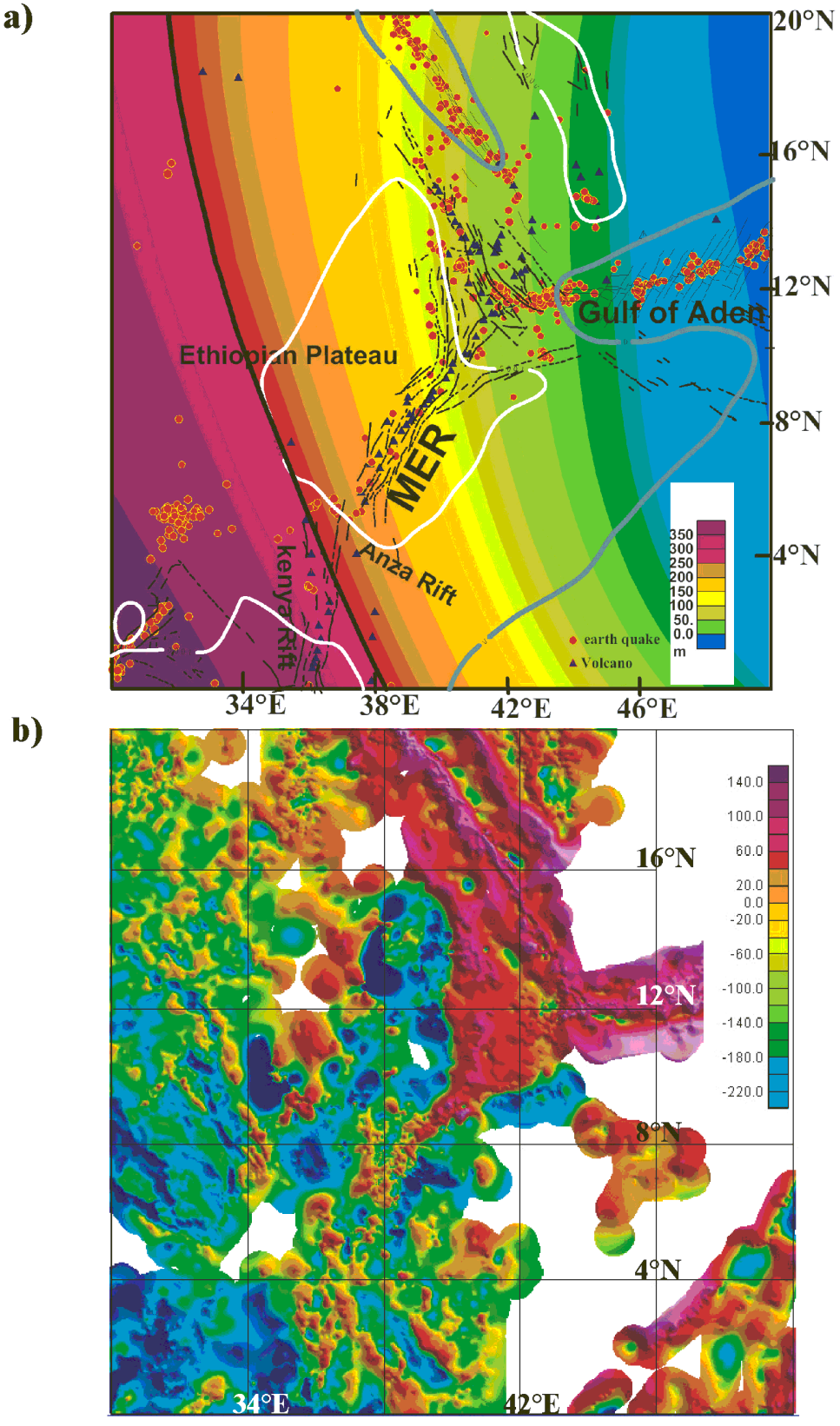

Figure 5.3 a: Dynamic topography of model-slab, based on subduction history (data source the same as in Fig. 5.2a). Features overlain are similar to Figure 5.2a and the thick black contour is the 300 m dynamic topography, roughly marking a probable suture zone. Significant dynamic topography exists west of this contour, but decreases to the east. b: The isostatic residual field modelled from the observed topography (Fig. 2a) corrected using the model in (a) and flexural rigidity (D=10^{23} Nm). In the rift zones the results are particularly similar with isostatic residual field in Figure 5.1a.

5.3.2 Isostatic residual field

Precambrian domains

There are vexing problems unsolved with regard to the geodynamic setting of the East African Orogen (EOG) and its relationship to the rift structures is an ongoing scientific debate. Some recent attempts have been made to investigate rift processes, tectonics and the role of Precambrian structures using seismic anisotropy (Ayele et al., 2004; Gashawbeza et al., 2004) and receiver function analysis (Dugda et al., 2005). The gravity data distribution covering these areas is relatively scarce, but the isostatic residual anomaly (Figs. 5.1, 5.2b, 5.3b) can be used to document the Precambrian structures in western, northern and southern Ethiopia. Though most of the prominent structures are labelled on Fig. 5.1, all figures show similar trends with varying amplitudes.

The Neoproterzoic basement rocks in western Ethiopia and southwestern Ethiopia are represented by low-grade volcano-sedimentary sequences associated with dismembered ophiolites and high-grade gneiss terranes (e.g. Braathen et al., 2001; Allen and Tadesse, 2003; Fig. 2.1). The zone is predominantly marked by relative positive isostatic residual gravity anomalies striking N-S to NE-SW along the western side of Ethiopia (SWP, Fig. 5.1). The zone is terminated to the south by the Gambela basin and probably continues to southwest Ethiopia underneath the volcanic rocks. It also extends north of 12°N latitude underneath the Phanerozoic basaltic cover rocks and terminates or is folded to join the northern Precambrian basement near the Ethiopia/Eritrea border. However, geological data (e.g. Kazmin, 1978) asserts that the zone can be traced south of Asmara as a belt of andesitic-dacitic metavolcanic rocks with abundant massive sulphides. This suggests that a densification of gravity stations in this area would be useful. On a regional scale, the existence of the Ingessana ophiolite complex at the Sudan/Ethiopia border and further north (Barka) and south (Sekerr), means that the entire zone is regarded as a suture zone (e.g. Berhe, 1990; Abdelsalam and Stern, 1996) or is considered to mark a subduction zone (e.g. Braathen, et al., 2001) with westward subduction of oceanic crust (only the margins of the western continental block exposed in Ethiopia). The western province of the ANS belt in Ethiopia, delineated by a relative positive isostatic residual gravity anomaly, may also mark the western margin of this subduction zone.

The northern Ethiopian basement rocks include low-grade volcanic, volcano sedimentary and plutonic rocks of ANS assemblage, where belts of mafic and ultramafic rocks (ophiolites) were identified (e.g. Tadesse, 1996). Mafic rocks overly the Mesozoic sandstones and Tertiary volcanics, particularly towards the eastern margin of northern Ethiopia (e.g. Kazmin, 1978).

The isostatic residual anomaly map is particularly important for geological interpretation in the mountainous areas of northern Ethiopia where most low gravity anomalies over high topographic areas were interpreted as only expressions/effects of high topography (e.g. Oluma and Zewuge, 2001). A closure of moderately positive gravity anomaly in northern Ethiopia (NP, Fig. 5.1) is related to the Precambrian low-grade rocks predominantly formed of meta-volcano-sedimentary and intrusive rocks of the ANS assemblage. Positive gravity anomalies are also well correlated with the mafic-ultramafic belts of Darotekli and Shirraro-Adi-Nebrid shear zones in the northern Precambrian domain (Oluma and Zewuge, 2001; Fig. 5.1). East of the major positive anomaly, the negative anomalies are associated with Palaeozoic-Mesozoic sedimentary formations of Adigrat (A, Fig. 5.1) and Mekele (M, Fig. 5.1) areas. The surrounding negative anomaly belt is associated with the Tertiary volcanics and sediments overlying the crystalline basement.

The strong positive anomalies along the Red Sea coastal areas of Eritrea are associated with the Tertiary marginal faults. The Barka zone (Bk, Fig. 5.1) is closer to the coastline (about 16°N latitude) and closely related with the earthquake epicentres. The Barka zone offers a good example of the association of Precambrian structure and rift geometry (Dixon et al., 1987). There are no gravity data to investigate the extensions of the MB/ANS belt in Eritrea.

To the south, the positive residual anomalies and moderately negative residual anomalies may be associated with basement rocks and meta-volcano-sedimentary sequences, respectively. In the southern part of Ethiopia, Precambrian basement rocks show a transitional zone between the low-grade volcano-sedimentary successions and mafic and ultramafic complexes of the ANS, and the high-grade gneisses and schists that form the MB (Worku, 1996; Yibas et al., 2002; Yihunie and Tesfaye, 2002; see also Fig. 2). The southern Precambrian province of Ethiopia is limited by the Anza graben in the south, and by the main rift margin to the west and north (SP, Fig. 5.1). The negative anomalies north and west of the Adola belt, limited by the rift, could be expressions of the weathered basalts/volcanic constructions overlying the crystalline basement (Figs. 5.1, 5.2b, 5.2b).

A north-south trending positive residual anomaly is evident near the Ethiopia/Kenya border (Moyale area) as the southward extension of the Adola belt (Figs. 5.1, 5.2b, 5.3b). Northeast of this belt, a relative positive residual anomaly intersecting the lower section of Dawa River (BL, Fig. 5.1) is associated with the Bulbul terrain rocks dominantly of amphibole schist, ultramafic schist, granitoids and gabbroic/dioritic rocks (Yihounie and Tesfaye, 2002). The Bulbul terrain is a west-verging thrust nappe, which is evidence of obducted ANS crust hidden beneath the sedimentary cover rocks of eastern Ethiopia (Yihounie and Tesfaye, 2002). There are no gravity

data east of this belt. Nevertheless, the positive closures near Ethiopia and the eastern border of Somalia may be the result of the same tectonic processes.

Other basement rocks, which are delineated by positive residual anomalies, include closures in southwest Ethiopia and in association with the southern rift system. Parallel to the major Omo and Weyto basins, the positive north-south trending anomalies are related to Precambrian structures of southwest Ethiopia that are dissected by the rift (see Fig. 5.1).

Along the Sudan/Ethiopia border (west), a suture zone is also discernible from relative positive isostatic residual anomaly with a brief east-west interruption by negative anomaly around the Akobo-Gambela sedimentary basin (Fig. 5.1). Further south, Vearncombe (1983) considers the dismembered ophiolites at Sekerr (Kenya), to mark a N-S suture zone, possibly extending northwards through Akobo of southwest Ethiopia to the Kurmuk-Ingessana region of eastern Sudan (e.g. Vail, 1983; Abdelsalam and Stern, 1996; and Fig. 5.1). Broad positive residual anomalies near Kampala and Sekerr are related to Precambrian basement rocks of the MB.

Contrasting gravity anomalies over the tectonic belts of Barka zone, western Ethiopia, southern Ethiopia (Adola) and Sekerr (Kenya) are shown in the isostatic residual maps. In general, positive residual anomalies are the expressions of juvenile island arc assemblages, ophiolite complexes, mafic intrusions and basement rocks, often locally showing reduced anomalies due to the associated volcano-sedimentary rocks, alteration and weathering. According to Kazmin et al. (1978) the absence of granulites in the north may suggest weak metamorphism and low temperature (i.e. ANS) while its presence in the south implies high-grade metamorphism (i.e. Mozambique belt). A normal increase in density with depth in the crust, related to increasingly higher metamorphic grades and increasingly mafic rock types with depth, has been observed in the conterminous US to describe positive residual anomalies (Simpson, et al. 1986). There is also a relative difference in the magnitude of the isostatic residual gravity anomalies between the western and the southern Precambrian basement rocks and locally within the same province, which probably reflects the degree of metamorphism. The density variations reflected in the isostatic residual maps are predominantly the sum effects of the isostatic and, in some part, the dynamic compensation processes.

Rift system

It is not necessary to delve into the detailed interpretation of the rifts. However, using the compilation of gravity data presented here, the MER and associated structures are examined in some detail. The isostatic models computed over a wider continental area also confirm and

enhance some of the inferences made by other researchers on the continental rifts and bring new information as well.

The entire MER is characterized by relative broad positive residual anomaly between Lake Chamo and Awash (Figs. 5.1, 1.1). The northern section of the MER is mapped by strong axial NE-SW trending positive residual anomalies. Around Awash, NW-SE trending strong positive anomalies delineate the margins of the northern MER and southern Afar rift systems respectively (Figs. 5.1, 1.1). To the south, below Lake Chamo, the trend of the rift is diffuse at the complex overlap of Mesozoic and Cenozoic rift systems, probably due to the NW-SE and E-W trending structures and associated rift basins.

Former surveys (e.g. Mohr and Gouin, 1967) attribute the broad negative Bouguer anomaly over the adjacent high lands and relative positive axial anomaly along the MER to the low-density upper mantle material under the western and eastern escarpment and intrusive bodies along the MER, respectively. Subsequent work in the Main Ethiopian Rift (Searle and Gouin, 1972) delineates the intrusive zone as the Wonji Fault Belt (WFB), which terminates around Lake Abaya and whose width decreases southwards. Similarly, Mahatsente (1999) arrived at the same conclusion, i.e. intrusive bodies beneath the rift floor, which mainly follows the Quaternary basalt along the WFB. The current faulting is localized within a 33 km wide zone and the Quaternary faulting includes a 7 km wide belt (Bilham et al., 1999). Estimates of the depth to the top of the intrusive body lie between 6 and 22 km, with a southward continuation (Mahatesente, 1999).

If the derived isostatic anomalies are reliable (Figs. 5.1, 5.2, 5.3), they show the continuity of the axial intrusive body southwards to join the Kenyan rift system. As demonstrated on the residual map, the intensity of the residual anomaly could be attributed to the variations of local swarms of faults and volcanic centres. Examples are the floor of the Gregory graben, including the step-fault platforms and ramps, which are cut by dense swarms of young, sub parallel minor faults (e.g. Baker and Wohlenberg, 1971), and the WFB local swarms of fault in the floor of MER (e.g. Searle and Gouin, 1972). The isostatic residual maps display major offsets in the orientation of the Afro-Arabian rifts by E-W and NW-SE trending cross structures or gravity lineaments (Fig. 5.1). In contrast, the western rift north of Kampala along Lake Albert shows a strong negative anomaly due to the thick sedimentary deposits above the Precambrian structure and the absence of volcanics (e.g. Upcott et al., 1996). In addition, magmatism is minor in the Western rift compared to Eastern rift (Kampunzu and Mohr, 1991).

The linkage of the rift systems is demonstrated by a constant T_e of ~20km (Ebinger and Hayward, 1996), the cross- cutting transfer or accommodation zones (e.g. Hayward and

Ebinger, 1996) or transverse fault zones (e.g. Chernet, 1998), and isostatic residual anomalies (Fig. 5.1).

Strong positive gravity anomalies over the Red Sea, Afar depression and upper section of the MER and Kenyan rifts are evident (Fig. 5.1). The magnitude of the residual gravity anomaly probably shows the tectonic activity of the region. Therefore, the central section of the main Ethiopian rift is relatively isostaticaly stable in comparison to the northern part. The near-zero values and/or moderate isostatic anomalies over the rift shoulders in the southern sections of South Afar, the Danakil Alps (southern Red Sea uplift), the central highland trap series of Ethiopia, and the southern sections of the Precambrian basement near Ethiopia/Kenya border reveal that these areas are nearly in isostatic equilibrium.

5.3.3 Comparison of different isostatic models

By and large, comparison of the different isostatic models shows similar features with maximum amplitude changes of about $45x10^{-5}$ m/s^2 for the negative residual anomalies and minimum variations of not more than $2x10^{-5}$ m/s^2 for the positive residual anomaly trends (Figs. 5.1, 5.2b, 5.3b). In addition, the isostatic residual maps display the following major differences: a) the isostatic residual map that incorporates only flexural models shows a slight positive bias indicating under-compensation and probably showing that there are upper-crustal features not compensated regionally. b) the isostatic residual map using the slab (subduction) model and total topography shows a moderate negative bias. Dominantly, regions in the western rift system and basins in Eastern Sudan are represented by more negative values. c) the isostatic residual anomaly computed using the Grand dynamic topography model shows a mean negative value twice as large as that of the subduction model. The dynamic topography calculated using this model (see Lithgow-Bertelloni and Silver, 1998) shows that active upwellings are dominating the southwest section, particularly in areas covered by the extensional basins, the MER, and East and Western rift systems.

Figure 5.5 shows histogram plots of the isostatic Mohos calculated using the different models of topography. The isostatic Moho for observed topography is ~1 km deeper than the isostatic Moho calculated using dynamic topography corrections. In all cases, the isostatic Moho displays similar variations (1-2 km).

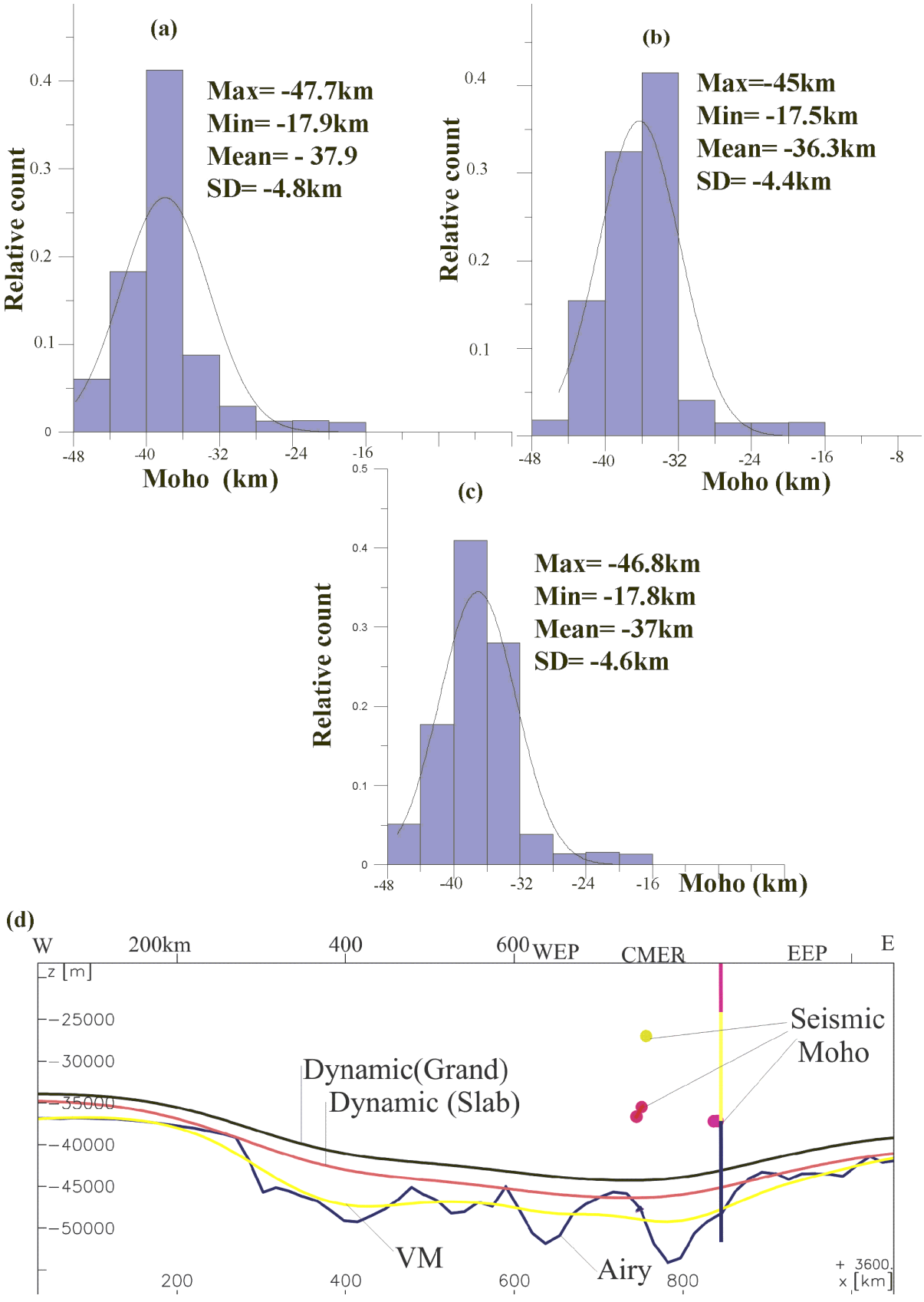

Figure 5.5 Histogram representation of calculated Moho depth using different models of isostasy. (a): using observed topography, (b): using Grand dynamic topography model, (c): using slab dynamic topography model. (d) shows variation of the Moho undulations across central main Ethiopian rift (CMER). Seismic Moho depths are projected into the plane of the section using a data tolerance of 6km.

The last panel in Fig. 5.5 is a section across the Central Main Ethiopian Rift (CMER) showing the variation in the different isostatic Mohos in relation to plateau uplift and the rift system. Seismically- determined Moho depths within 6km are included to show correlations. The isostatic Mohos corrected for dynamic compensation, in particular the one based on the Grand model, closely corroborates the seismic Moho, if the seismic Moho depths are translated to their real position.

It is difficult to determine which is the best compensation model. All models are limited by the approximations required for some parameters (e.g. density of mantle, viscosity, crustal thickness, flexural rigidity etc). However, isostatic residual maps are all similar and helpful for examining upper crustal structures and for performing geological correlations. The results of the qualitative interpretation form the basis of continuing three-dimensional gravity modelling and quantitative analysis that also integrate some of the latest EAGLE results (Chapter 6).

6 Integrated three-dimensional density modelling

A model is an approximation of reality and can be used as a method/tool to further understanding of complex problems. Models that simplify a wide range of parameters can be developed within a relatively short time and with minimum effort. However, using simple models is complicated by the complex nature of geological processes and these processes are also difficult to simulate using mathematical expressions. Thus, the simple models in some cases fail to explain the real world. On the other hand, our knowledge is limited, meaning that it is difficult to understand every single parameter and to develop a robust complex model. Complex models are not easy to apply to real-world problems or to comprehensively understand or interpret. We need to arrive at a solution by optimizing the model so that it is complex and robust enough to express reality and, at the same time, easy to understand without being too cumbersome.

In potential field/density modelling, the constraints available to make realistic density models are limited. In the East African Rift System (EARS), three fundamental seismic constraints, spanning over 1500 km length of the rift and plateau region are available (Chapter 3), along with geological synthesis and petrological, geophysical and geochemical data. In such a broad region, the available information and hard data provide the opportunity to bring them together in a unified system so as to enable the preparation of a reasonable complex model. In short, we require an object-oriented three-dimensional geographic information system and modelling approach (3D-GIS) that allows interactive modification of the model to match all available constraints.

6.1 Forward modelling in gravity interpretation

Forward modelling is an approach to interactively manipulate an assumed well-constrained geometry of a geological structure by trial and error to match the observed potential field data. Forward modelling, both in 2D and 3D, has been in use at least for the last 50 years. Some of the initial works used a line integral approach to compute the gravitational attraction of a 2D object (e.g. Hubbert, 1948; Talwani, 1959; Bathacharya, 1964; Plouff, 1976) and in 3-dimensions (e.g. Talwani and Ewing, 1960; Vogel, 1964; Barnet, 1976; Götze, 1976, 1984; Okabe, 1979; Götze and Lahmeyer, 1988; Singh, 2002). Despite the extensive development of 2D and 3D gravity data interpretation schemes over the years, development of suitable interactive modelling packages that allow integration of data across disciplines was possible only recently.

In this work, the mathematics behind the forward interactive modelling package, IGMAS, are only briefly mentioned. In a later section (section 6.2), some general descriptions of IGMAS's GIS functions with respect to lithospheric-scale modelling are included. Details of the background mathematics can be found in the references mentioned.

IGMAS is a forward potential field-modelling program. The method uses numerical approximations of closed polyhedron with constant charge and density. It has been constantly developed and updated over the last 25 years (e.g. Götze, 1976, 1978, 1984; Götze and Lahmeyer, 1988; Schmidt and Götze, 1998, 1999). Mathematically, the volume integral (eq. 6.1) is transformed into a surface integral using Gauss and Green integral theorems, and then to a line integral suitable for computer programming (Götze, 1976; Götze and Lahmeyer, 1988). It solves the problem of body definition by triangulating the outer faces of the polyhedron.

The gravitational potential 'U' at a point 'P' is expressed in terms of the volume integral:

$$U(P)= G\rho\iiint_{poly} (1/R)dv \qquad 6.1$$

where R is the distance between the station and the mass (dm=ρdv). The vertical attraction of the closed (homogeneous) polyhedron at a station 'P' is given by:

$$\partial U/\partial Z (P)= g_z (P)= G\rho\iiint \partial/\partial z (1/R)dv \qquad 6.2$$

The above two equations and the derived analytical solutions form the major algorithm within IGMAS structure (for details see Götze, 1976; Götze and Lahmeyer, 1988). The program package IGMAS is used to construct a three-dimensional density model of the EARS.

The model is constructed using vertical planes/sections (as shown in Figure 6) for the modelling area of the EARS shown in Figure 4.3. In the IGMAS model of the EARS constructed here, the planes making up the model are oriented west-east across and covering the entire rift and adjacent plateau regions (see Fig. 4.3). The planes are more or less perpendicular to the major rift orientations in the EARS. Along these modelling planes, the geometry of the modelled objects is given to the program via a structured input system. Between each modelling plane, the vertices of the given geological structure are interconnected by triangulation in order to form layer boundaries of constant density. The program performs triangulation between adjacent modelling planes automatically (see Fig. 6). Other modifications with regard to shape of the body, adding or removing new vertices, shifting layer boundaries and change of density, are made interactively. Furthermore, the program accounts for Earth curvature, an important consideration when modelling very large-scale structures like the EARS.

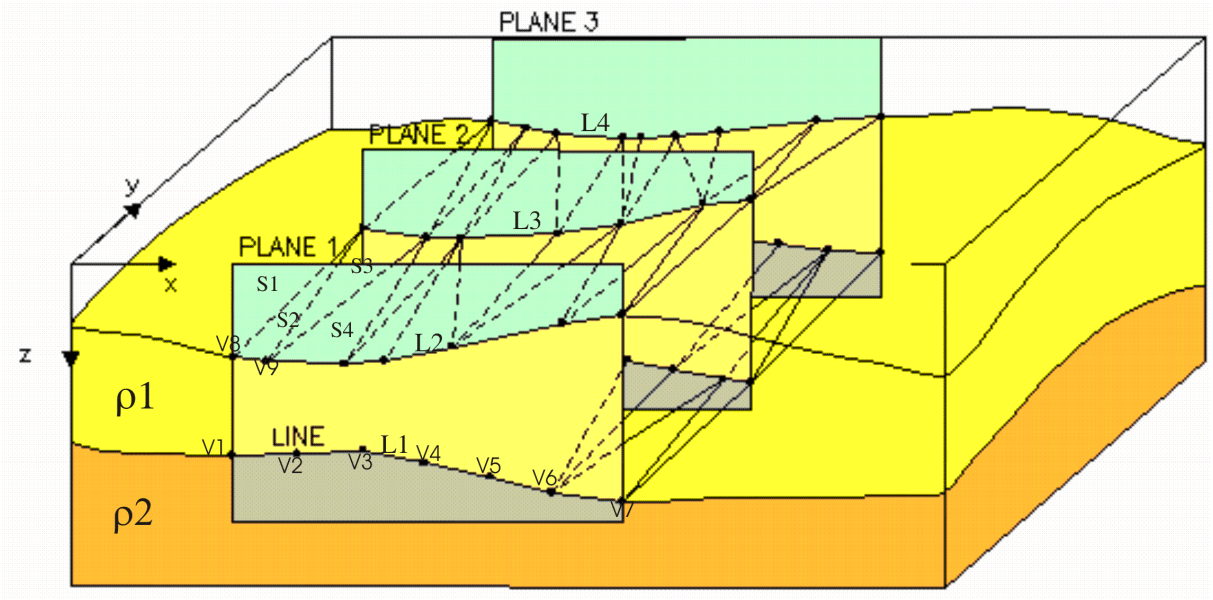

Figure 6 Construction of IGMAS 3D model using triangulated polyhedra surfaces where constant density is assigned. Plane 1, 2, 3 are vertical planes (30), across EARS. Vertices are (V1, V2, V3...), layer boundaries are (L1, L2…); triangles are (S1, S2, S3…). In each plane the vertices are interconnected to establish lines separated by densities ρ1 and ρ2 (after Götze and Lahmeyer, 1988).

IGMAS has previously been used for modelling in different geological environments. For example, ocean continent boundaries, continent-continent collision zones, sedimentary basins and continental rifts and transforms (Götze et al., 2004). This is the third of IGMAS application within Africa. The first application of IGMAS in Africa was to model the Anza rift (Dindi, 1994) and later the Main Ethiopian Rift (Mahatsente, 1998) using an older version of IGMAS called IGAS. However, the use in this work of the latest version of IGMAS, with its complete GIS functions, is the first in Africa to cover a large area of complicated geology that integrates a wide range of geo-constraints.

6.2 Three dimensional modelling using the functionality of GIS

This section explains how constraining data for the EARS (e.g. earthquakes, Moho geometry, isostatic models, geological and petrological information) are integrated in the IGMAS potential field-modelling program. Integration of these data allows the development of robust models of the EARS and associated plateau. Here, the general 3D-GIS method is briefly described in relation to the three-dimensional GIS modelling processes. The whole modelling procedure can be summarized into the four steps described below. These steps are similar to those involved with existing GIS applications.

The first step (see also the previous chapters) is to assess existing and new primary and constraining data sets and to re-evaluate, describe and build a spatial database system consisting of point data, vector and raster formats and, wherever possible, in three dimensions.

The second step involves processing, analysis, and interpretation, and also generates new information (e.g. isostasy models, qualitative interpretations, wavelength filtering). In many cases, Steps 1 and step 2 overlap.

Step 3 consists of reformatting data to suite the requirements of the 3D GIS modelling program (IGMAS) and integrating all data into a unified database.

Step 4 involves an interactive modelling process with all the primary and constraining information included directly within the modelling software.

It should be emphasized that the integration of the data and visualization alone does not solve the problem. The final task is up to the modeller, who must look for viable solutions. This step requires decisions from the modeller, guided by some intermediary steps, calculations and options, to define geometry and parameters. In the kind of 3D GIS applied used here, the system supports the solution of particular geophysical problems (e.g. inversion) and offers very particular intermediate or final solutions (e.g. the maximum allowable range of density variations for all bodies in the model).

The other common options we have in other GIS routines such as spatial query, visualization (2D and 3D), combination, analysis, prediction, outputs (ascii, raster, meta files etc.) and export and import capabilities of processed and semi processed data sets are supported. The flow chart in Figure 6.1 depicts the whole process. The four steps discussed above are summarized into three major categories shown in the flow chart.

1. Potential field and constraining database (step 1 and step 2).
2. Modelling processes (step 2 and step 3 and part of step 4).
3. Interpretation (mainly step 4).

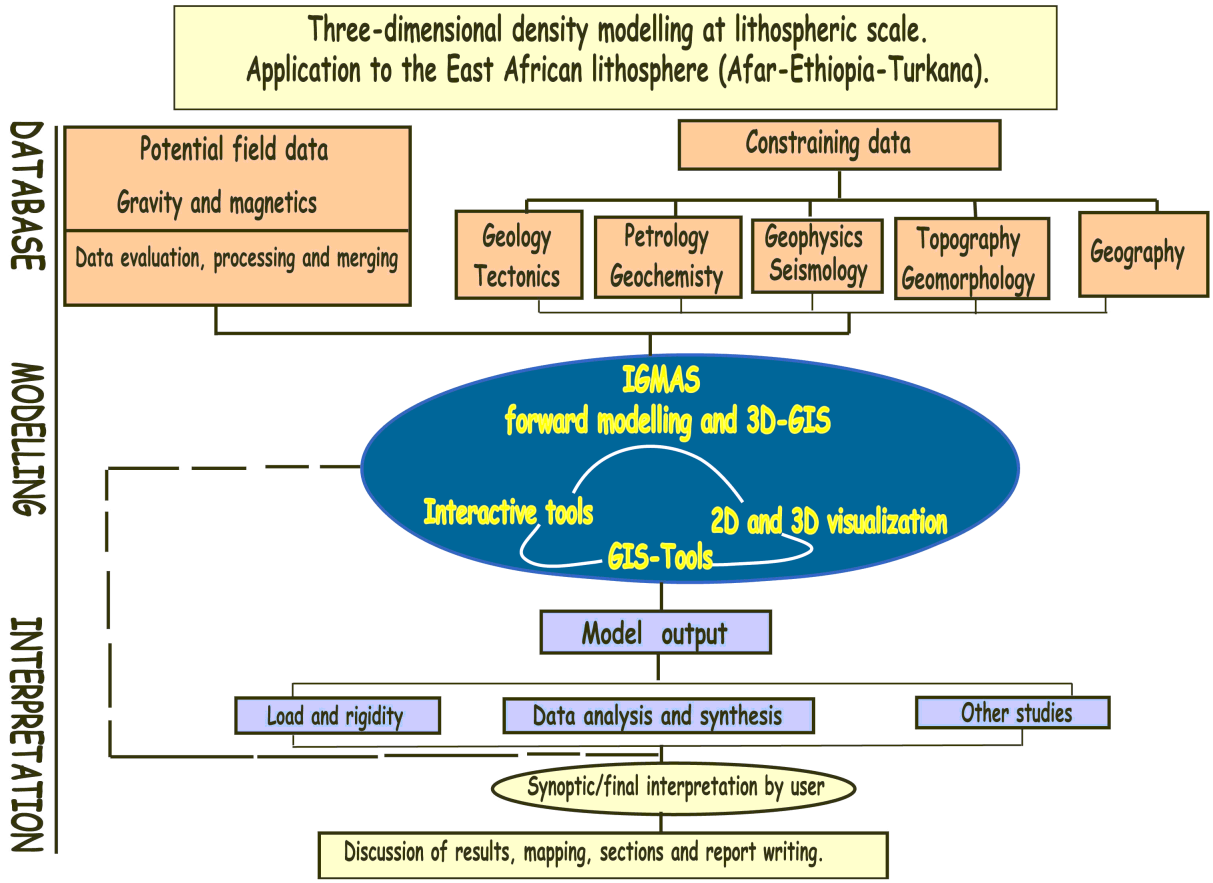

Figure 6.1 Flow chart showing the general process of three-dimensional modelling.

6.3 The initial model and general assumptions

The three-dimensional modelling area does not include the entire area as shown in Figure 1.1 or the area analysed using isostasy and Bouguer gravity anomaly. It is generally preferred to construct the modelling space within a region where there is a reasonable gravity data distribution. Therefore, the model covers the whole rifted block of the EARS and adjacent plateau, as indicated in Figure 4.3. The local data gaps within the modelling area are accepted so that geologically interesting zones for regional synthesis are not avoided.

The discussions on regional geological and tectonic setting, density measurements and calculations, previous models, concepts in crustal and upper mantle processes (Chapter 3) form the basis for the initial and final model construction. The basic modelling geometry uses the concept which Hay et al. (1995) applied for modelling an equatorial profile (the southern end of this modelling area) and extends the later model developed by Simyu and Keller (1997) that incorporates asthenospheric upwelling beneath the East African lithosphere. The new model presented here may have some similarities with the intrusive model developed for the MER by

Mahatsente (1998) on a crustal scale, but it differs in the underlying mechanisms of upper and lower crustal modification and upper mantle structures.

The most important concept to consider is the modification of the lower crust by magmatic processes (e.g. Hay et al., 1995). This concept, based on KRISP (1991) results (i.e. thinning along Turkana), axial thinning in the Main Ethiopian Rift (Keller, et al., 2004) and complete thinning of the Afar lower crust, is incorporated in the model presented here. The 10 km thick basal lower crust in southern Kenya becomes thinner to the north (a major results from KRISP 91). Therefore, with more lithospheric process, the lower crust further north is extremely modified or replaced by upper mantle material. In other words, the upward arching of the lithosphere (asthenospheric upwelling) pushed the Moho interface shallower and, as a result, upper mantle low-velocity layers are observed northwards along the axis of the rift.

Hay et al. (1995) used a density of 3.00 Mg/m^3 for the basal lower crust and 3.15 Mg/m^3 for the underlying low-density lithospheric mantle. North of this basal lower crust, the Turkana low velocity anomaly is modelled. The thinning or absence of the lower basal crust could also be directly correlated to the systematic younging of the Ethiopian volcanism from north to south. This in turn could be related to the direction of movement of mantle material. Therefore, more lithospheric material and more intensive magmatism and lithospheric modification exist in the north than in the south, as noted in the previous discussions.

Earlier models (e.g. Baker and Wohlenberg, 1971) emphasize crustal modification under the rift or assume an intrusive body. Mahatsente et al. (1999) expand the intrusive model by including two intrusive bodies with different densities. In a recent development, Keranen et al. (2004) use an intrusive model beneath the magmatic segments to explain the high mid-crustal velocity (~ 6.0 km/s).

Similar to the earlier models this work emphasises lower crustal modification, but with more replacement of mantle material axial to the rift and more intensive replacement in Turkana (north to south) and in Ethiopia northwards from the NMER to Afar. In contrast, in the southern Ethiopian rift and CMER, lower crustal modification is assumed to be less intensive. The crustal density under the rift and outside the rift differs. This has also been suggested using the density calculations for pre-rift and post-rift lavas that highlight density patterns (i.e. pre-rift lavas dominate the plateau and post-rift lavas are within the rift). Other evidence supporting the model geometry is derived from the broadband seismic experiments and tomographic images that consistently map a low velocity layer beneath the EARS (see Chapter 3). Recent laboratory experiments that include a melt zone at the base of the lithosphere (e.g. Mulugeta, 2004) support the kind of model geometry used here.

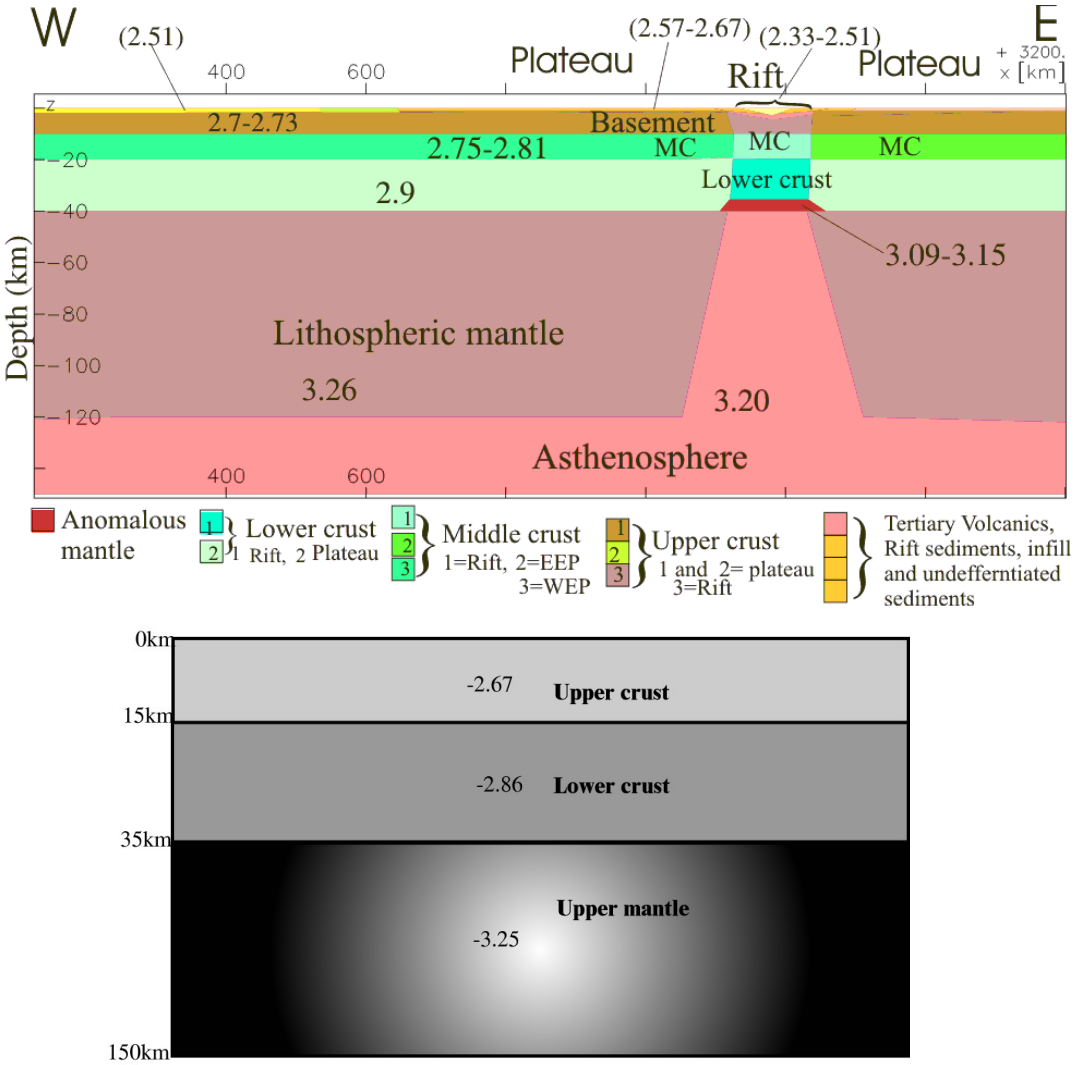

Figure 6.2. Upper panel: general structure of three-dimensional model geometry, which is divided into basement, middle crust (MC), lower crust, anomalous mantle, lithospheric mantle and asthenosphere. Overlying the basement are Tertiary volcanics atop the plateau, rift volcanics and sediments in the rift. Lower panel is the background model.

The 3-D density model is constructed using the following bodies (Fig. 6.2) i) upper crust, ii) middle crust, iii) lower crust, iv) anomalous upper mantle (modified lower crust), v) asthenosphere, vi) lithospheric mantle vii) Tertiary volcanics/sediments, viii) Quaternary-Tertiary sediment, ix) sediments/rift infill/rift volcanics. Crustal densities are different under and outside the rift, as explained in section 3.3.2. The final densities used are indicated in the various discussions under modelling results and the model sensitivity and variation of allowable densities for the various units are discussed in section 6.4.5. In addition to the initial model, a reference model is needed in the background, as explained below (see also the lower panel in Figure 6.2).

The reference model

The gravity field at any point is an integral field is caused by the superposition of all masses

(attraction from nearby masses and the mass of the Earth). In modelling small-scale features, it is not possible to incorporate the long-wavelength gravity field of the Earth that arises from its mass. These long-wavelength features are supported by the strength of the lithosphere (Cochran and Talwani, 1978; Vogt, 1978) and produce a constant shift in the local three-dimensional gravity predicted by the model. Nearby effects can be accounted for by expanding the modelling space to 20-40 % of its size in all directions (personal experience). Then, in the IGMAS modelling program, one has to apply a constant shift to the output model to adjust the difference between the measured and modelled gravity field. Kirchner (1997) introduced an alternative. He constructed an equivalent density layer called a reference density model. This reference model is integrated into the three-dimensional model in the background. In effect, the reference model takes care of the offset between the measured and modelled gravity field. The densities of the reference model are negative, as shown in the lower panel of Figure 6.2. There are several ways to construct the reference model, but the end result is to remove the constant offset between the measured and modelled values. In the present case, the reference model is divided into a simple three-layered Earth (upper crust, lower crust and upper mantle, Fig. 6.2). The depth to the lower crust is allocated using the mean crustal thickness from the isostatic model (see chapter 5) and densities close to the mean crustal density in Christensen and Mooney (1995). For reasons explained under constraints (Chapter 3, section 3.1) the maximum depth of the model is set to 150 km.

6.4 Interpretation of modelling results

According to the methodology explained above and data integration, constraint development and model set up, 30 parallel planes, more closely spaced in the MER and equally spaced in the rest of the area, are used to define the three-dimensional model. Figure 6.3 shows the location of all modelled planes along with the observed and modelled Bouguer gravity anomaly. In the following sections, the results of the model are described and discussed.

The statistics of the fit shows a standard deviation of 16×10^{-5} m/s^2 with a correlation coefficient of 96%. The small accompanying map in Fig. 6.3 shows the difference between the observed and modelled field. Some finer details, especially in Eastern Sudan, the southeast-northwest- trending Anza rift and associated upper-crustal structures, are not well modelled. Also, many details atop the plateau are excluded from the model to avoid additional complexity. The gravity difference is not only due to unconsidered structures, it is also due to the errors in the gravity database described in chapter 4.

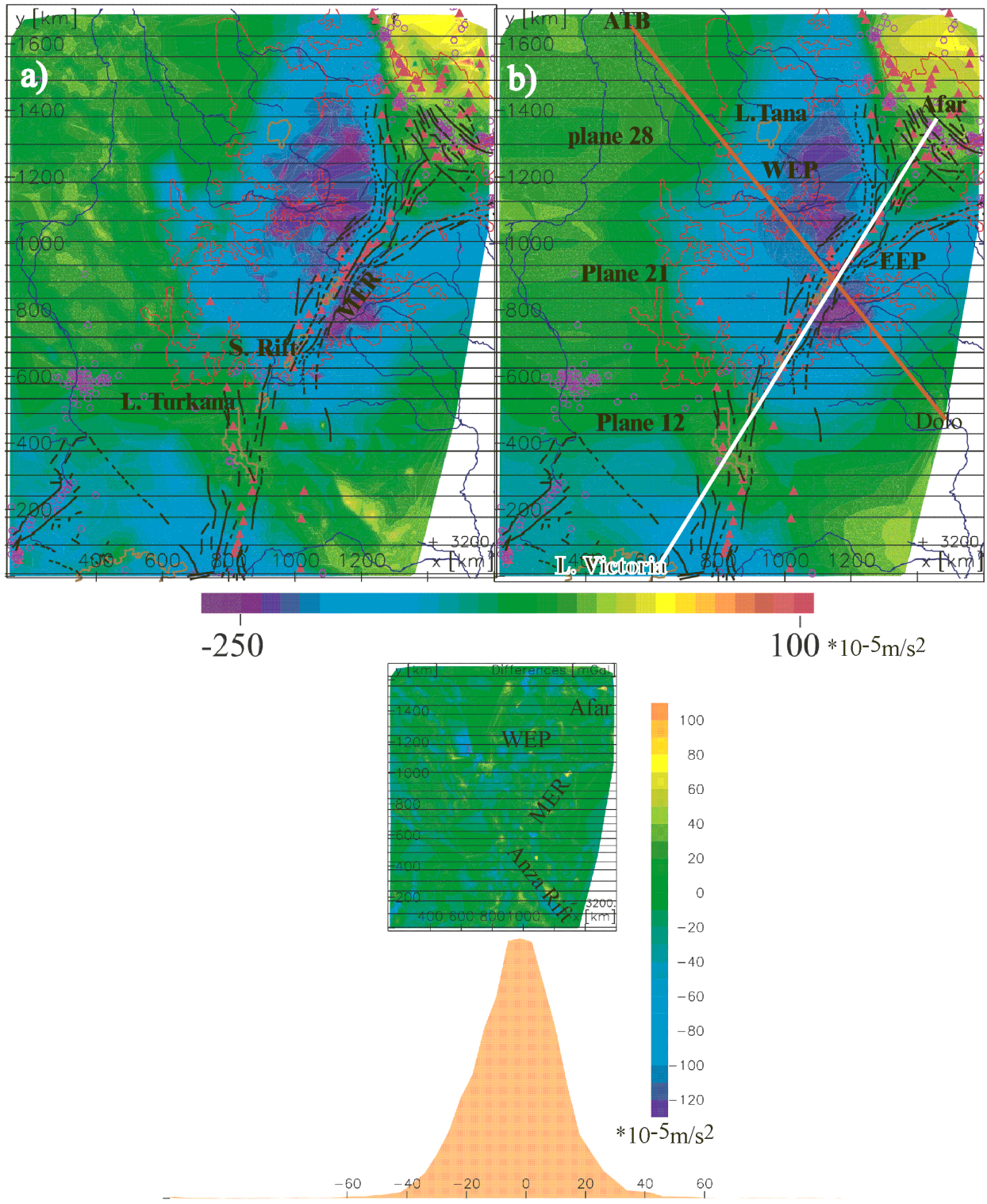

Figure 6.3 Measured (a) and modelled (b) Bouguer anomaly. Thirty west-east parallel planes (black lines) are used to construct the three-dimensional model. The panel below shows the difference between the measured and calculated anomaly. A histogram plot of the difference displays a normal distribution. Most differences are close to zero and have a standard deviation of about 16.20×10^{-5} m/s^2 and a correlation coefficient 0.96. The rift-perpendicular Atbara (ATB)-Dolo profile (red line in b) and the rift-parallel Afar-Lake Victoria profile (white line b) are presented in Figure 6.5.

6.4.1 Crustal models and rift structures

The north-south variation of crustal and upper mantle structures associated with the EARS can be regionally observed from the three sections 28, 21 and 12. These sections extend from 12°N to 4°N (Fig. 6.4).

The first section in Figure 6.4 runs along 12°N from Eastern Sudan to Serdo in Central Afar (see also Fig. 6.3). It intersects the lower section of Lake Tana in the Western Ethiopian Plateau (WEP). Along this plane, the crust is very thick (40-48 km) under the WEP and this is consistent with the seismic results. The crustal thickness generally decreases southwards until the southern margin of the WEP. The thick Tertiary volcanics on the WEP and some discussions on volumes and thickness of sediments in the WEP are presented in section 6.4.3. The second section, along 8°N, extends from southeastern Sudan to the Eastern Ethiopian Plateau (EEP), intersecting the southern margin of the WEP and Central Main Ethiopian Rift (CMER). The third section along 4°N is from the northern end of the western Rift system through northern Turkana, and ending in Moyale (Mozambique Belt).

The allocation of densities to the anomalous crust or upper mantle in Afar, MER and Turkana is based on the extent of lower crustal modification under the rift. The modification of the lower crust is more extensive in Central Afar and Turkana, with an eastward-dipping, sharp gradient in Afar and MER, but is symmetrical and uniform in Turkana. The apparent geometry is partly due to the direction of the cross-section, i.e. perpendicular to the rift in the case of Turkana and oblique to the NE-SW trending MER. In the EEP, the extent of volcanism is less than in the WEP. Therefore, there are less Tertiary volcanics and sediment and uniform upper crust (see Figure 6.4, middle panel).

In the rift, there is thin upper crust under Afar and Turkana (6-10 km), whereas relatively thick upper crust exists under the CMER. This shows that the crustal modification and extension are less prominent or a minimum in CMER. Presently, the ascent of the asthenosphere/plume is only directly influencing the upper mantle and crust under Turkana and Afar by shallowing the Moho topography. It is not possible to directly alter a wider section of the CMER crust. Only a small section of the lower crust and adjacent plateau could have been directly modified by this anomalous mantle plume. The model shows wide rifted zones in Afar and Turkana (up to 300 km) and narrow ones in the MER (less than 200 km). This is because the Cenozoic extension and volcanism could have affected a large area only in Afar and Turkana. This may imply that there are different channelling mechanisms for plumes or plume heads in Afar and Turkana, and that the plume head might be deeply seated under the MER and subsequently cannot directly alter rift structures there.

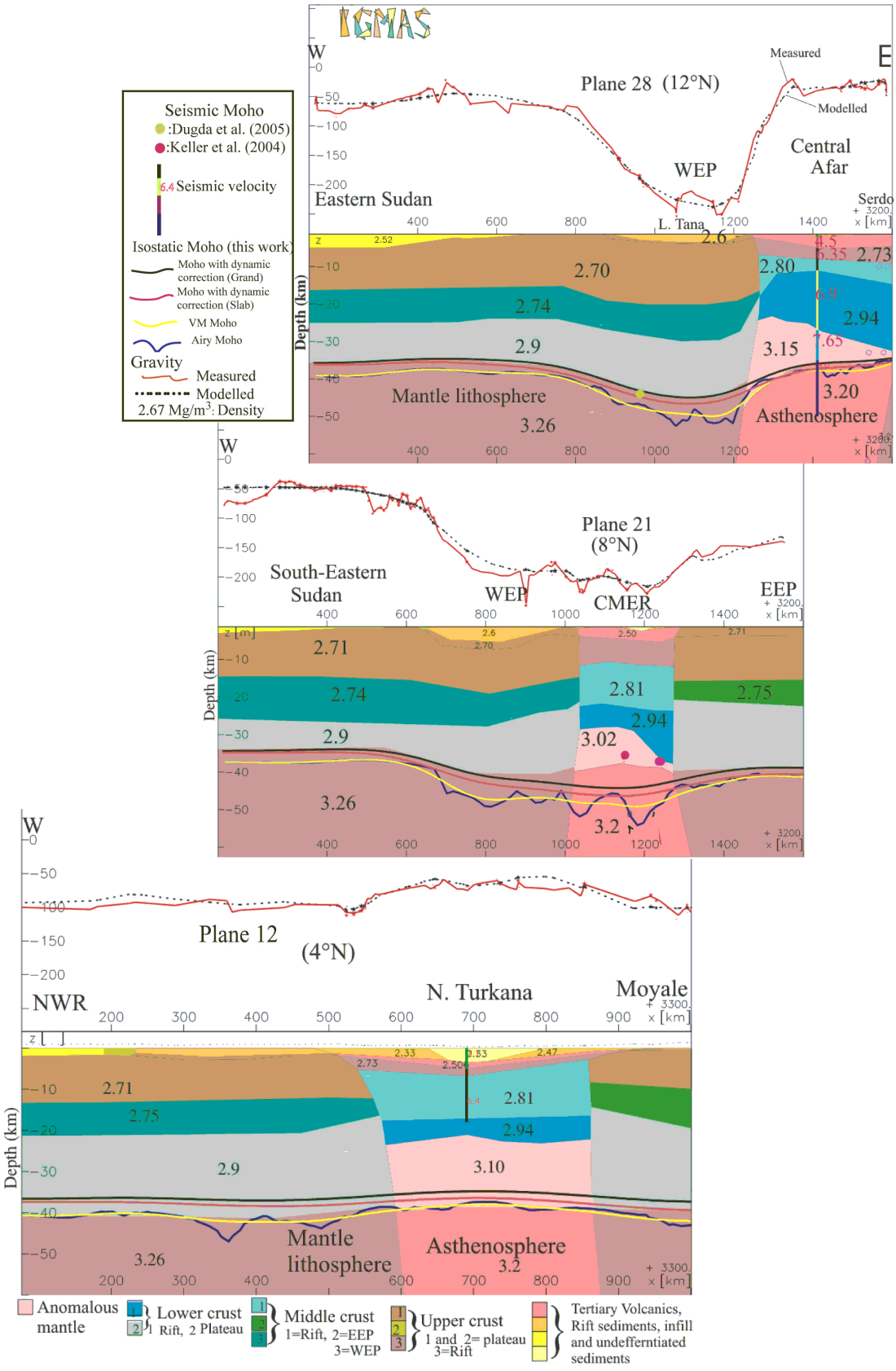

Figure 6.4. N-S variation of the crustal and upper mantle structure. The approximate location of the W-E modelling planes are indicated. CMER: Central Main Ethiopian Rift, EEP: Eastern Ethiopian Plateau, NWR: Northern end of the western Rift system, WEP: Western Ethiopian Plateau. The corresponding constraining data within 6 km of each profile are projected into the plane of the section. The crust adjacent to the rift is thicker in the northern (plane 28) and the thickness decreases southward (see text).

6.4.2 Vertical and horizontal cross sections (Earth models)

vertical cross sections

Two important cross-sections to consider (for locations see thick white and red lines in Fig. 6.3) are axial to the rift (Turkana-MER-Southern Afar) and rift-perpendicular (Nubia plate-MER-Somalia plate) and are shown in Figure 6.5. The cross-sections are not parallel to the general modelling plane (W-E). Examining cross-sections in any arbitrary direction confirms the quality, robustness and true three-dimensional nature of the modelling. The two cross-sections show the entire EARS crustal and upper mantle structures from two directions. The axial view is to investigate the role of the asthenosphere (plume) in modifying lithospheric structure and Moho topography. The rift-perpendicular section is to show the unmodified or slightly modified lithospheric structure underneath the two plates (Nubia and Somalia). The two plates are moving away from each other, forming a loose contact at the rift and with a sharp gradient in the lithosphere-asthenosphere boundary towards the Somalia plate. *Southern Afar-*

MER-Turkana (a)-axial to the rift

This profile (see white thick line on Figure 6.3 for location) shows the variations of crustal and lithospheric thinning along the rift. The model is based on the low velocity layer identified by the KRISP experiment in Turkana, the Afar and EAGLE experiment in Ethiopia and extrapolation through the broadly-rifted zone of southern Ethiopia. A broad region of the entire EARS, except at the marginal contact of the WEP and the southern rift is underlain by upwelling asthenosphere/plume. This has predominantly changed the Moho topography by modifying the lower crust in Afar and Turkana and in a narrow region under the MER. The model is consistent with most of the seismic Moho depths determined by different investigators (1975-2005). At the southwest end of the profile, the northern edge of the cold and rigid Tanzanian craton with intact lithosphere is evident. This craton has largely resisted modification by the Cenozoic extension and volcanism and is believed to be a bifurcation point for the eastern and western rift systems (e.g. Nyblade and Brazier, 2002). The large area dominated by asthenosphere under Afar and intensive modification of the lower crust indicate that the Afar plume might be very hot and strong, but is not able to affect areas beyond the southern rift. On the other hand, the Turkana asthenosphere is restricted to the Turkana rift. Therefore, the plume under the Turkana might be relatively less hot or more deeply seated. Further discussions are made under plumes and melts in Chapter 7.

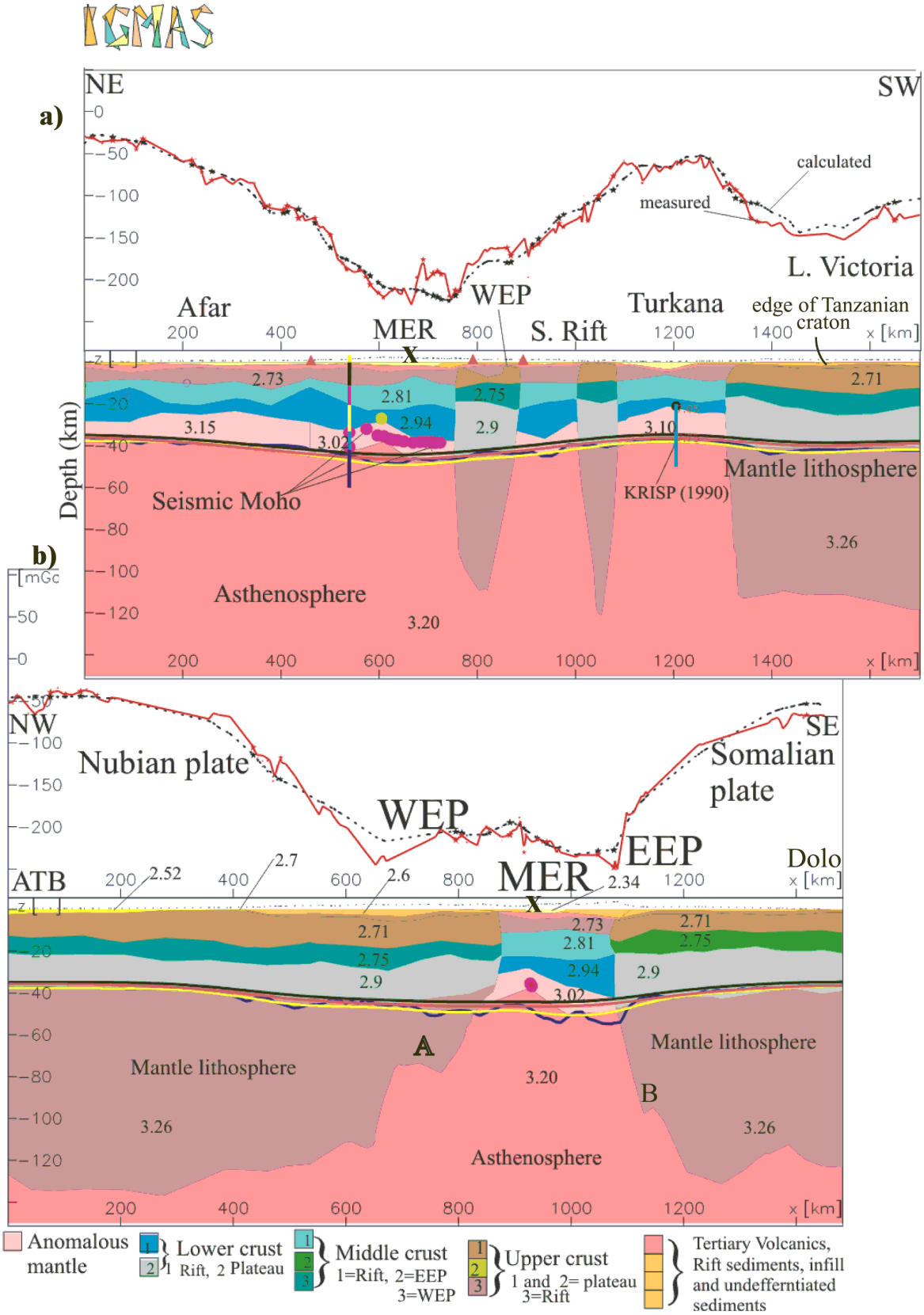

Figure 6.5 Axial (NE-SW) and perpendicular (NW-SE) profiles of the Main Ethiopian Rift (MER) that intersect each other at position X. Each profile is about 1500 km long. Profile (a) runs from Central Afar via the MER, touching the southern end of Western Ethiopian Plateau (WEP) and southern rift systems, Turkana and ends up at about Lake Victoria. Profile (b) runs from Atabara in eastern Sudan (Nubia plate), crosses the WEP, MER and Eastern Ethiopian Plateau (EEP). Constraining data within 6 km of each plane is projected onto each section (see for Fig. 6.4 for the legend).

Nubia-MER-Somalia (b)-rift perpendicular

This profile runs NW to SE from the Atbara (ATB) confluence in Sudan to Dolo (Dawa, Genale and Weyeb rivers confluence) in Ethiopia and intersects the Sudan craton, Western Ethiopian Plateau (WEP), Main Ethiopian Rift (MER) and Eastern Ethiopian Plateau (EEP).

The mantle lithosphere is intact at the northwest and southeast ends of the profile. It shows plateau uplift right under the WEP due to the ascending asthenosphere at a relatively shallow depth (80 km, A, in Fig. 6.5). Beneath the Somalia plate, the lithosphere-asthenosphere (LAB) boundary is steep, with only a small bump at about 90 km depth (B in Fig. 6.5) owing to the flexural uplift of the EEP. However, the LAB rises at the east end, most likely due to the sediment loading in Ogaden basin of Ethiopia (eastern Ethiopia) and consequent asthenospheric flow, as postulated by Woldegabriel (1987). A similar mechanism could work for the Nubia plate, i.e. sediment loading in Eastern Sudan by erosion from the WEP and asthenospheric flow beneath the Ethiopian plate. Both processes should not be seen as separate developments for postulating the cause of plateau uplift, rift development, erosion, loading and asthenospheric flow. Therefore, simultaneous sediment loading in the western (eastern Sudan) and eastern (Ogaden) basins can be proposed. The loads from the Tertiary constructs atop the WEP and EEP affected the rapid ascent of the asthenospheric upwelling and consequently also the Moho topography and rift development.

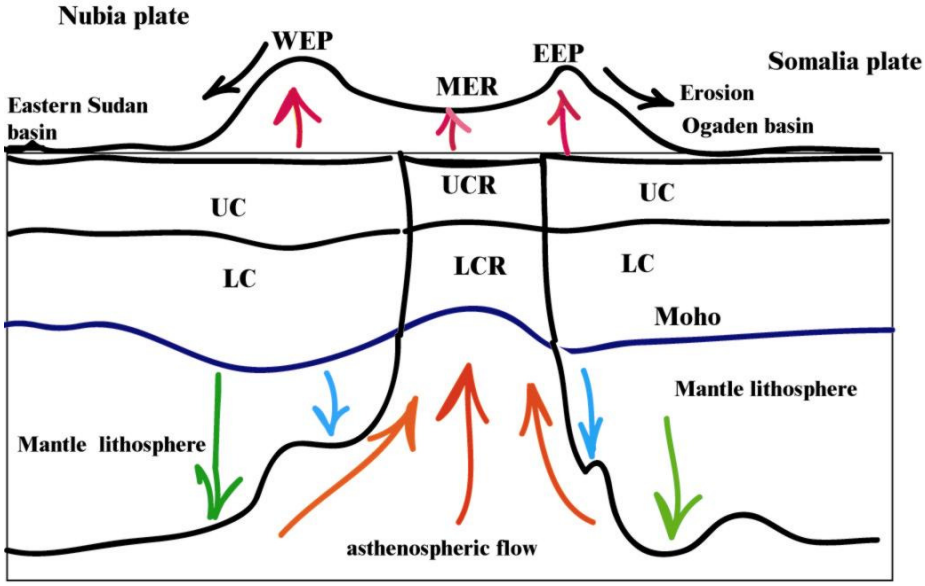

Figure 6.6. Simplified schematic presentation of the model of the EARS (not to scale). Red arrows indicate uplift of the Ethiopian plateau and rift and asthenospheric flow or mantle upwelling. Erosion of the plateau is indicated by black arrows that form sediment load in the Eastern Sudan and Ogaden basins. Green arrows indicate downward movement of the lithosphere due to sediment loading and blue arrows downward movement largely due to loads from Tertiary constructs atop the plateaus (WEP and EEP). LC: Lower crust, LCR: Lower crust under rift, UC: Upper crust, UCR: Upper crust under rift.

A cartoon that summarises this model is shown in Figure 6.6. The loads in the Eastern Sudan and atop the plateaus are estimated in the following sections. The model does not include the Ogaden basin (Eastern Ethiopia), so the sediment loading from this area cannot be quantified.

Horizontal cross sections

Figure 6.7 shows the lateral and vertical distribution of the crustal density variations at relative shallow depths (20-35 km) and the role of the upwelling mantle in the modification of the lower crust. At shallow depths less than 25 km, the whole crust away from the rift is dominated by middle crust compositions (lower crystalline basement). However, in northern Afar, anomalous crust/upper mantle material is exposed because of the thinning observed in seismic results (Berckhemer et al., 1975) (see also Fig. 6.5a). At 25 km, the northern Afar, central Afar, northern terminus of MER and Turkana are dominated by the anomalous crust, which has largely modified the lower crust beneath these areas and also the rift as a whole (Fig. 6.5a). A large part of the MER and northern Kenya rift partially resisted the lower crustal modification. The model in Figures 6.7a, b shows thick middle-crustal material in the Western Ethiopian Plateau (WEP), whereas in EEP it is very localized or non-existent. At a depth of 30 km (Fig. 6.7c), the entire region shows lower crustal composition, except in the Afar, Turkana, and axial (central zone) of NMER where asthenospheric material dominates. At 35 km, the whole of the rift, except the central parts of MER and southern end (northern part of Kenya Rift), is dominated by anomalous crust/asthenospheric material.

The depth slice map at 39 km shows four types of crustal and upper mantle compositions (Fig. 6.8). In this Figure, surface faults, volcanoes, earthquakes and drainages are shown for reference. Other information, e.g. Moho depths from seismic and isostatic analysis are projected with a data tolerance of 4 km, mainly to show correlations. This particular depth (39 km) represents the average crust mantle interface (CMI) for this region.

The zone of the large igneous province in Ethiopia marked by thin red in contour in Figure 6.8 correlates well with the boundary of the lower crust, particularly in the western plateau. However, on the Eastern Ethiopia Plateau (EEP) it does not show a good correlation, except for regions closer to the rift shoulders or rift margins. This is mainly because of the intensive erosion on the eastern plateau that causes the surface exposure of the LIP to be closer to the rift margins, whereas at depth it covers a substantial region to the east. Therefore, what is observed in topography and geological maps is basically a reflection of the deep lithospheric structure.

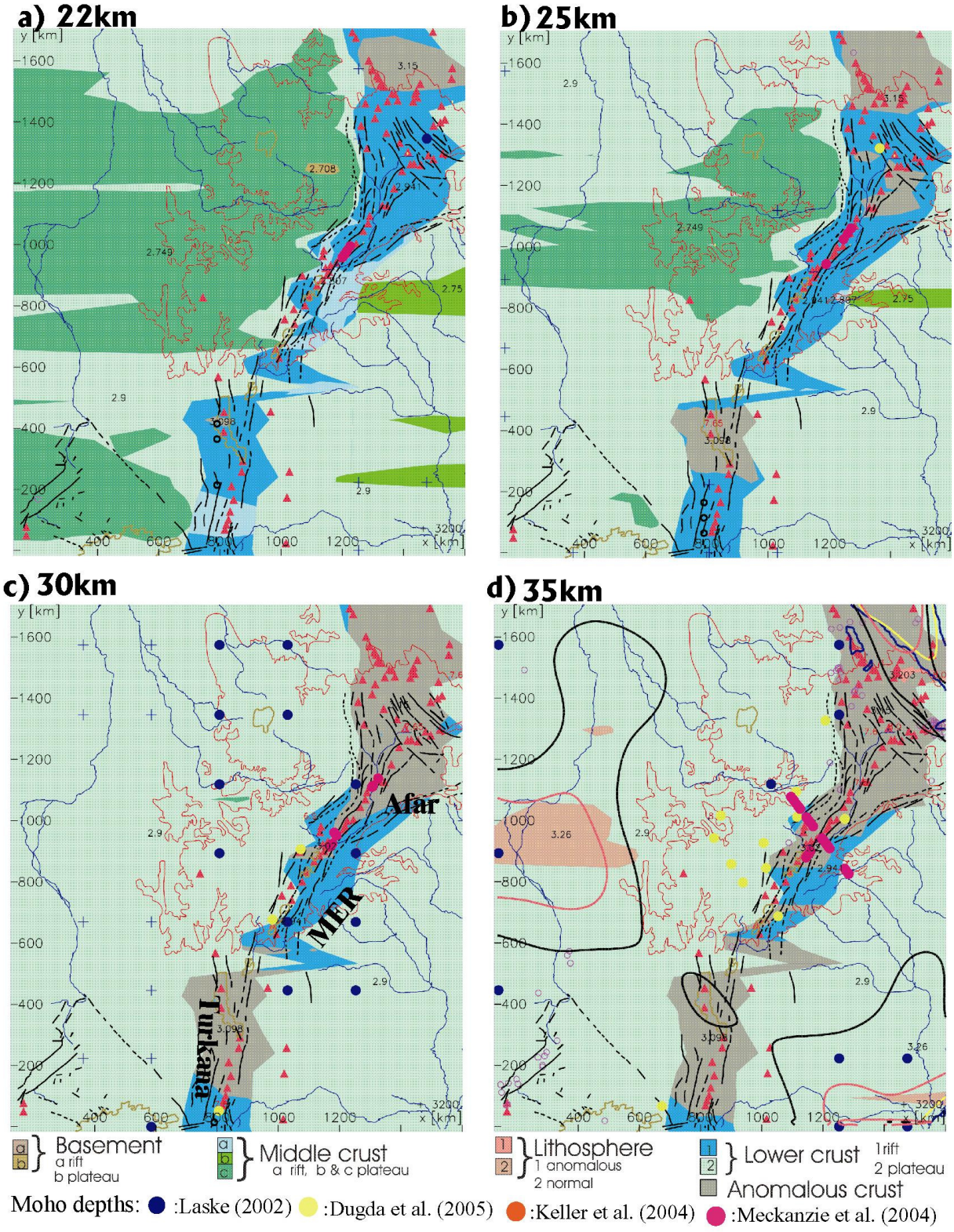

Figure 6.7 Depth slices from the 3-D model a) 22 km, b) 25 km, c) 30 km and d) 35km showing lateral and vertical crustal variations. Anomalous crust is exposed at shallow depth in Afar in a broad area and in central Turkana related to the thinning observed by the seismic experiments. The anomalous zones of crust or upper mantle at a depth of only 30 km completely covers the Afar and Turkana areas and a substantial region of the northern MER. This indicates that the MER is intact and still dominated by thick crust. Both plateau areas of the Nubia plate (west) and the Somalian plate (east) have a thick crust, even beyond 35 km depth (see detail view at a depth of 39km which more or less marks the crust mantle interface, Fig. 6.8). Dots show seismic Moho when it is within 2 km of the appropriate depth. Other surface information (volcanoes, faults and drainage) is for reference only. The contours show isostatic Moho depths when they are within 2 km of the depth in question.

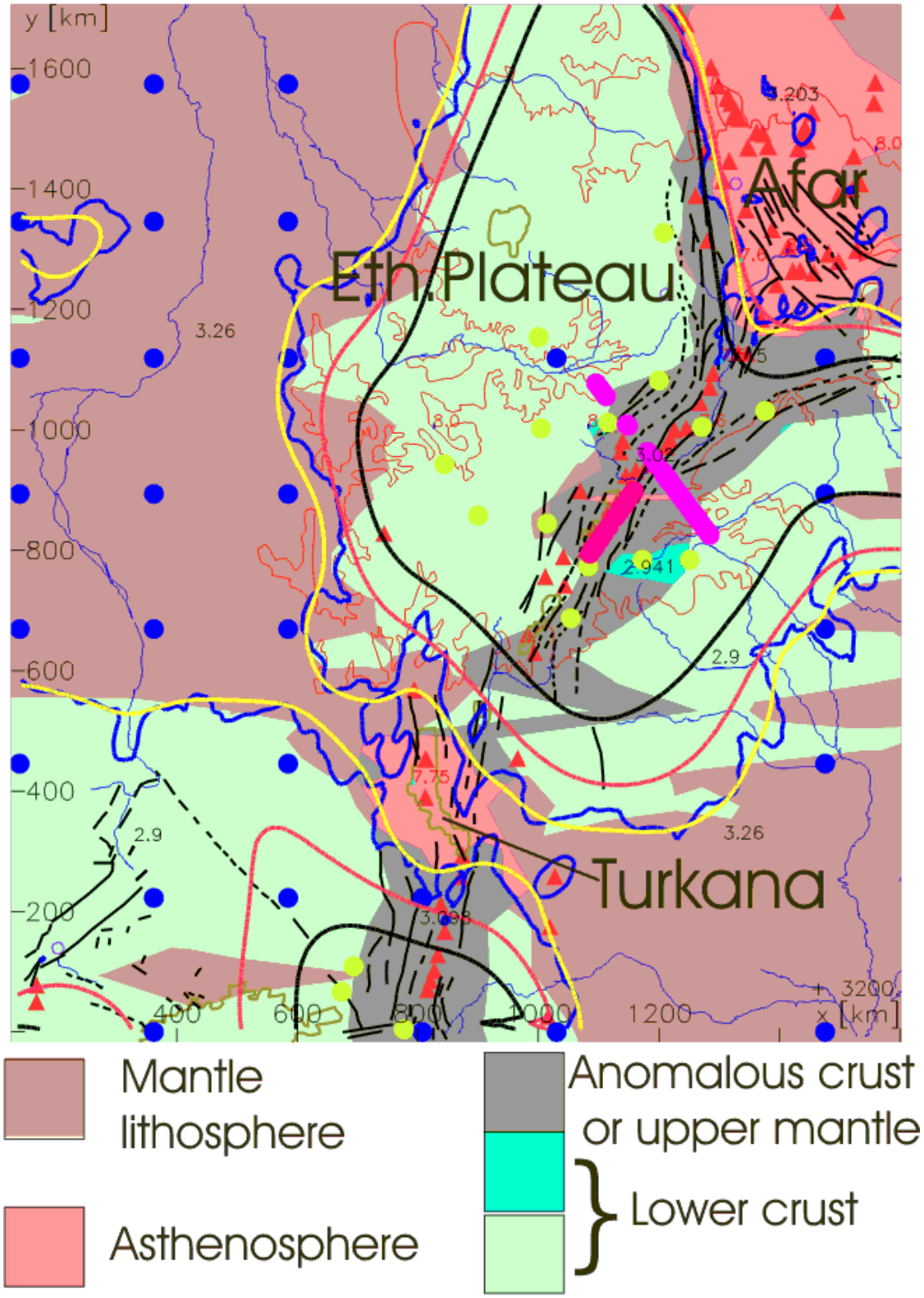

Figure 6.8 Horizontal slice at a depth of 39 km (ca. crust-mantle interface). The seismic Moho depths (dots are Moho depths, see Fig. 6.7 for the legend). Seismic Moho depths are shown by dots when they are within 4 km of the section plane (see Fig. 6.7 for the legend). Thick contour lines represent isostatic Moho intersecting with the section plane (black and red with dynamic topography correction; yellow: VM isostatic Moho; blue: Airy Moho). Other features are shown for reference. Faults: medium black lines; major rivers: thin blue lines; lakes: light green and zone of large igneous provinces in Ethiopian plateau: thin red contours. Densities of the lithologies are indicated in the map (Mg/m^3).

The similarity of the filtered topography map (Fig. 2) and the 39 km depth section (Fig. 6.8) suggest that both the Ethiopian and Kenyan plateaus are supported by dynamic compensation rather than isostatically.

The mantle lithosphere (Fig. 6.8, dark-brown colour) is intact away from the plateau areas. This is related to the Nubian craton to the west and Somalia craton to the east. An anomalous crust/upper mantle (grey) and asthenospheric material (red) dominate the rift and rift shoulders. The asthenospheric (red) is partly exposed in the MER axial zone (see Fig. 6.8) and fully exposed in the Afar and Turkana areas where, according to seismic observations, maximum thinning is observed.

6.4.3 Volume and mass of bodies and load maps

The volume and masses of modelled bodies are calculated using the IGMAS modelling program. Quantification of volumes and masses helps to define the extent of deposited sediments/volcanics or modelled layers. It also assists geological interpretations.

The volumes and masses of the different layers from the final density model are summarized in Table 8. The estimation does not include the topographic masses that may reach thicknesses of about 3-4 km on the plateau. The largest volume contribution comes from the lithospheric mantle. The asthenosphere under Afar is not completely represented because the eastern edge of the model does not extend as far as the edge of Afar. Thus, the volume estimate is smaller than for Turkana, which is completely modelled and shows the largest volume for this layer in the whole rift. In the MER, the volume and mass of the anomalous mantle is the least because the MER and its surrounding regions are not completely modified by the ascent of the asthenosphere. This also indicates the intact nature of the rift in this region.

Other estimates shown in Table 8 include the volume of rift sediments and the Tertiary-Quaternary sediment which dominates the area beyond the Western Ethiopian Plateau (WEP) and covers most of eastern Sudan (about 129 x 10^6 km^3). This area covers a large part of the Nile basin. Although the model is very regional and simplifies all sediments to a single sedimentary unit, the large volume is consistent with the accumulation of sediment since Tertiary time in an environment believed to have once been an oceanic basin. Furthermore, the large volume may be indicative of the intensive erosion of Quaternary sediments from the adjacent plateaus by the Nile and its many tributaries. Thus, the erosion and accumulation of sediment in such a large basin is an isostatic response to plateau uplift, rifting and continuous erosion (to the west) on the Ethiopian plateau.

Table 8
Volumes and masses of bodies relative to the surrounding (reference density model).

Bodies/layers	Volume ($x10^6$ km^3)	Mass ($x10^{18}$ kg)
Sediments/rift infil/rift volcanics	6.18	15.1
Quaternary-Tertiary sediment	129	326
Tertiary volcanics (plateau)	5.26	13.7
Upper crust/Precambrian basement (incl. rift)	906	2460
Precambrian basement under rift only)	5.38	14.70
Lower crystalline basement	1150	3180
Lower crystalline basement (outside rift)	1140	3130
Lower crystalline basement under rift	17.5	49
Lower crust	2340	6800
Lower crust under rift	19.7	58
Anomalous mantle under Afar	11.5	36.3
Anomalous mantle under MER	1.07	3.22
Anomalous mantle under Turkana	17.8	55.1
Anomalous mantle under the entire rift	30.4	94.6
Anomalous lithospheric mantle/asthenosphere	2340	7500
Lithospheric mantle (west/ Nubia plate)	5810	18900
Lithospheric mantle (east/ Somalia plate)	4800	16000
Lithospheric mantle (east+west)	10700	34900
Whole mantle (incl. anomalous mantle)	13000	42400

A conservative estimate of the combined volume of Tertiary volcanics and rift sediments in the entire region is 11.4 million km^3 (or $28.8x10^{18}$ kg mass). If we take the area covered by the Tertiary trap series (about 750000 km^2 and average height 2.5 km), a volume estimate of 1.3 million km^3 can be made for the topographic component of sediment and volcanics. Thus, the total volume that has been accumulated in the region may reach 12 million km^3. Kampunzu and Mohr (1991) estimate only about 400000 km^3 of volcanics in the Ethiopia-Yemen region (central in Afar), of which 90% is in Ethiopia. In Kenya, the total volume of the volcanic succession may reach 220000km^3 (Williams, 1982) and in western rift not more than 100000km^3 (Kampumzu and Mohr, 1991). Therefore, the total estimation is not more than a million km^3 less than the estimation here. The volume of Tertiary volcanics (flood basalts) on the western Ethiopian plateau is more than three times than the Eastern Ethiopian Plateau (EEP) (Table 8). This is mainly because volcanism is more profuse on the WEP than EEP (e.g. Mohr, 1983). Another possible reason could be the large volume of thick successions deposited from the southeast (Somalia plate) during marine transgression in middle Jurassic and ocean regression in the Upper-Jurassic (e.g. Mohr, 1983) and subsequent Cenozoic volcanism.

The thickness of the Tertiary volcanics and sediment in the WEP (Fig. 6.9) is particularly important as it is of interest for hydrocarbon exploration in the Tana basin. Hautot et al. (2004)

recently conducted 27 magnetotelluric soundings below Lake Tana from southwest to northwest across the plateau along a 220 km long profile (Fig. 6.9). The area is covered by Tertiary basalt that masks underlying formations (Mesozoic sediments). The major objective of the survey was to investigate the thickness of the volcanics. The area near and around Lake Tana is speculated to be the site of a failed junction of three rift systems (Chorowicz, et al., 1998). Sediments might have accumulated here and reached a thickness of 1-2 km during the episodes of transgression and regressions in the Jurassic. Hautot et al. (2004) suggest that sediments lie above Precambrian basement (resistive medium, see also the MT section in Fig. 6.10) to about 3.5 km in a syncline structure inherited from the basement topography. This is in general agreement with the density model in which the Tertiary volcanics, Mesozoic and undifferentiated sediments extend over the entire western plateau and have a thickness of 2-6 km (Fig. 6.9). Two broad zones of thick sediment north and south of Lake Tana are probably of similar importance to the Tana basin. The broad basin south of Tana is related to the earliest flood basalt sequences (e.g. Davidson and Rex, 1980). On the other hand, in the EEP the maximum thickness of sediment reaches 3.5 km.

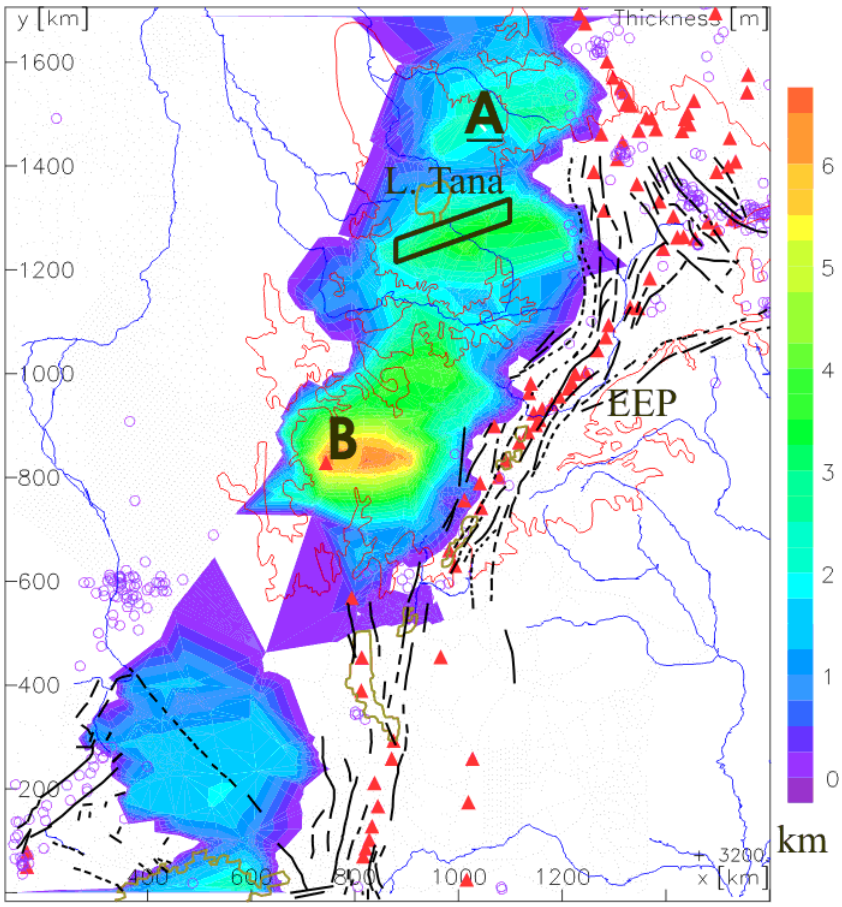

Figure 6.9 Thickness of Tertiary volcanics across the Western Ethiopian Plateau. Three broad basins are indicated (Tana basin, north (A) and south of Tana (B)), the small box, near Lake Tana marks the MT survey, results from which are shown in Figure 6.10 and discussed in the text.

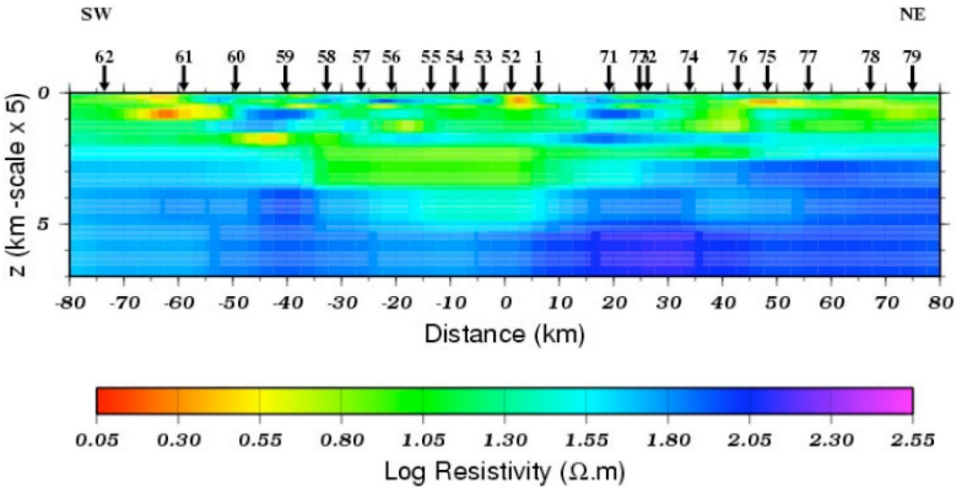

Figure 6.10 2-D vertical resistivity cross-section from modelling MT data in the vicinity of Lake Tana (see location in Fig. 6.4). Arrows show location of MT sites (after Hautot et al., 2004).

The intensive erosion on the EEP (see the drainage patterns) contributed to the huge sedimentary loading in the Ogaden basin (south east). Woldegabriel (1987) suggests that the sedimentary loading in Ogaden basin since the Jurassic might have caused asthenospheric upwelling beneath the Ethiopian plateau (see section 6.4.2). Maximum loading in the model section that crosses Lake Tana (12°N, Fig. 6.11) also corresponds to the location of maximum sediment thickness.

The total load across a modelling plane or at a specified depth can be estimated using the function available in IGMAS. This facility is also used in Section 6.5 for rigidity calculations. The section along the modelling plane 28 (about 12°N latitude) is shown along with the corresponding load map in Figure 6.11. The thick Tertiary volcanics/sediments discussed above are also evident under Lake Tana.

The flexure and upward bending under the rift due to thermal upwelling and the downward bending of the lithosphere outside the rift (plateau) due to combined loading of external (topographic) and internal (subsurface) density contrasts are evident in Figure 6.11. The estimated loads reach $8x10^{18}$ kg/m^2 underneath the plateau. The loading may have produced a downward flexure of the Moho topography from a mean value of 35 km to about 45 km. Near the margins of the rift (east of Lake Tana) flexural uplift of the rift shoulders is clearly seen.

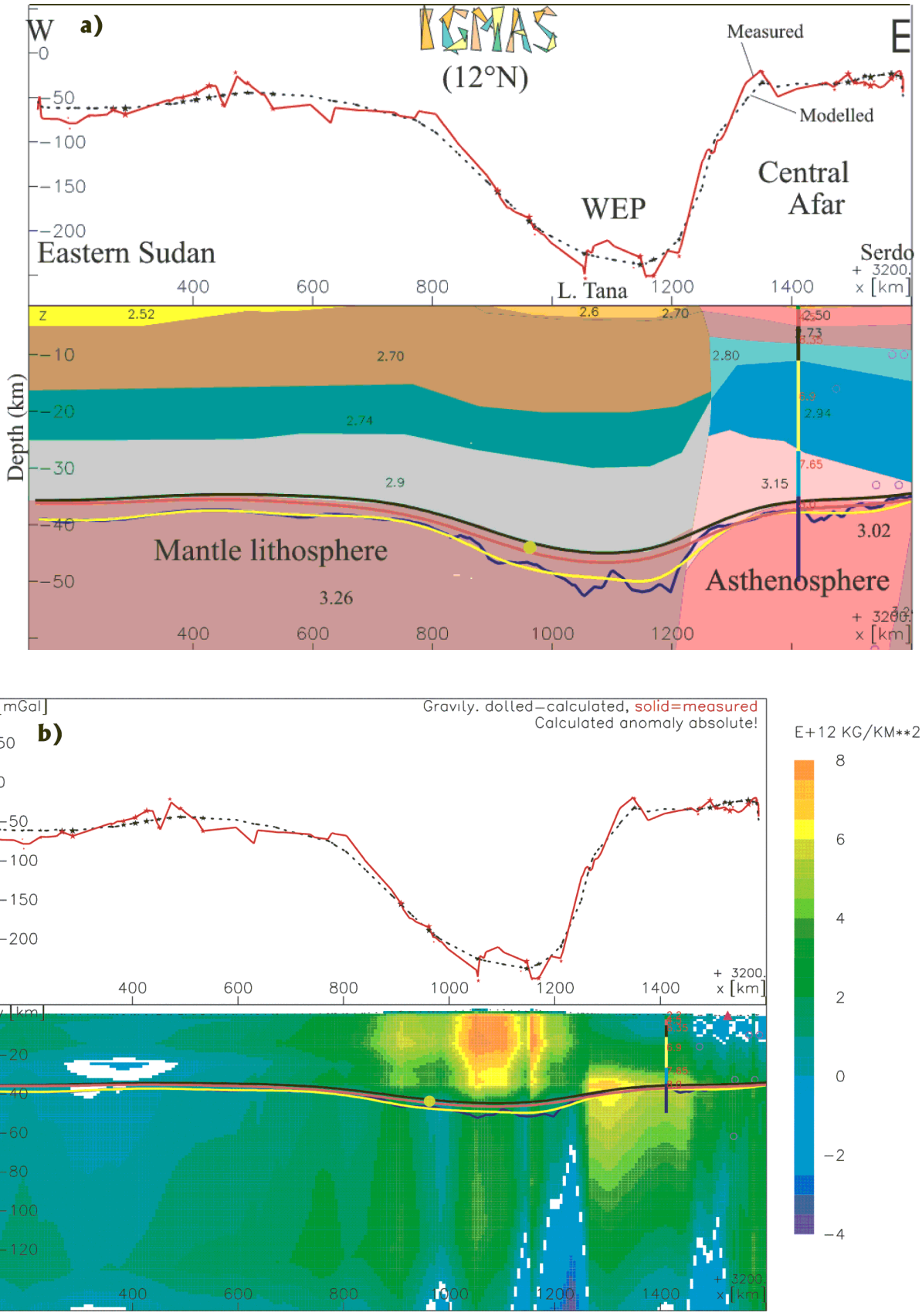

Figure 6.11 (a) Crustal structure along 12°N from eastern Sudan through the western Ethiopian plateau (WEP) to central Afar (Serdo). (b) Corresponding total load (internal plus external). The maximum total load corresponds to the thick crust (WEP) under Lake Tana.

As explained in Section 5.3.3, the isostatic Mohos under the rift are deeper than the seismic Moho, which suggests under compensation. For this reason, isostatic Mohos are not particularly relevant under the rifts. However, some general correlation with the different isostatic Mohos can be made. The Airy Moho (see Fig. 6.11a, thick blue line) does not consider the strength of the lithosphere and consequently shows pronounced Moho undulations. In contrast, the regional VM Mohos (black and red thick lines corrected for dynamic compensation, yellow without correction) show that regional flexure correlates much better with seismic Moho estimates (green dots and vertical thin bar in Figure 6.11) than do the Airy Moho estimates. The correlation between different Mohos is particularly good outside the rift. Central Afar is also characterized by a thin upper crust that is conformable to seismic observations.

6.4.4 Deep Lithospheric structure

In this section, the deep lithospheric structure beneath the EARS is discussed. Two cross-sections from the density model across the rift are used to show narrow and wide rift structures and horizontal slices of the modelled lithospheric structure (50-115 km) are also discussed.

The upper panel in Figure 6.12 shows a very good correlation with new seismic data from Keller et al. (2004) and global Earth model of Laske (2002). The profile almost uniformly intersects the entire northern part of the Western Ethiopian Plateau (WEP) from Tekeze to Erer (Eastern Plateau) via the southern terminus of southern Afar. A complete section of the WEP over more than 500 km is seen. The section depicts the irregular basement structure beneath the WEP that influenced the succession of Tertiary and Mesozoic sediments deposited during episodes of marine transgression, regression and volcanism over a million years. As previously discussed (Section 6.4), the rift shows thin lower crust to the west and thick lower crust in the east towards the EEP. Thus, the modification of the lower crust is more intensive towards the WEP. At greater depths, the topography of the anomalous lithosphere generally looks similar to the basement structure, probably suggesting that basement uplift and topography are partly a consequence of dynamic compensation due to sub-lithospheric density contrasts. The thickness of the mantle lithosphere beneath the plateau areas is similar on both sides of the plates (about 100 km), except at the northwest end of the WEP where the thickness is more than 100 km.

Figure 6.12 shows two cross-sections that demonstrate the development a continental rift (MER) to an oceanic rift (Afar). Away from the rift these sections may also give an indication of lithospheric geometry before continental break up.

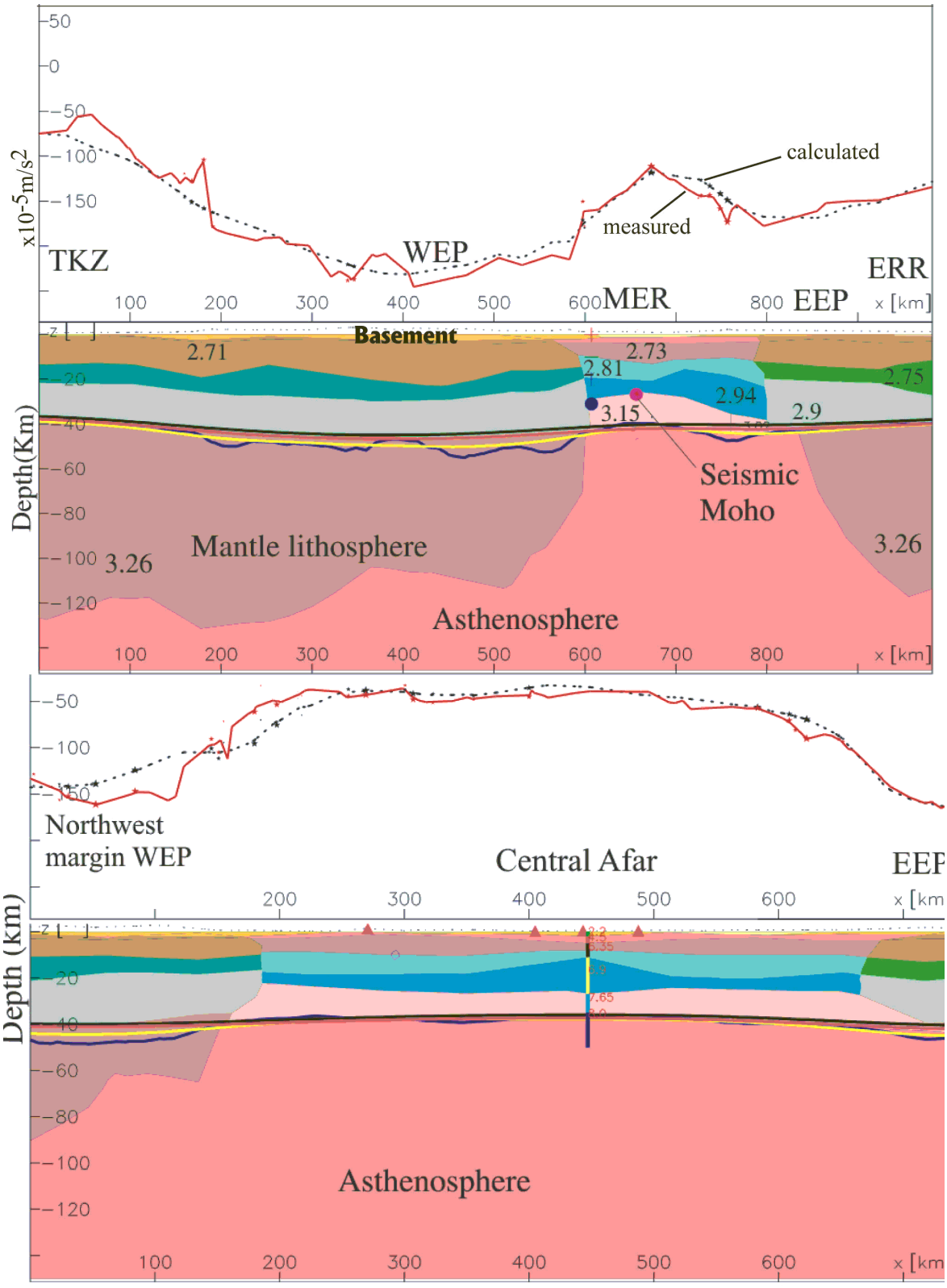

Figure 6.12 Upper panel: a cross-section perpendicular to the northern end of the MER from the northwest end of the WEP-Tekeze river (TKZ) along a wide section of the WEP. The profile ends in the eastern Ethiopian plateau (EEP) near Erer. The lower panel is a complete NW-SE (parallel to the trend of the Red Sea) section through Afar and shows a lithosphere thinned (more than 100%) by the asthenosphere/lithospheric material (~500 km width), and thin upper crust with less than 8 km thickness.

The lower panel of Figure 6.12 is a complete cross-section of Afar from the northwest margin of the WEP to the EEP. It shows a lithosphere thinned by more than 100% over a region more than 500 km wide. Assuming ideal conditions, the modified lower crust could on average reach 60% of the original lower crust. This simple estimate is made with the major assumption that the present anomalous mantle region in the lower crust was part of the lower crust before modification, hence:

mass or volume of lower crust before modification= lmb

mass or volume of lower crust after modification= lma

*% of modified lower crust=(lmb-lma)/ lma)*100,*

The values in Table 8 have been used to calculate the 60% modification of the original lower crust. The modified lower crust may be variable from rift to rift and the calculation here uses the total mass or volume of the whole rift section.

The lower panel in Figure 6.12 also demonstrates to what extent the mantle lithosphere below Afar is eroded and replaced by the buoyant lithospheric material. The thinning of the mantle part of the lithosphere and replacement by asthenospheric material lead to uplift (Meckenzie, 1978), i.e. the dynamic uplift of the East African plateau.

The deep lithospheric geometry from 50 km to 100 km is shown in Figure 6.13. Below 50 km, the lithosphere is simplified into two units (mantle lithosphere and asthenosphere). The lithospheric processes related to these units are the interaction of the hot ascending mantle (asthenospheric material or plume) and the normal lithosphere. Surface references, such as faults, major drainages, volcanoes and boundaries of Large Igneous Provinces (LIPS) are overlain to correlate regions affected by the expansion of the assumed plume material. Below 50 km, almost no crustal material is present. At 50 km the asthenosphere is limited to the rift and rift shoulders, while the whole region outside of the rift is normal mantle lithosphere. At 80 km, asthenosphere expands to the east and west, eroding the mantle lithosphere, and affects the whole of rift and adjacent blocks. At 100 km, it covers a substantial region of the plateau and the whole of the rifted blocks. This may further indicate that the thick crust beneath the plateau is a favourable region for further development of rifts. It has also been noted in earlier works that rifting generally prefers a thicker crust, that contains a higher proportion of weaker minerals like quartz and feldspars (e.g. Keller et al. 1994). At 112 km, a large area of the EARS is dominated by the hot mantle lithosphere/asthenosphere that preferentially expands to the thickest crust of the western and eastern plateau regions.

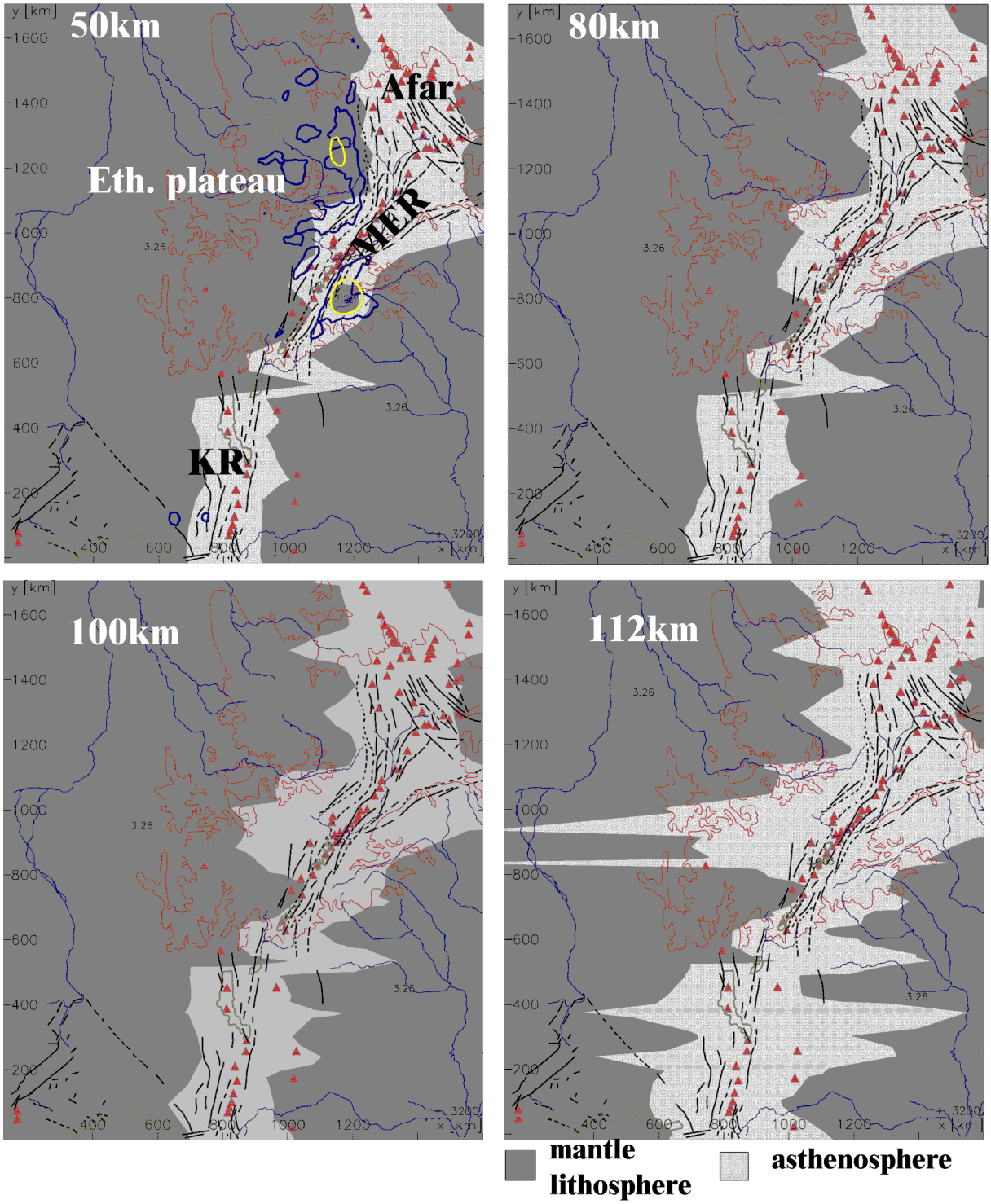

Figure 6.13 Deep lithospheric structure derived from the 3D model. The expansion of the asthenosphere (ascent) shows that it is presently restricted to the rifted zone at shallow depth (50 km) and underlines large section of the plateau at greater depth (> 100km). The deep expansion regions are well correlated with Oligocene-Miocene volcanoes far from the rifted regions. This may indicate that the anomalous mantle is not sufficiently buoyant to rise up, or alternatively that hot mantle is currently eroding the intact lithosphere under the Nubia and Somalia plates.

The expansion directions and the bending of the drainages are apparently correlated, but are very difficult to relate it to a particular process at this stage. The pattern of the expansion further indicates two separate general areas of expanded mantle material: the MER and Afar regions and the Kenya Rift (KR). As discussed in Section 6.4.2, this could be related to two channelling mechanisms from a single plume or to two separate plumes with an overlap in the broadly rifted region of Southern Ethiopia.

6.4.5 Model sensitivity (density)

A new experimental IGMAS procedure (Schmidt, pers. comm.) assists to reduce the subjectivity in varying the density parameters by estimating the maximum allowable density variations that maintain a satisfactory fit between observed and calculated gravity profiles. However, the subjectivity is not totally avoidable because a priori assumptions remain important at the start of the model. Therefore, careful allocation of density parameters is important. In this study, densities were allocated using the approach of Sobolev and Babyko (1994) and also partly based on many other density measurements and calculations (see Chapter 3). Allowable density variations for the major modelled units are indicated in Table 9.

Table 9
Allowable density variations for the modelled units

Unit	density (Mg/m^3)	Allowable variation (Mg/m^3)
Mantle lithosphere	3.26	0.003
Asthenosphere	3.20	0.003
Anomalous mantle under Afar	3.15	0.016
Anomalous mantle under MER	3.02	0.029
Anomalous mantle under Turkana	3.09	0.019
Lower crust under Rift	2.94	0.018
Lower crust out side Rift	2.90	0.011-0.012
Lower crystalline basement (Rift)	2.81	0.017
Lower crystalline basement (outside Rift)	2.75	0.019
Precambrian basement/upper crust (Rift)	2.73	0.026
Precambrian basement (outside Rift	2.71	0.077-0.096
Precambrian exposure	2.70	0.106
Tertiary volcanics	2.60	0.039-0.069
Sediments/rift infill/rift volcanics	2.33-2.51	0.070-0.079

Table 9 shows the maximum flexibility in density values is for the Precambrian exposures. Surface measurements show that the density of this unit is highly variable and ranges between 2.5-2.8 Mg/m^3 (Table 2). The next most flexible units are the sediments and rift infill. For these units, density measurements using samples and boreholes from Eastern Sudan also exhibit a wide range of values. Thus, density allocation for upper crustal units is more uncertain than for

the lower crustal and mantle densities which are extremely sensitive to very small variations (e.g. greater than 0.003 Mg/m^3 for mantle densities).

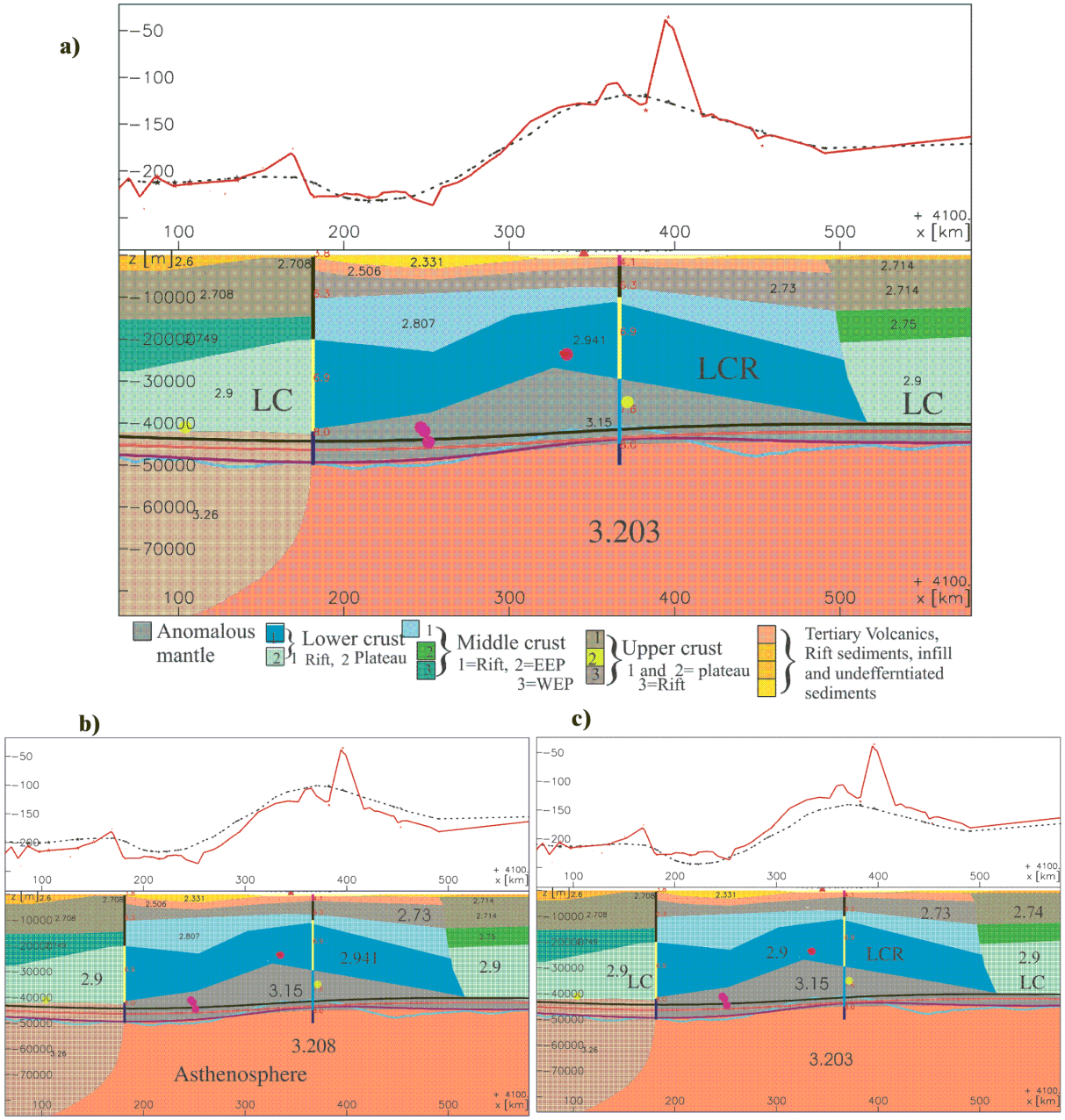

Figure 6.14 (a) Part of a cross-section across the northern end of the Main Ethiopian Rift, b) calculated gravity after changing the asthenosphere density by 0.005 Mg/m^3, an increment of only 0.002Mg/m3 greater than the allowable variation (see Table 9) and c) assuming no lower crustal modification. The adjustments in both b) and c) produce an unacceptable misfit. LC: lower crust, LCR: lower crust under rift.

A part of a section across the northern end of the Main Ethiopian rift (Figure 6.14a) is used to demonstrate changes produced by changes in density. A small variation of the asthenospheric density above the allowable variation, i.e. an increase of 0.006 Mg/m^3, leads to a significant

misfit (Figure 6.14b). The same section is also tried with the assumption of similar lower crustal density variation (no lower crust modification) and the density of the lower crust is kept constant at 2.9 Mg/m^3. This case also gives a misfit (Fig. 6.14c). In general, the final density model could be variable within the above range of density limits and the number of possible solutions is reduced.

6.5 Rigidity of the East African Lithosphere

Effective elastic thickness for the Afar and Red Sea areas ranges between 6 and 17 km (Ebinger et al., 1989; Hartley et al., 1996; McKenzie and Fairhead, 1997), for the east African Plateau about 46 km, and cratonic areas, 77 km (Ebinger et al., 1989). Other East African regions show a range of values between 25 and 29 km (Forsyth, 1985; Bechtel et al., 1987). Low estimates of T_e have been determined for the African lithosphere Cretaceous/Tertiary rifts such as the White Nile Rift (11 km) and the Red Sea margin (5km) (Hartley et al., 1996). Tessema and Antoine (2003) estimated different, but generally comparable T_e values, with differences probably related to differences in data sets and inherent problems of the techniques (e.g. Watts, 2001). The estimates are usually made using admittance and coherence methods by taking the topography and the gravity field and assuming a thin elastic plate. The response of the thin elastic plate (deflection) 'W' is calculated using the following differential equation:

$$Dk^4W(k)+g\Delta\rho W(k)-q(k)= 0 \qquad 6.5.1$$

where $D=\frac{E T_e^3}{12(1-\sigma^2)}$ *is the flexural rigidity of the lithosphere, k= wave number*

$\Delta\rho$= *the density contrast between the material above and below the plate*

$q(k)$= *the applied load (Forsyth, 1985; Bechtel et al., 1987).*

The estimates outlined above show that within distinct tectonic regions, such as Afar, T_e estimates vary significantly. Partly to overcome the inherent problems and general limitations with admittance/coherence methods and to suggest reasonable solutions, the estimation of elastic thickness here is approached using the alternative method from Braitenberg et al. (2002).

The method of Braitenberg et al. (2002) does not calculate the admittance function, instead a set of point-load response functions are used (Airy type) in order to generate optimal flexure parameter from the relation between topographic and internal loads and the Moho interface. In the method, it is also possible to include both surface and subsurface loads using the concept of pseudo-topography (explained below).

The flexure calculations for the EARS are made using the program code developed (Braitenberg et al., 2002) according to the following procedures. The major inputs for the

program code are taken directly from the 3-D model and this procedure gave extra advantages. The inputs are:

a) The Moho map generated from 3-D modelling (Chapter 7, Fig. 7)

b) Total load (L) is directly calculated from the 3-D model using eq. 6.5.2-6.5.3 and used to estimate the pseudo-topography (h_{PT}) following the approach developed by Ebbing et al. (2002). The flow chart in Ebbing et al. (2002) is modified with respect to the new additions of dynamic topography models (Fig. 6.15).

$$L = h_T \rho_T + \Sigma h_i (\rho_i - \rho_c) \qquad 6.5.2$$

$$h_{PT} = L / \rho_T = h_T + \frac{\Sigma h_i (\rho_i - \rho_c)}{\rho_T} \quad i=1, N \qquad 6.5.3$$

Calculations are effected using the smoothed Moho shown in Figure 7 (see Chapter 7 section 7.1 under Moho and residual gravity) and:

a) using loads from observed topography and loads from topography corrected using dynamic topographic models;
b) total load estimated from pseudo-topography, which is calculated using the above relations, in one case with observed topography alone, and in another case with topography corrected by dynamic topographic models.
c) sub grid dimension in all cases is 200x200 km with a shift 20x20 km, reference depth of the flexure 35 km and reference mean crustal density 2.8 Mg/m^3. The loads are calculated at a reference depth of 50 km.

Following the above procedure, Figures 6.16, 6.17 and 6.18 are produced. The sequence of the process is summarized by the flow chart in Fig. 6.15.

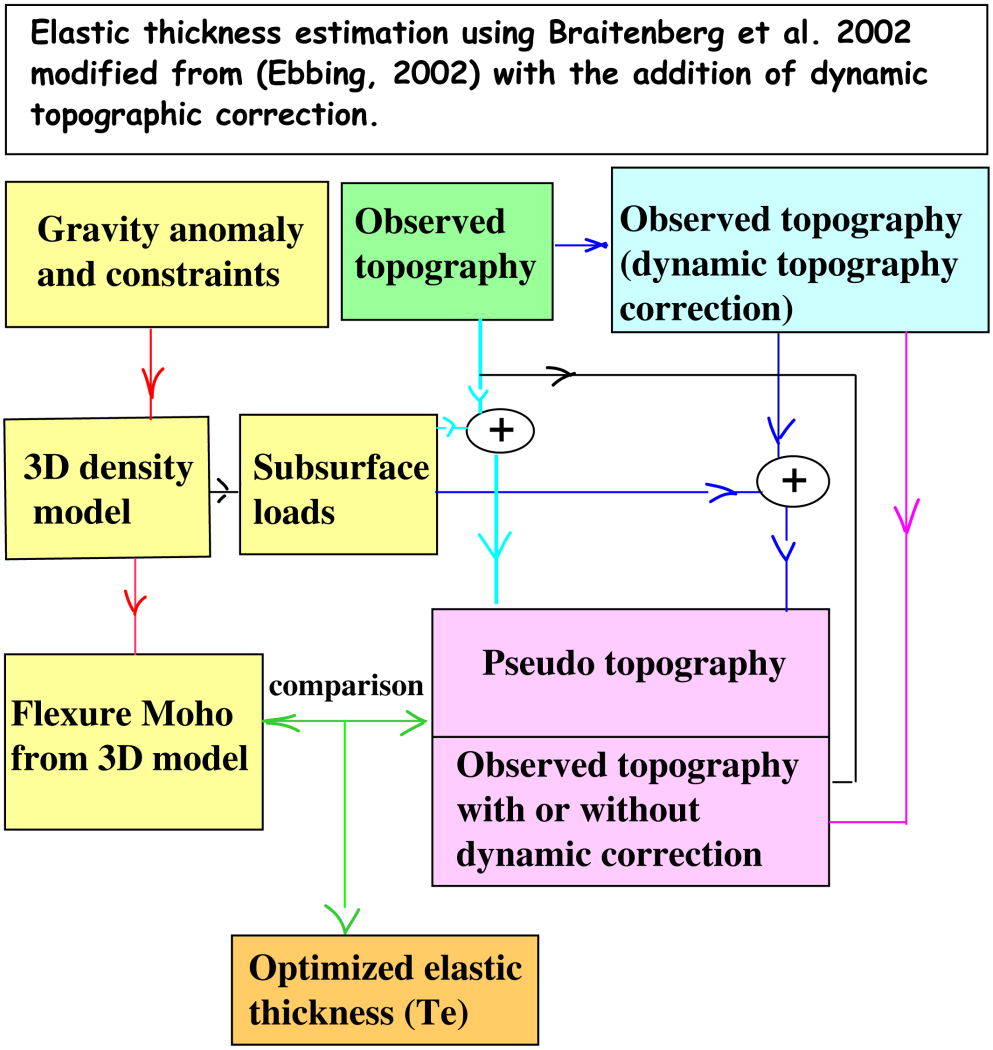

Figure 6.15 Flow chart showing the steps involved in elastic thickness estimation (modified from Ebbing, 2002) with the addition of dynamic topographic correction.

1) Effective elastic thickness from observed topography

Figure 6.16 shows the effective elastic thickness computed using observed topography (Fig. 6.16a) and with internal load from the 3D model (Fig. 6.16b). In both cases the low elastic thickness (less than 15 km) is computed for Afar and Turkana, and high values (above 40 km) are computed for the plateau regions of Ethiopia, Kenya and a large section of the MER are similar. The low rigidities in Afar and Turkana are consistent with estimates made using admittance method (e.g. Ebinger and Hayward, 1996). There are differences in the MER axial region, but these are less than 20km (Ebinger and Hayward, 1996). In Figure 6.16a the whole of eastern Sudan is represented by low rigidity, whereas Figure 6.16b shows medium rigidity only in the southern Sudan basin while the rest of the Sudan craton displays high rigidity, consistent with other elastic thickness estimates (e.g. Tessema and Antoine, 2003). Therefore, estimation of elastic thickness should ideally incorporate internal loads (Figure 6.16b).

2) Effective elastic thickness from topography corrected by dynamic topographic model.

Grand dynamic topography model

The results from topography corrected using the Grand dynamic topographic model are shown in Figure 6.17a (only topographic load) and Figure 6.17b (with internal load). Both results are similar, except that in Figure 6.17b the zone of high rigidity in the MER and adjacent plateau is narrower than in Figure 6.17a. The results are more consistent with the results of other estimates, especially when internal loads are incorporated.

Slab dynamic topography model

The case without internal load (Fig 6.18a) shows a different estimation to the east of the rift and a larger area of high rigidity in the plateau region (including the MER). Here, the slab model with internal load (Fig. 6.18b) gives a similar picture to the results using the Grand model.

The following could be possible reasons for the differences in elastic thickness estimates from this study and the earlier work using admittance and coherence techniques.

a) the new method of calculation based on Airy compensation may not be completely applicable in this region, at least in the Main Ethiopia Rift (MER).
b) the MER is relatively intact, the amount of extension is very small, and the locus of strain is now localized towards the centre, therefore high rigidity away from the border faults and plateau areas might dominate the expected low values towards the centre of the rift.
c) the MER is completely underlain by Precambrian basement, not highly tectonized and the lithosphere might be more rigid than expected.

In general, estimates that incorporate internal loads and dynamic topography corrections gave consistent results in most areas. Based on all the estimates, some of the salient features include:

- in highly tectonized zones of Afar and Turkana all the models consistently show low values.
- Precambrian / basement areas are more or less characterized by medium to high elastic thickness, with some differences from model to model that could be attributed either to the nature of the basement rocks or to the type of model in use.
- in Afar near the Tendaho-Goba'ad discontinuity, a change in lithospheric strength is shown by all models (Figs. 6.16, 6.17, 6.18). This discontinuity may be an incipient plate boundary (Ebinger and Hayward, 1996) and marked by accommodation zones (Tesfaye et al., 2003).

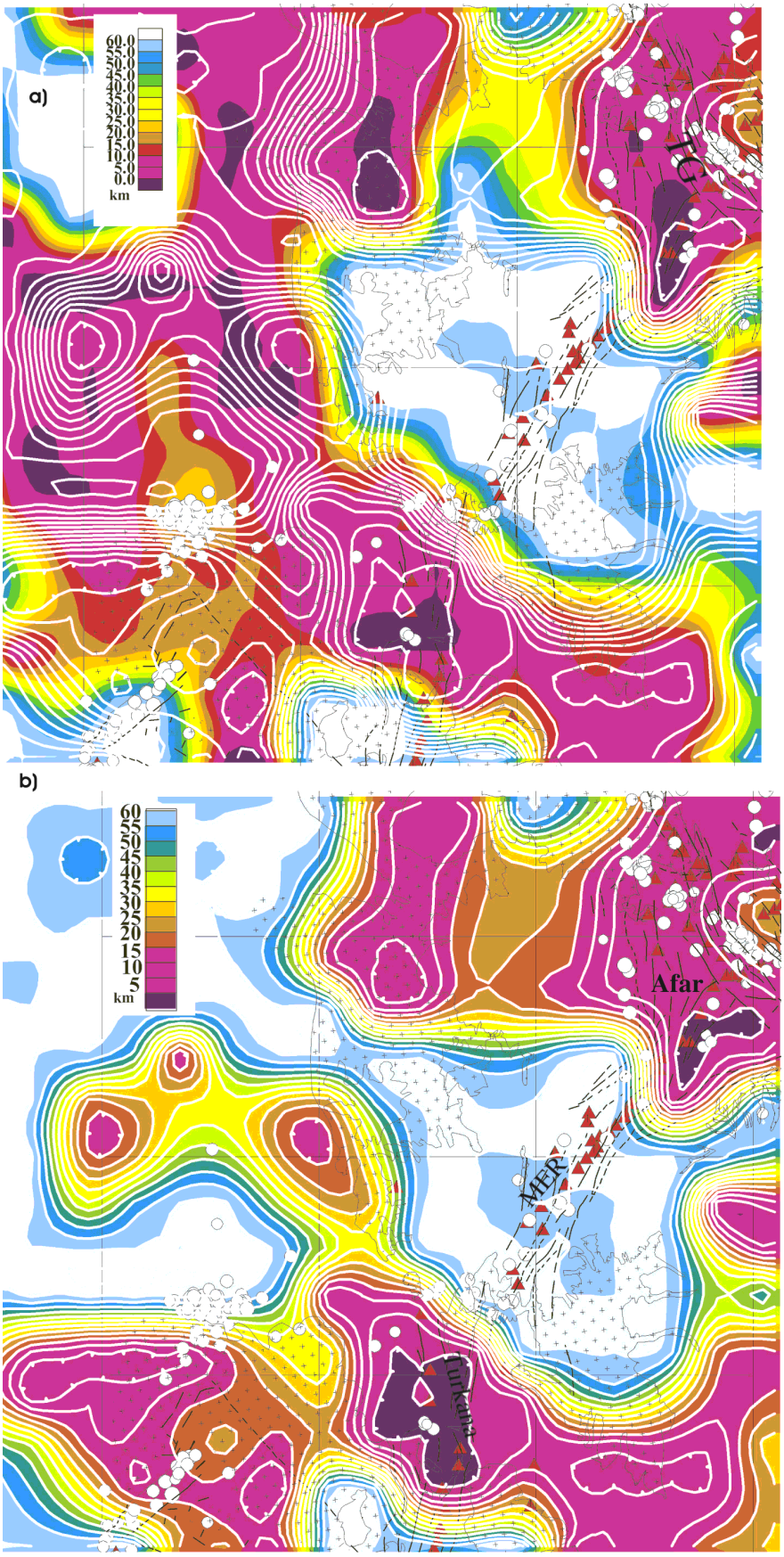

Figure 6.16 Effective elastic thickness computed: a) Observed topography without internal load b) Observed topography with internal load from the 3D model. Reference depth 50 km, mean crustal density 2.8 Mg/m^3 and window width 200 km x 200 km. Basement areas are indicated with crosses. TG: Tendaho-Goba'ad.

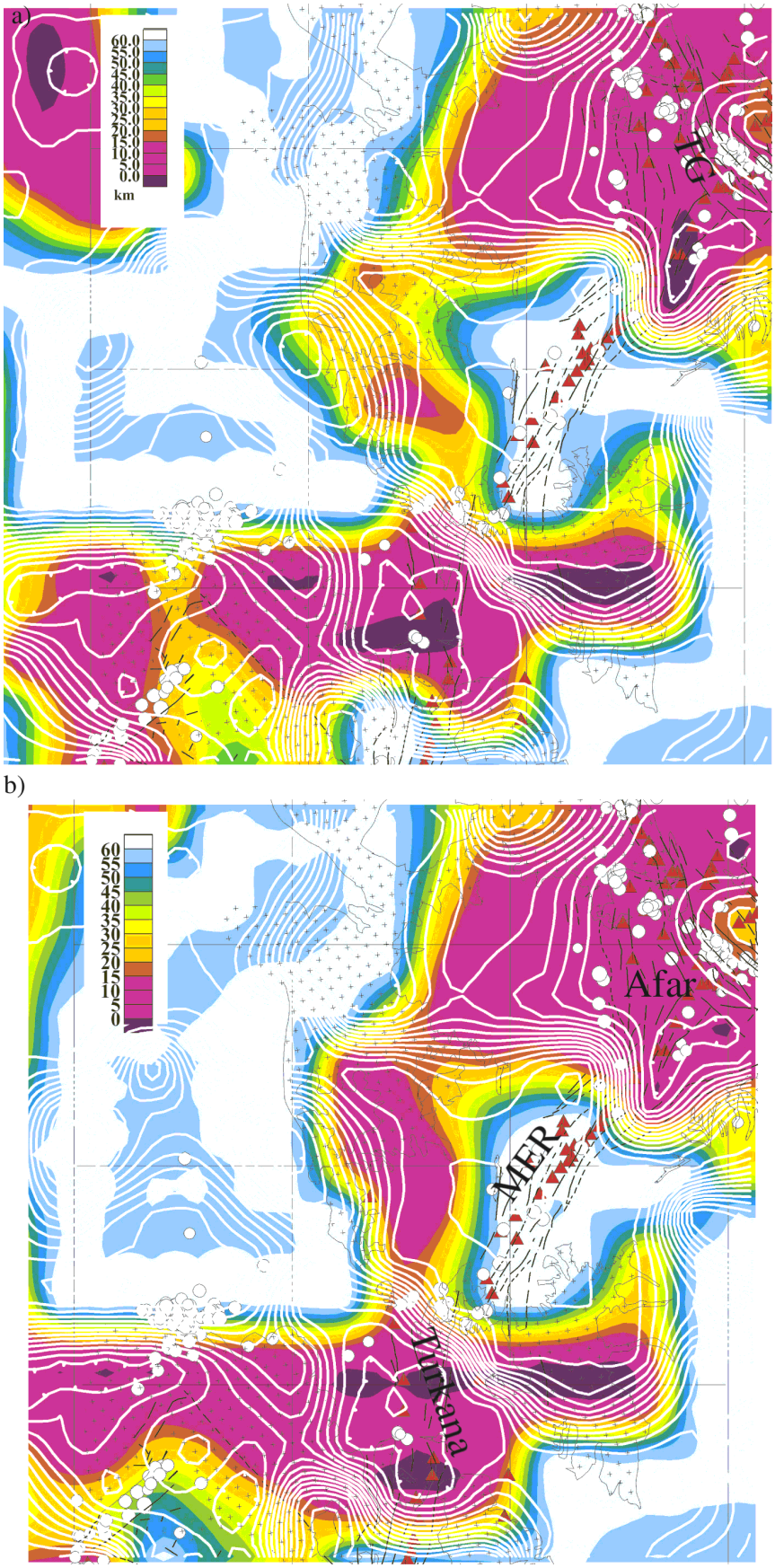

Figure 6.17 Effective elastic thickness: a) Without internal loads and topography with dynamic correction (Grand model). b) With internal load and topography with dynamic correction (Grand model). 50 km reference depth, 200 km x 200 km moving block and reference density 2.8 Mg/m^3

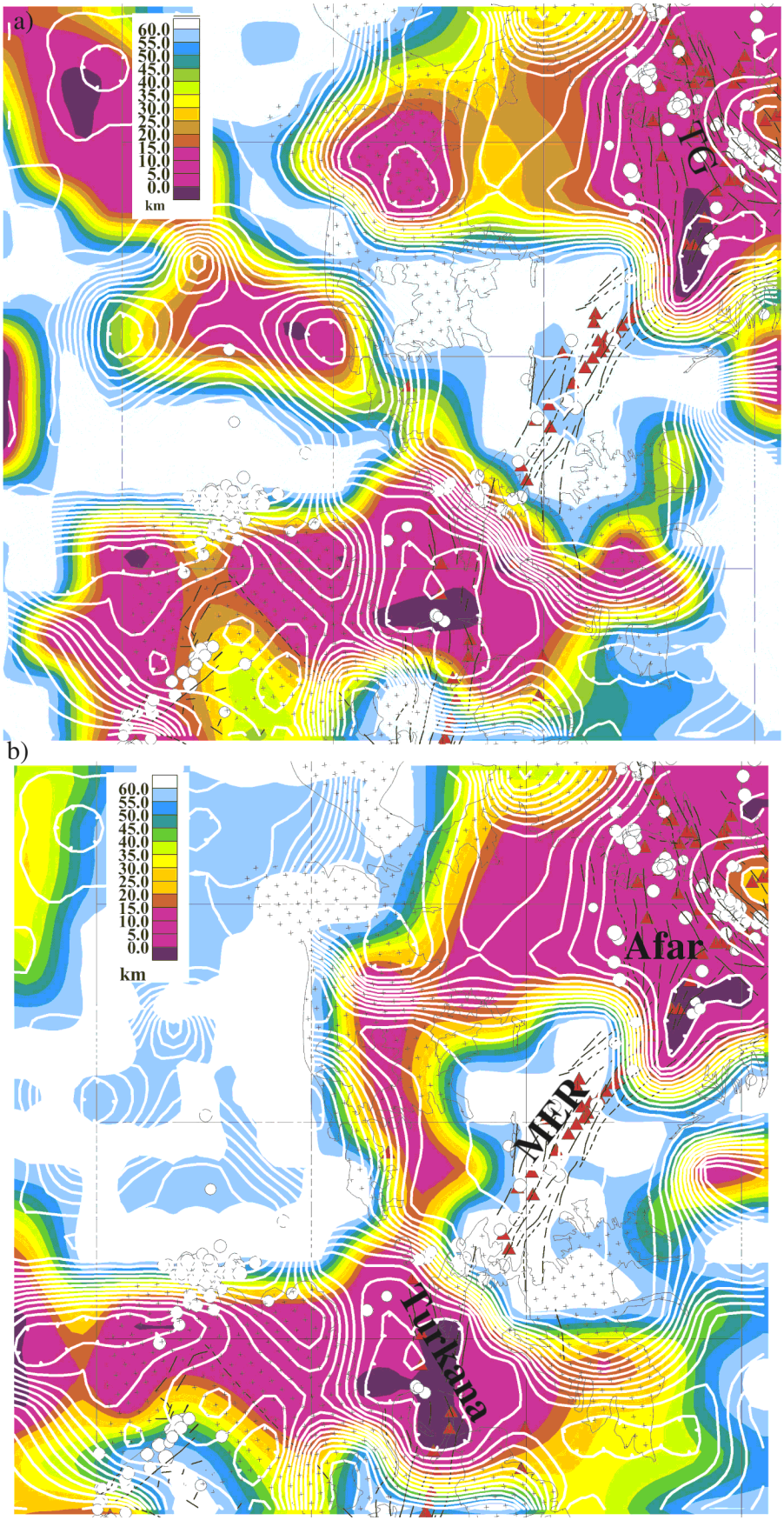

Figure 6.18 Effective elastic thickness: a) Without internal load and topography with dynamic correction (slab). b) With internal load and topography with dynamic correction (slab). 50 km reference depth, 200 km x 200 km moving block and reference density 2.8 Mg/m^3.

The calculation could be improved with a more smoothed version of the Moho map as it gives better results than the unsmoothed Moho version. The method of Braitenberg et al. (2002) may be improved by incorporating a regional flexural compensation model, but this is beyond the scope of this work.

7 Discussion and conclusions

7.1 Discussion

Why rifts are important?

The entire East African rift has become an important open laboratory for applying Geoscience methods for different purposes with varied scale and intensity. This study, although made at a regional scale, important for many aspects other than solving academic problems. Many useful and practical applications can be envisaged, as discussed below. Continental rifts like the ones in East Africa, are homes for millions of people. The present population explosion along the rift and its margins call for a sustainable integrated study of the rift resources, geodynamics and environment. The eastern branch of the East African rift is also known for its untapped thermal resources. Current projections show that Eastern Africa alone could generate about 2500 MW (Teklemariam, 2004). However, in spite of the favourable conditions (high reservoir temperature and pressure fluids), only about 121 MW are generated in Kenya (Mariita, 2004) and a pilot plant with a capacity of 7.2 MW exists in the Main Ethiopian Rift (Teklemariam, 2004). Nevertheless, studies and research are continuing in the entire East African region. The very limited heat flow data does not allow the preparation of a regional heat flow map or reliable thermal structure model, which is useful for assessing thermal resources and for related geodynamic research. The present work and other forthcoming research in this area should give some consideration for collecting more heat flow data. Such data could be acquired relatively easily as part of ongoing projects (as sub projects).

The Ethiopian rift also offers an environment for a variety of sources of industrial minerals: e.g. potash, diatomite, kaolin, bentonite, sulphur, common salt, zeolite, soda ash and various types of industrial raw minerals (Fentaw and Mengistu, 2004). This wealth of resources is due to the widespread volcanism and early development of topographic depressions within the rift, which in turn gave rise to favourable depositional environment. There are recent indications of epithermal gold deposits that have changed the old notion of finding gold and base metal deposits only in the Neoproterzoic rocks (Precambrian exposures) of Ethiopia. The thick Tertiary sediments in some places reaching three to five km depth and that extend from Eastern Sudan to the western border of Ethiopia (e.g. Blue Nile Rift, Atabra rift) are important sites for looking hydrocarbon exploration. Some of the results from this work could assist in this regard. The Mesozoic sediments at the margins of the rifts may also be of economic interest. Mamo et al. (2004) have tried to look the recent EAGLE data in this direction. Another area of active research is paleoenvironmental reconstruction in the Horn of Africa (e.g. Woldegabriel et al.,

2000, 2004). This is because the thick sedimentary successions and recent Quaternary units are epitomes of the past Millennium. Therefore, experiments and modelling to understand the deep processes underlying the rifts must continue.

From integrated 3-D modelling, many additional syntheses can be prepared, such as:

1) Depth to the basement: This could be combined with some out puts from regional geological mapping (in all scales) and aeromagnetic interpretations;
2) Sedimentary thickness map;
3) Volume estimates of important lithological compositions (e.g. volumes of the volcanic constructs atop the East African plateau as discussed in the previous section);
4) Balanced and well-optimised Moho map useful for geodynamic and related studies and which help to constrain crustal and upper mantle structures, reduction or separation of regional and residual Bouguer gravity anomalies, and are useful in hazard studies.

Extension and rift models

Classical rift models and this study

Currently there are three types of rift model: active, passive and core complexes (e.g. Corti et al., 2003). In active rift models, the thermal anomaly (asthenospheric upwelling) is important for extension (e.g. East African rift Systems) and, in passive rift models, the far field forces, Absolute Plate Motion (APM), ridge pull and push systems are important (e.g. Turcotte and Emerman, 1983). Many analogue experimental models in the laboratory apply such models in order to understand the evolution of rifts (grabens and half grabens), their development, trends of asymmetry, and associated lithospheric-scale processes. Summary and review of some of the experimental studies related to the three-dimensional model are made by, for example, Mullegeta and Ghebreab (2001) and Corti et al. (2003).

This work (the derived 3-D model) does not favour one particular model over the other. Classifications as such may not be necessary for complete understandings and the analogue experiments rely heavily on our choices of parameters. Of course, there is a need to shape the initial model based on previous results, assumptions, data and information. Both thermal processes activated by mantle convection currents or plumes and the far field forces (APM and plate ridge push) contributed to the present geometry of the rift structures and continue to act with different degrees of intensity. Therefore, the idea of distinct classification does not help as the end result in both or in all cases are nearly similar. However, the hard facts we see in such classifications remain true.

The current GPS data, though contradictory in some ways, shows that the current activity (strain) is now concentrated in the central part of the rift rather than at the border faults (e.g. Bilham et al., 1999). Models by Ebinger and Casy (2001) also support these results. The GPS data further shows that the African plate is currently stationary (e.g. Burke, 1996). The relative plate motion and extension between the Nubian (NW), Somalia (SE) and Arabian plates (NE) are very small (e.g. Chu and Gordon, 1999; Argus and Gordon, 1991; Fernanades et al., 2004) compared to the magnitudes of plate motion and extension observed for other plates. Thus, the contribution of the far field stress to rift development could be negligible.

In the model derived here, it is not possible to include the effect of the far field forces other than by assuming their presence during interactive modelling. The effects and contributions are indirect or 'implicit'. The model fundamentally takes into consideration the so-called active rift model with the understanding that mantle convection/thermal upwelling or plume encroachment beneath the East African rift and plateau are affected by the far field forces. How and to what extent the vigour of these forces affects the reconfiguration of the East African lithosphere, the ascent and distribution of partial melt or plume material, and the interaction of crust and mantle over a period of the last 40 Ma or so (since the first volcanic pulse) requires other methods (e.g. thermomechnical modelling that takes into consideration the heat flow data and thermal structure of the region). This is one of the important data sets that, despite large rift related literature and interdisciplinary experiments, lacking in this region.

The first approach to understand the nature of the East African lithosphere using gravity data was to try different types of isostatic methods (local and regional types) and to consider their implication. A regional type of isostasy (i.e. VM) that takes into consideration the flexure or the rigidity of the lithosphere is preferred. The analysis in this regard demonstrated that the method is useful for studying the state of isostasy and for geological interpretation. However, it cannot completely explain the large negative Bouguer gravity that we observe in East Africa. With the then available data, Ebinger et al. (1989) suggested the need to consider the dynamic compensation mechanisms. Others (e.g. Lithgow-Bertlleoni and Silver, 1998) estimated that the dynamic topography using slab and global tomography models is on the order of 500 to 600 m in the East African plateau (see Chapter 5). These dynamic compensation mechanisms are at the mantle lithosphere/asthenosphere boundary and contribute to most of the plateau uplift. Therefore, we need to combine the isostatic compensation usually made at the crust-mantle interface (Moho) with the dynamic compensation. Ultimately, we have seen that all these combinations are not able to completely explain the gravity differences. However, there may still be buried loads in the upper crust or bodies that were not totally modelled by these simple

compensation mechanisms. This is also evidence of the dynamic nature of the rifts (tectonically active). The results of both models and combinations help the study of first order effects and also assist the three-dimensional forward modelling.

The model derived here is in effect a combination of the active and passive rift models. It assumes a balance between the two if such classifications of rifts are useful and correct. According to the models of Turcotte and Emmerman (1983) and Bott (1992), both models are affected by the far field and local stresses acting under the lithosphere. As indicated before, most argue that the African plate is almost stagnant, though GPS data are conflicting (East African conference in Addis Ababa, June 2004) as are plate motion analyses. Therefore, the effect of the far field forces is negligible. The SKS splitting data in Ethiopia (Gashawabeza et al., 2004; Kendal et al., 2005) does not highlight the correlation between absolute plate motion and fast SKS splitting direction, both in the plateau (Neoproterozoic rocks) and rifts. The recent EAGLE data show also that the lithosphere under the rift area is locally thinned, whilst the adjacent plateau is intact or thick.

The new regional 3D density model shows that the east and the west mantle lithosphere remains largely intact, although it is affected by the ascent of the asthenosphere or the superposition of the two plumes of Afar and Kenya. At shallow depths, the mantle lithosphere (see Figs. 6.12 and 6.13) is generally less affected by the ascent of the asthenosphere (associated plumes or plume) away from the rift zones or border faults. This may imply that the effect of the far-field forces is able to alter the configuration of the lithosphere, while the near-field stresses under the lithosphere are important for the lithospheric modification observed under the rifts (see also the various sections of the models and the discussion under melts and plumes). It is not possible to directly quantify the effect of these stresses. But, as shown in the following section, gravity back stripping (calculation of the gravity effect of the interfaces in the model) suggests that a significant effect on the gravity field is coming from the density contrasts within the crust and that remaining effect corresponds to the density contrast at the crust-mantle boundary and sub-lithospheric mantle.

Moho and residual Bouguer gravity

The Moho as a crust-mantle boundary has different geophysical, petrological and geochemical definitions. Geophysical definitions consider the layer where the seismic velocities show a drastic jump from normal crustal velocities to upper mantle P-wave velocities (approx. 8.0 km/s). P-wave velocities below this layer generally remain constant. Along with the change in velocity, the chemical and petrological compositions also change. P waves in the mantle

suggest that the bulk density predominantly reflects peridotite (Olivine+Orthopyroxene+Clinopyroxene) or Ecologite (Clinopyroxene+Garnet) (Richardson and McSween, 1989). The petrological definition of the crust is a layer having a composition of felsic-quartz/feldspar lithology underlain by mafic granulites and gabbros (Giese et al., 1999). Similar to the above definition, the crust-mantle boundary is then considered as the transition zone where felsic/mafic rocks grade into peridotities (e.g. Mengel and Kern, 1992). Therefore, the petrological Moho discontinuity is characterized by a compositional change, whereas the geophysical Moho discontinuity marks a prominent change of elastic and density properties (Giese et al., 1999). More discussions on the nature of the Moho discontinuity and the processes causing its alteration are given by Giese et al. (1999).

The velocity layer 7.3-7.6 km/s, which shallows in central Afar to about 18 km, is defined as a mantle layer (Berckhemer et al., 1975). Thus, following the geophysical definition of the Moho and based on the 3-D density model, the Moho map (Fig. 7) is produced for EARS. The map depicts a minimum Moho depth of about 16 km under central and northern Afar, a maximum of 48 km atop the Western Ethiopian Plateau (WEP) and a mean Moho of 36 km for the EARS. Figure 7 shows an anomalous Moho region associated with the axial crustal thinning in Afar (Berckhemer et al., 1975), MER (Keller et al., 2004) and the Turkana area (KRISP, 1991), and disturbed Moho features /interruptions where the Turkana rift and the Afar-MER rift systems join at the broadly rifted zone in southern Ethiopia. Moderately deep Moho features (about 38 km) mark the transition zones from shallow Moho to deeper Moho. The transition is sharp and with a high gradient between the WEP and Afar and from the plateau areas to the rifts. The gradient is more gentle and smooth between the plateau and the depressions. Examples include the northern termination of the western rift, the transition from the WEP to the Eastern Sudan, and the northern termination of the Mozambique belt. The irregular pattern of the western margin of the Moho near 34°E longitude could be related to the suture zone on the northern (e.g. Abdelsalam et al., 1996) and on the southern side of the Turkana area (e.g. Simyu and Keller, 1997). Thus, the suture is clearly marked by a broad feature up to 5°N, but tapers off at about 4°N and continues further south. This result is consistent with the earlier isostatic analysis. Deepening of the Moho with separate closures related to the thickening of the lower crust are central features in the WEP, EEP and at the termination of the NMER at about 8°N. This shows that the part of the lithosphere underlying these areas is not affected or modified by the Cenozoic volcanism and associated rift development. The area south of the NMER (south of 8°N) and north of Turkana is characterized by deepening of a relatively intact Moho. The narrowing of the Moho from Afar to the MER before it deepens is consistent with

the Ebinger and Casey (2001) model or to the Bilham et al. (1999) GPS analysis that show the locus of strain is now moving towards the centre of the rift away from the border faults. It may further indicate that the crustal extension in the MER is very small.

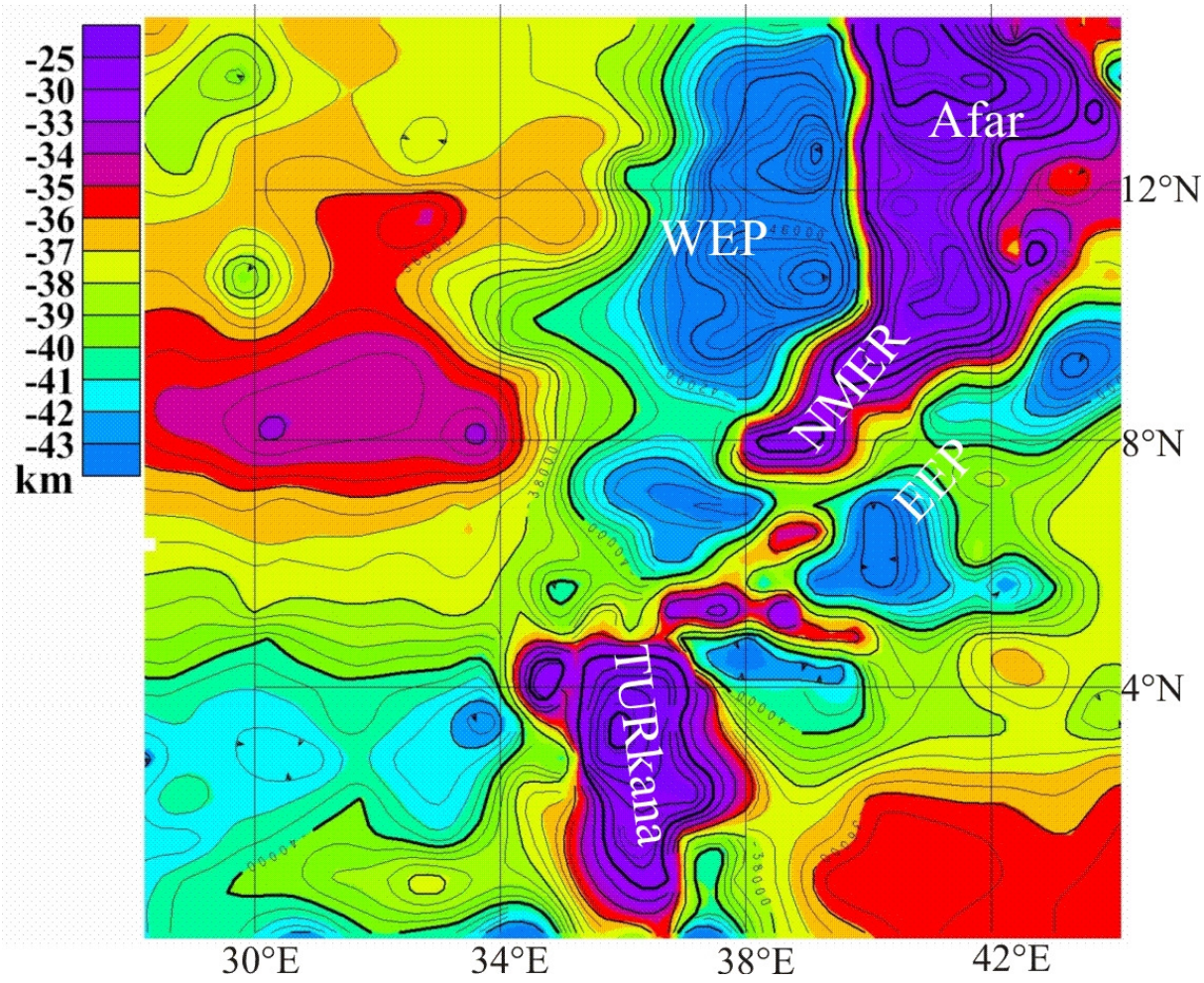

Figure 7 Optimized Moho of EARS from three-dimensional modelling (see text).

The modelled Moho could be used for further gravity modelling or for any other geodynamic studies at any scale. In the next section, the Moho is used to calculate a residual gravity field.

Residual Bouguer gravity

The density contrast between the lower crust and mantle is variable under the rift and plateau regions. Within the EARS itself, it is slightly variable (see Table 10). Therefore, the gravity effect of the Moho or any other preferred layer should be calculated by taking this change into account. To avoid further complications, a Moho layer (Fig. 7.1a) is defined that include only the adjacent plateaus and an average density contrast of 0.148 Mg/m^3 and a mean reference depth of –20 km are used to calculate the corresponding Bouguer gravity effect (Fig.

7.1b). Figure 7.1c is the residual gravity after eliminating the Bouguer gravity effect of the Moho. In a second case the gravity effect of the anomalous lithosphere/asthenosphere below the EARS is estimated using a density contrast of -0.183 Mg/m^3 at a depth of –35 km (Fig. 7.1).

Table 10.
Density contrast below the rifts between modified lower crust/anomalous mantle (A) and density contrast with respect to anomalous mantle/asthensosphere (B).

Zone	Case A (Mg/m^3)	Case B (Mg/m^3)
Turkana rift	0.157	-0.105
MER/CMER	0.079	-0.183
Afar	0.209	-0.053
average	0.148	-0.114

A positive density contrast (0.209 Mg/m^3) in Afar produces positive residual gravity anomalies due to the addition of masses (underplating) or dyke injection and local crustal thinning. A comparatively similar process occurs in Turkana with a density contrast of 0.157 Mg/m^3. The dyke injection zone or thinning in the MER is in a relatively narrow area and could be attributed to a small density contrast of 0.079Mg/m^3. The residual Bouguer gravity anomaly exhibits a strong positive in Afar and relative positive features in the whole rift. It decreases locally, which is related to sedimentary basins. The Precambrian basement areas are also marked by relative positive to positive anomalies. The strong positive anomalies are related to the mafic-ultramafic belts, as noted in the isostatic residual anomaly. Differences are evident with the previous isostatic residual field. The differences however are related to the differences in choice of parameters, density contrast and the definition of the Moho layer. The residual field computed with consideration of dynamic compensation, is more similar to the residual Bouguer field in Figure 7.1c, even though its amplitude is much more reduced in the rift area.

The negative contrast is useful for explaining the ascent of the mantle material (negative buoyancy). The small negative density contrast shows a petrologically homogenous layer where large area of thinning of the lithosphere or modification exists, (e.g. in Afar, see also the cross section in Fig. 6.12).

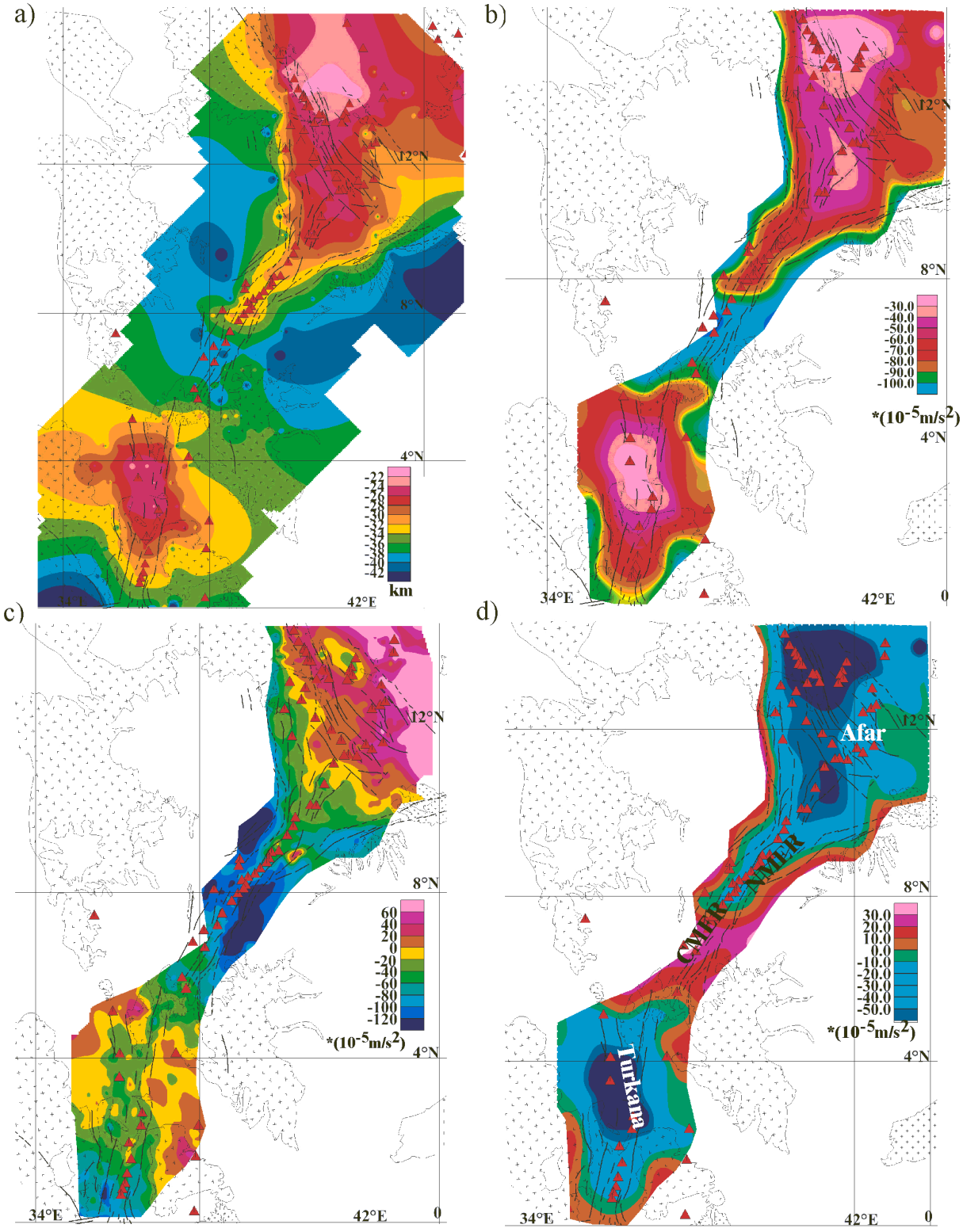

Figure 7.1 The Moho under the Rift system and adjacent plateau from the 3-D model (a). The corresponding Bouguer gravity using the density contrast 0.148 Mg/m3 and a reference depth of –20 km calculated using the Parker algorithm (b). The residual gravity computed by eliminating the Bouguer gravity of the Moho in b from the Bouguer gravity field in Fig. 4.3 (c). The Bouguer gravity effect of the anomalous lithosphere (asthenospheric upwelling) using the negative density contrast of –0.183 Mg/m^3 and reference depth of –35 km (mean Moho)(d). Faults (black lines) and volcanoes (red triangles) and boundaries of the Precambrian units (dark crosses) are overlain for reference.

Figure 7.1d shows the Bouguer gravity effect of the asthenospheric upwelling. The asthenospheric upwelling produces a negative Bouguer gravity field of about -60×10^{-5} m/s^2 that is more prominent in Afar and Turkana, the extremely thinned parts of the EARS lithosphere. Regions modified by such upwelling include the complete Turkana rift up to the broadly rifted region of Southern Ethiopia, and to the north, the whole Afar region and the northern part of the MER up to 8°N about Lake Shala. To the south, the region between Lake Shala and Chamo forms the CMER and the positive Bouguer gravity effect (Fig. 7.1d) may imply that this part of the lithosphere remains largely very intact. It is to be noted here that the region up to 4°N is poorly constrained by crustal-scale seismic refraction data. The entire plateau region is dominated by positive residual Bouguer gravity effect (about 30×10^{-5}m/s^2) due to the positive density contrast between the intact mantle lithosphere and the lower crust and is thus unaffected by the ascent of the upwelling mantle or plume. As explained in the forgoing, a single mantle plume under Afar may not be sufficient to explain all the lithospheric features and processes.

Removing both fields, i.e. the gravity effect of the Moho, and the upwelling mantle/asthenosphere, produce a residual gravity field (Fig. 7.2) more or less comparable to the isostatic residual anomaly in the rift (see Chapter 5). The reason for this similarity is that in the isostatic residual field the gravity effect of the mantle upwelling is implicit (see also the isostatic regional anomaly), whereas in the present case, effects are calculated separately and eliminated.

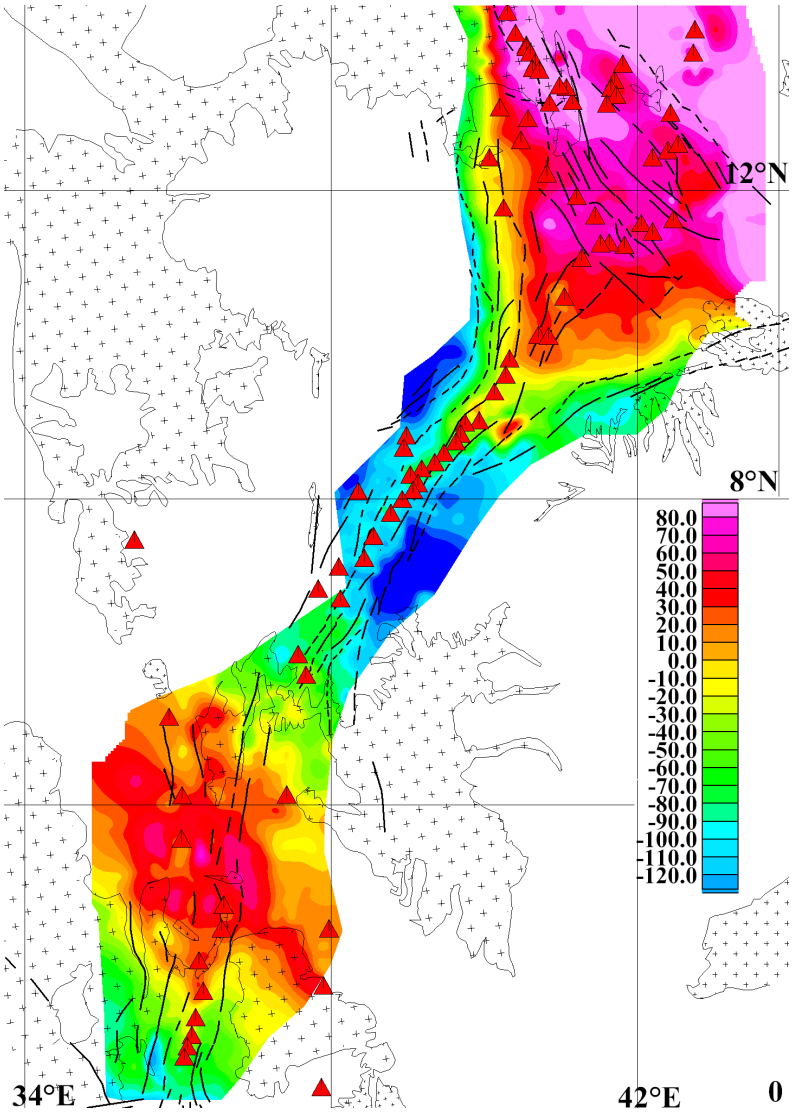

Figure 7.2 The residual gravity field after eliminating the gravity effect of the Moho (Fig. 7.1b and the upwelling mantle (Fig. 7.1d) from the Bouguer gravity field.

Melts and plume

The Pliocene-Quaternary volcanoes (Mohr and Wood, 1976), and the contemporaneity of tectonic and volcanic cycles (Baker and Wohlenberg, 1971) have been cited, among other factors, as evidence that the Ethiopian and Kenyan rifts are part of a single mega-structure and can not be related to independent causative phenomena such as separate mantle plumes (Gass, 1975). There are also many geophysical similarities between the Ethiopian rift and northern Kenya rift: broad negative isostatic regional anomaly, Bouguer anomaly, relative positive isostatic residual field along the axis of the rift, relatively elevated heat flow data, geothermal manifestations, uplift and extreme thinning in Turkana and Afar.

Mantle plume advocators suggest many possibilities: a single plume under Afar, two plumes, one in Afar and one near L. Victoria, a single plume with different channelling

mechanisms etc. Based on the density models presented here, it is not possible to argue for a particular number of plumes, but the model may favour one or a combination of the different possibilities, depending on the pattern of the deep structures (see Fig. 6.13).

A single mantle plume could be channelled in the thinned lithospheric zones of:

a) Afar and currently expanding to the northwest and southwest Ethiopian plateau (see Fig. 6.13);
b) Turkana and could be expanding to the east while it is blocked or unable to penetrate the strong craton to the west (e.g. Nyblade and Brazier, 2002). Similarly, to the north expansion is blocked by the thick and relatively intact Sudan craton and by basement uplift in southwest Ethiopia.

This suggestion may support the separate structure and modification of the Ethiopian (Nubia) plate. Notably, the lithosphere in the northwest is largely modified by the Afar plume and the Somalia plate by the Turkana (Kenya) plume. The Turkana rift may mark the contact between the two plates. North of Turkana, there is diffuse contact also noted as a broadly rifted region in southern Ethiopia (e.g. Ebinger and Ibrahim, 1994) that results from the overlap of the NE-SW trending MER, the N-S Kenya Rift and associated basins and Precambrian structures. It may also be also an overlap zone for the expansion of the Afar plume and Turkana plume if two plumes or two channelling mechanism of a single plume are accepted.

The deep lithospheric model may support two mantle plumes, depending on the radius of influence the plume head (usually about 1000 km). For the Afar-Turkana area, having more than 1500 km in length, it may be unlikely that the Afar plume alone or Turkana plume (about L. Victoria) would affect the entire Afar-Turkana zone. The earliest volcanism (Oligocene-Miocene) may have facilitated further thinning of the lithosphere. The plume material prefers a thin lithosphere to allow lateral spreading and ponding to produce the greatest thickness in the pre-existing thin lithosphere (Sleep, 1997). Thus, the expansion of the plume material covers a large area in Afar and Turkana. Therefore, two plumes or a single plume with two different heads could explain the geophysical model (Fig. 6.13). Figure 7.3 show a three-dimensional view of the modelled Moho and the ascent of the upwelling anomalous mantle that indicates the ponding of plume material after it is channelled selectively in the thin lithosphere of the Kenya Rift (KR) and Afar.

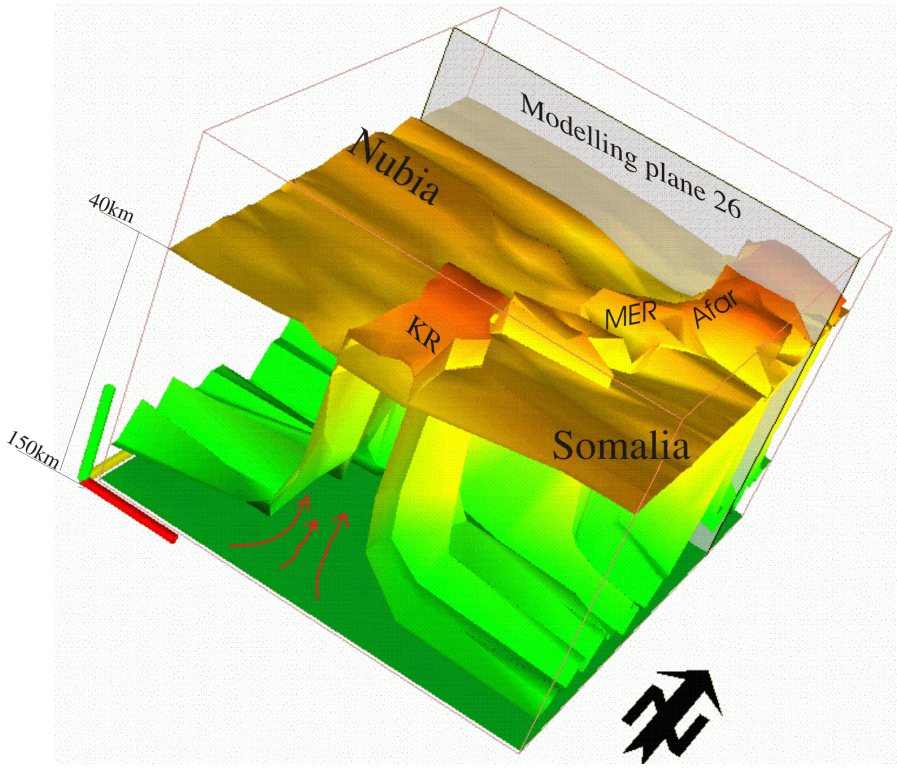

Figure 7.3 The undulation of the Moho interface above the ascending anomalous lithosphere (ascent is indicated by red arrows).

Another important aspect that is often discussed in relation to plumes in extension zones is the presence of melts or partial melts. The existence of partial melts in the EARS is not well constrained. Geophysical observations, such as high conductivity zones, low velocity zones, high heat flow, high negative Bouguer anomaly and high Vp/Vs ratio, are used to point out amounts of melts in some orogens like in the Central Andes (e.g. Schilling and Partzsch, 2001). The following paragraph outlines some attempts by different investigators to identify the presence of melts in the EARS.

Melts could be generated by increased mantle temperatures or upwelling mantle beneath extension zones. As a result, the melts may extrude at the surface or be underplated. The observed upper mantle velocities (7.5-7.7 km/s) in the Kenya rift could be explained by the presence of 3-5% basaltic melt rising from greater depths to be trapped below the Moho (Mechie et al., 1994). Similarly, the velocity reduction below the Kenya rift based on teleseismic tomography (Achauer et al., 1994) is explained by the joint effects of melt and temperature increment (e.g. Zeyen et al., 1997; Sobolev et al., 1996).

Using laboratory experiments Mullugeta (2004) demonstrated the dynamic consequences of mantle upwelling in the presence of a melt system in stratified lithosphere that undergoes episodic extension. Bastow et al. (2004) suggested high temperature and partial melt in the

upper mantle beneath the rift using the teleseismic tomographic inversion of P and S wave travel time data in the MER. Al-augite silicate melt metasomatism associated with continental rift development has been observed in the MER using xenoliths and megacrysts from Quaternary basaltic eruptions (Rooney et al., 2004). Rooney et al. (2004) further suggest that Al-Augite veining dominates the regional lower crust and lithospheric mantle.

As shown in the 3-D density model, lower crustal modification under the rift may affect up to 60% of the original lower crustal composition, particularly in Afar and Turkana. This modification of the lower crust could be related to infiltration of the silicate melts that produced Al-Augite veining in the MER (Rooney et al., 2004) or other alkali basaltic magmas in the southern Kenya rift (Hay et al., 1995). Stewart and Rogers (1996) extrapolate their result from southern Ethiopia to the whole of Ethiopia and suggested that plume derived melt production rates increased three-fold in syn-rift basalts from its pre-rift value ca 0.01 km^3/a. One can see that with the present limited data, although it is very difficult to quantify the volume percent of melt, a rift model must incorporate the presence of melt that has significantly altered physical properties.

Depth to the top of basement

The depth to the top of the crystalline basement (Neoproterzoic) for the EARS can be determined directly from the 3D density model (Fig. 7.4). The map is restricted only to the modelling area indicated in Figure 6.3. This map gives a regional view of the basement relief of the EARS that is useful for resource exploration and planning of further work. It could be also integrated with other maps (e.g. bedrock geology) for better definition and use.

Basement highs include all exposed Precambrian domains (NP, SWP, SP, MB) and basement lows correspond with sedimentary basins in eastern Sudan, southwest Ethiopia and the whole rift region.

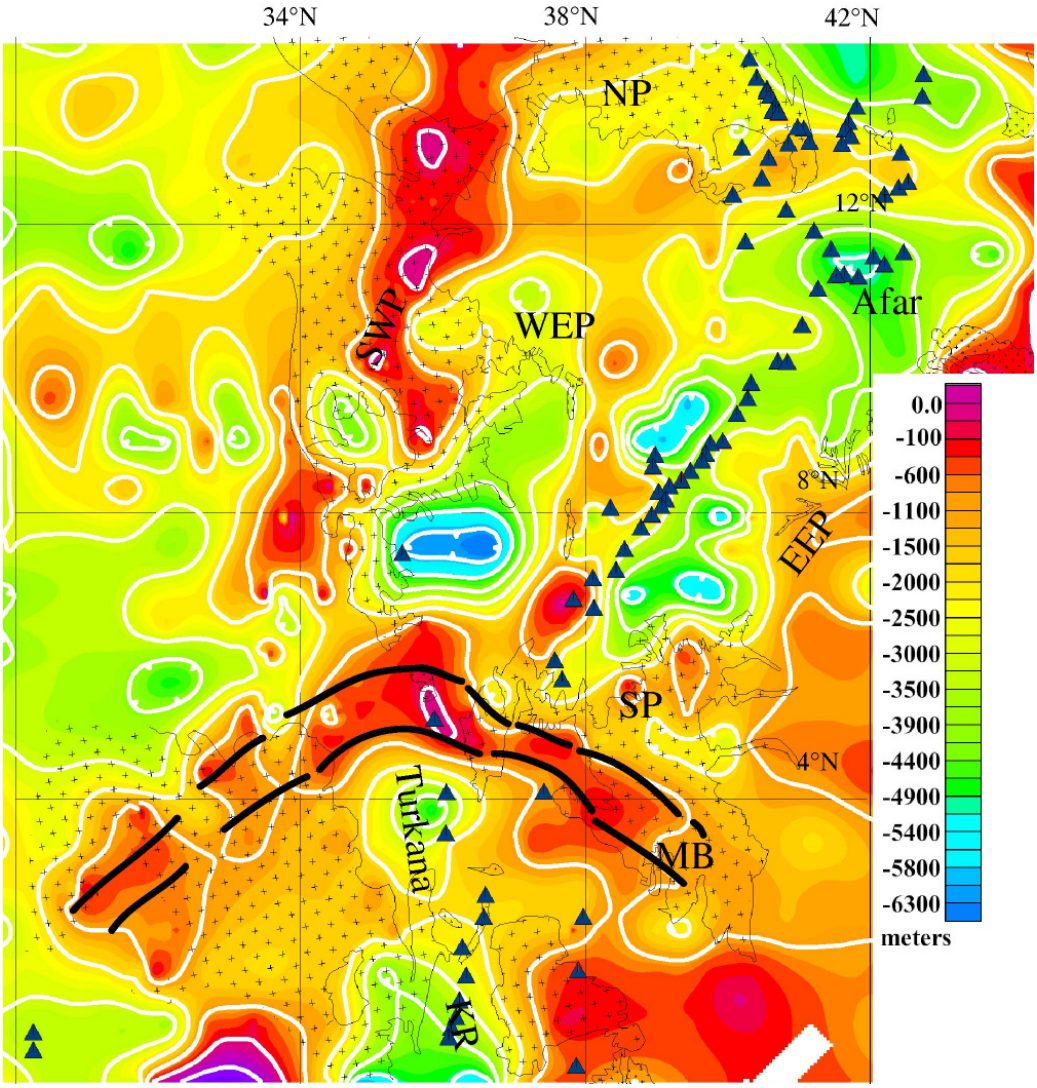

Figure 7.4 Basement topography from the 3D density model. Precambrian basement exposure dark crosses) and volcanoes (blue triangles) are overlain. Deep basement related to sedimentary structures exists in the rift, south west Ethiopia, Afar, Turkana and Eastern Sudan. Shallow basement corresponds to Precambrian rocks (East African Orogen). Precambrian domains: SWP, NP, SP, MB are as described in Figure 2b. A basement high above Turkana is indicated by the thick black lines. The outer northern margin of the rigid Tanzanian craton is indicated by high basement contours west of Kenya Rift (KR).

In general, the basement topography varies from a few hundred meters in the Precambrian exposures to a maximum of 7 km in the sedimentary basins and rifts.

It appears that the rifts may preferentially follow and propagate by intruding the weakest basement structures. Similarly to the matured Red Sea rift (e.g. Cochran, 2005), basins and rifts are the result of the break away of Precambrian basement structures. In some places, the Precambrian terranes resisted modification by the Cenozoic extensional tectonism. The weakness of the basement is also related to the underlying deep-seated lithospheric processes and magmatic modification of the lower crust. The propagation of Turkana northwards may

have been partly blocked by the strong Precambrian basement structure or basement uplift shown in Figure 7.4. North of this basement high the thick basin in southwest Ethiopia tapers off to the north-south trending Precambrian domain (SWP) to the west. The basin is bounded by high basement topography to the east and west that is related to Precambrian rocks. This relationship is also apparently also true for all the basins and rifts in this region.

The basement topography map could be improved by integrating results from aeromagnetic data analysis and interpretation, bedrock geology, sedimentary thickness maps and other studies in this region.

7.2 Summary conclusions

The major outcomes of this work are summarized below.

(1) In this work, a new regional database that covers Ethiopia and surrounding regions was prepared using unified and consistent processing procedures. With this database, a complete regional interpretation with respect to important geological features (e.g. Precambrian areas and rifts) is possible. Satellite-derived gravity data (GRACE) was shown to be useful for filling remaining data gaps.

(2) The negative Bouguer anomaly observed in the East African rift system and adjoining plateau is probably due to upwelling of the asthenosphere complemented by local crustal thinning and/or underplating.

(3) Isostatic residual anomalies have been calculated using both Airy and Vening-Meinesz models. Additionally, isostatic residual anomaly maps that incorporate both isostatic and dynamic compensation were prepared. In all cases, the isostatic residual anomalies outline the major Precambrian belts, the Cenozoic rifts and associated major structures. Positive residual anomalies associated with the Main Ethiopian Rift (MER) and Kenyan rift systems could be the expressions of an axial intrusive body and swarms of local faults and fractures. The residual anomalies give an indication of the degree of tectonic stability in the region. In the MER residual anomalies are less prominent, suggesting relative tectonic stability. In the areas of the Red Sea, Gulf of Aden and Afar and northern end of MER, residual anomalies are more pronounced and suggest on ongoing tectonic activity. Near-zero isostatic residuals flank the MER and Kenya rifts and are found within the Danakil Alps and some plateau regions.

(4) The small mean isostatic residual anomaly (about 8 mGal) and the isostatic analysis show a slight positive bias. This bias is indicative of under-compensation. The under-compensation may imply that there are upper-crustal features that are not compensated regionally (probably supported by the rigidity of the lithosphere) or isostatic disequilibrium in the region. Therefore, the high topography of Ethiopia and the East African plateau must be partly compensated by thicker crust (broad negative isostatic regional anomaly) and partly by dynamic forces.

(5) There are no definite Bouguer gravity distinctions between the Arabo Nubian Shield (ANS) and Mozambique Belt (MB) that could be gleaned from the new gravity database. However, major geological structures, such as the margins of the rifts, the Neoproterozoic belt, the ocean–continent boundaries and shear zones, are indicated by positive residual gravity anomalies in both models. The Tertiary volcanics mostly covering the plateaus (age >25 Ma) and the Quaternary volcanic belts in the rift (age < 25Ma) show contrasting isostatic residual anomalies owing to the density contrast arising from the magmatic segments/mafic intrusions in the rift.

(6) To minimize the uncertainties resulting from a lack of sufficient constraints for the whole of the EARS, a combination of both isostatic and dynamic models is preferred. The isostatic Mohos without or with dynamic models cannot completely explain the Bouguer gravity anomalies under the rifts. All models are limited by the approximation of some parameters (e.g. mantle density, viscosity, crustal thickness, flexural rigidity, etc). However, isostatic residual maps are helpful for examining upper-crustal structures and for performing correlations with geology.

(7) The three-dimensional model offers qualitative and quantitative estimate of the depth, thickness and volumes of different geological interfaces and bodies and an optimised Moho and basement topography map. The volume of volcanic constructs on the western plateau of Ethiopia is three times larger than the eastern plateau. The load map derived from the model indicates maximum crustal loads at the crust/mantle interface (ca. 40 km) on the eastern and western flanks of the Main Ethiopian Rift.

(8) The shallowest Moho depth is about 16 km under Afar, while the deepest is 48 km under the Western Ethiopian Plateau (WEP). The mean Moho depth for the

entire EARS is 30 km. The maximum combined load (external and internal) in the WEP may reach $8x10^{18}$ kg/m^2 and this could have produced a deepening of the Moho from average values of 35 km to 45 km. In general, the Moho map reflects the influence of upwelling anomalous mantle beneath the EARS.

(9) A three-dimensional image of the deep structure below the northern part of the Main Ethiopian Rift (MER), Afar and Turkana shows shallow Moho depths and a large area affected by asthensopheric upwelling and lower crustal modification.

(10) The controls on the rift architecture are very much governed by the lower crustal modification and underlying asthenospheric processes. The huge sediment loading in Eastern Sudan (west of WEP) and the Ogaden basin (East of EEP) have played an important role in the rapid ascent of the asthenospheric material or plume heating of the EARS lithosphere. Variations in loadings may have also controlled the general rift architecture (symmetry) in the whole of the EARS. This may be an over simplification, as the modelling does not include large areas to the southwest and southeast of the Nubia and Somalia plates, respectively.

(11) Elastic thickness estimates use combined internal and external loads and the Moho geometry, both of which are direct outputs from the three-dimensional model. An attempt is also made to include dynamic topography corrections while calculating loads from topography. In general, the elastic thickness estimates derived during this work are consistent with the results of earlier studies using other methods.

7.2 Further work and recommendation

In the present work, a three-dimensional density structure using limited constraints is presented. With this model, it has been possible to discuss many scientific issues related to the East African Rift System and plateau. However, there are still many unsolved problems that require further research and study by using: a) the present data and output, b) additional new and important data sets. The following recommendations for long-term scientific goals in this region are made:

- Testing of different elastic thickness calculation methods using the output from the present 3-D density model or future improved models;

- improvement of the basement map using analysis of aeromagnetic data and bedrock geology;
- detailed interpretation and three-dimensional density modelling of the Main Ethiopian Rift using the latest seismic results from the EAGLE experiment;
- joint modelling and interpretation of gravity and aeromagnetic data on selected Precambrian blocks and sedimentary basins in Ethiopia;
- regional three-dimensional density model using uniform and consistent gravity data set (e.g. GRACE, GOCE or similar missions) and the inputs from the present model for the entire East African Rift system.

b)

- update of the gravity network in Ethiopia and adjacent regions for accurate gravity data validation;
- further compilation and integration of gravity data south, north and west of the present area for continental-scale geodynamic and related studies;
- heat flow measurements in the Main Ethiopian Rift, Afar and Southern Ethiopia rift systems;
- densification of gravity data on the Western Ethiopian Plateau, Afar and between Turkana and Southern Ethiopia;
- aerogravity in the Nile basin, a possible suture zone between 14°N- 4°N Latitude and 34°E-38°E Longitude;
- seismic and integrated geoscientific experiments similar to the recent EAGLE project in the broadly-rifted region of Ethiopia (Turkana and Main Ethiopian Rift overlap area).

References

Abdelsalam, M.G., Stern, R.J., 1996. Suture and shear zones in the Arabian-Nubian Shield. Journal of African Earth Sciences 23, 289-310.

Achauer, U., and KRISP Teleseismic Working Group, 1994. New ideas on the Kenya rift based On inversion of the combined dataset of the 1985 and 1989/90 seismic tomography experiments. Tectonophysics 236, 305-329.

Alemu, A., 1992. The gravity field and crustal structure of the Main Ethiopian Rift. PhD Thesis, Royal Institute of Technology, Sweden, 126 pp.

Allan, T.D., 1970. Magnetic and gravity fields over the Red Sea. Phil. Trans. Roy. Soc. London

Allen, A., and Tadesse, G., 2003. Geological setting and tectonic subdivision of the Neoproterozoic orogenic belt of Tuludimtu, western Ethiopia. Journal of African Earth Sciences 36, 329-343.

Ayele, A., Stuart, G., Kendall, J.-M., 2004. Insights into rifting from shear wave splitting and Receiver functions: an example from Ethiopia. Geophysical Journal International 157, 354-362.

Argus, D.F., and Gordon, R.G, 1991. No-net-rotation model of current plate velocities incorporating plate motion model NUVEL-1. Geophysical Research Letters 18, 2039-2042.

Artemieva, I.M. and Mooney, W.D., 2001. Thermal thickness and evolution of Precambrian lithosphere: A global study. Journal of Geophysical Research 106, 16387-16414.

Baker, B.H, Wohlenberg, J., 1971. Structure and Evolution of the Kenya Rift Valley. Nature 229, 538-542.

Banks, R.J., Parker, R.L. and Huestis, S.P., 1977. Isostatic compensation on a continental scale: local versus regional mechanism. Geophys. Journal of Royal astronomical Society 51, 431-452.

Barberi, B.F., Borsi, S., Ferrara, G., Marinelli, G., Varet, J., 1970. Relations between tectonic and magmatology in the northern Danakil depression (Ethiopia). Philosophical Transactions of the Royal Society of London 267, 293-311.

Barnett, C.T., 1976. Theoretical modelling of the magnetic and gravitational fields of an arbitrary shaped three-dimensional body. Geophysics 41, 1353-1364.

Barton, P.J., 1986. The relationship between seismic velocity and density in the continental crust- A useful constraint? Geophysical Journal Royal Astronomical Society 87, 195-208.

Barrat, J., A, Fourcade, S., Jahn, B.M., Cheminée, J. L., Capdevila, R., 1998. Isotope (Sr, Nd, Pb, O) and trace element geochemistry of volcanics from the Erta' Ale range (Ethiopia). Journal of Volcanology and Geothermal Research 80, 85-100.

Bastow, I.D., Stuart, G.W., Kendall, M.J., Ebinger, C.J., Ayele, A., 2004. Upper mantle structure of the Northern Ethiopian Rift- a region of incipient continental breakup. Eos Trans. AGU 85(47) Fall meet. Suppl., Abstract T41G-01.

Bechtel, T.D., Forsyth, D.W., and Swain, C.J., 1987. Mechanism of isostatic compensation in the vicinity of the east African Rift, Kenya. Geophysical Journal Royal Astronomical Society 90, 445-465.

Bedini, R.M., Bodinier, J.-L., Dautria, J.-M., Morten, L., 1997. Evolution of LILE-enriched small melt fractions in the lithospheric mantle: a case study from the East African rift. Earth and Planetary Science Letters 153, 67-83.

Belaineh, M.1983. Petrology, chemistry and physical properties of core samples from well LA-3, Aluto langano geothermal field. Univ. Auckland, NewZeland, no.83.

Berckhemer, H., Baier, B. Bartelsen, H., Behle, A., Burckhardt, H. Gebrande, H., Makris, J., Menzel, H., Miller, H., Vees, R., 1975. Deep seismic soundings in the Afar region and

on the highlands of Ethiopia. In: Pilger, A. and Roesler, A. (Editors), Afar Depression of Ethiopia. Schweizerbart, Stuttgart, I, 89-107.
Berhe, S.M., 1990. Ophiolites in northeast Africa and east Africa: implications for Proterozoic crustal growth. Journal of Geological Society of London 147, 41-57.
Berktold, A., Haak, V., Angenheister, G., 1975. Magnetotelluric measurements in the Afar area. In: Pilger, A. and Roesler, A. (Editors), Afar Depression of Ethiopia. Schweizerbart, Stuttgart, I, 67-79.
Bhattacharyya, B.K., 1964. magnetic anomalies from prism-shaped bodies with arbitrary polarization. Geophysics 29, 517-531.
Bilham, R., Bendick , R., Larson, P., Mohr, P., Braun, J., Tesfaye, S., Asfaw, A., 1999. Secular and tidal strain across the Main Ethiopian Rift. Geophysical Research Letters 26, 2789-2792.
Braathen, A., Grenne, T., Selassie, M.G., Worku, T., 2001. Juxtaposition of Neoproterozoic units along the Baruda-Tulu Dimtu shear-belt in the East African orogen of western Ethiopia. Precambrian Research 107, 215-234.
Braitenberg, C., Ebbing, J., Götze, H.-J., 2002. Inverse modelling of elastic thickness by convolution method-the eastern Alps as a case example. Earth Planetary Science Letters 202, 387-404.
Bullard, E.C., 1936. Gravity measurements in East Africa. Transactions of the Royal Society of London 235, 445-531.
Bott, M.H.P, 1992. Modelling the loading stresses associated with active continental rift systems. Tectonophysics 215, 99-115.
Burke, K., 1996. The African plate. South African Journal of Geology 99, 339-410.
Burov, E.B. and Diament, M.., 1995. The effective elastic thickness (T_e) of the continental lithosphere: what does it really mean?. Journal of Geophysical Research 100, 3905-3927.
C.G.M.W., 1968. Carte Tectonique Internationale de l'Afrique. Choubert, G., Faure-Muret Coordinators UNESCO Paris. Sheets, 3, 5, 6, 1: 5000000.
Chernet, T., Hart, W.K., Aronson, J.L., Walter, R.C, 1998. New age constraints on the timing of volcanism and tectonism in the northern Main Ethiopian Rift-southern Afar transition zone (Ethiopia). Journal of Volcanology and Geothermal Research 80, 267-280.
Chernet, T., and Hart, W.K., 1999. Petrology and geochemistry of volcanism in the northern Main Ethiopian Rift-southern Afar transition region. Acta Vulcnologica 11(1) 21-41.
Chorowicz, J., Collet, B., Bonavia, F.F., Mohr, P., Parrot, J.F., Korme, T., 2004 (Abstract). EARS conference June 20-24, Addis Ababa, Ethiopia.
Chu, D., and Gordon, R.G., 1999. Evidence of motion between Nubia and Somalia along the south west Indian Ridge, Nature 398, 64-67.
Cochran, J.R., and Talwani, M., 1977. Free-air gravity anomalies in the world's oceans and their relationship to residual elevation. Geophysical Journal Royal Astronomical Society 50, 495-552.
Cochran, J.R, 1983. A model for the development of the Red Sea, American Association of Petroleum Geologists Bulletin 67, 41-49.
Cochran, J.R., 2005. Northern Red Sea: Nucleation of an oceanic spreading center within a continental rift. Geochemistry, Geophysics, Geosystems, doi: 10.1029/2004GC000826.
Corti, G., Bonini, M., Conticelli, S., Innocenti, F., Manetti, P., Sokoutis, D., 2003. Analogue modelling of continental extensions: A review focused on the relations between the patterns of deformation and the presence of magama, Earth-Science Reviews 63, 169-247.
Davidson, A., Rex, D., 1980. Age of volcanism and rifting in southwestern Ethiopia. Nature 283, 657-658.

Davis, P.M., Slack, P.D., 2002. The uppermost mantle beneath the Kenya dome and relation to melting, rifting and uplift in East Africa. Geophysical Research Letters 29 (7), 21-1-21-4.

Davies, D., and Tramontini, C., 1970. The deep structure of the Red Sea. Philosophical Transactions of Royal Society London 267, 181-189.

Debayle, E., Lévêque, J.-J, Cara, M., 2001. Seismic evidence for a deeply rooted low-velocity anomaly in the upper mantle beneath the northeastern Afro/Arabian continent. Earth and Planetary Science Letters 193, 423-436.

Dindi, E.W. 1994. Crustal structure of the Anza graben from gravity and magnetic investigations. Tectonophysics 236, 359-371.

Dixon, T.H., Stern, R.J., Hussein, I.M., 1987. Control of Red Sea Rift geometry by Precambrian structures. Tectonics 6, 551-571.

Doucouré, C.M., de Wit, M.J., 2003. Old inherited origin for the present near-bimodal topography of Africa. Journal of African Earth Sciences 36, 371-388.

Döring, J.,1998. Dichteverteilung und Modellierung des isostischen verhaltens der Lithosphäre im Südural. PhD Dissertation, Freie Universität Berlin, 136pp.

Dugda, M.T., Nyblade, A.A., Julia, J., Langston, C.A., Ammon, C.J., Simiyu, S., 2005. Crustal structure in Ethiopia and Kenya from receiver function analysis: implications for Rift development in East Africa. Journal of Geophysical Research 110, B01303, doi: 10.1029/2004JB003065.

Ebbing, J.,2002. 3-D Dichteverteilung und isostatisches Verhalten der Lithosphäre in den Ostalpen. PhD Dissertation, Freien Universität Berlin, 143 pp.

Ebinger, C.J., Bechtel, T.D., Forsyth, D.W., and Bowin, C.O., 1989. Effective plate thickness beneath the East African and Afar plateaus and dynamic compensation of the uplifts. Journal of Geophysical Research 94, 2883-2901.

Ebinger, C.J, Ibrahim, A., 1994. Multiple episodes of rifting in Central and East Africa: A re-evaluation of gravity data. Geologische Rundschau 83, 689-702.

Ebinger, C.J., and Hayward, N., 1996. Soft plates and hot spots: views from Afar. Journal of Geophysical Research 101, 21858-21876.

Ebinger, C.J, Sleep, N, 1998. Cenozoic magmatism throughout East Africa resulting from impact of a single plume. Nature 395, 788-791.

Ebinger, C.J, Yemane, T., Harding, D., Tesfaye, S., Rex, D., and Kelley, S., 2000. Rift deflection, migration, and propagation: Linkage of the Ethiopian and Eastern rifts, Africa. Geological Society of America Bulletin 112 (2), 163-176.

Ebinger, C.J., and Casey, M., 2001. Continental break-up in magmatic provinces: An Ethiopian example. Geological Society of America 29, 527-530.

Fadaie, K. and Ranalli, G., 1990. Rheology of the lithosphere in the East African Rift System. Geophysical Journal International 102, 445-453.

Fairhead, J.D., Girdler, R.W., 1970. The seismicity of the Red Sea, Gulf of Aden and Afar triangle. Philosophical Transaction of the Royal Society of London 267, 49-74.

Fairhead, J., 1976. Structure of the lithosphere beneath the Eastern African rift, East Africa, deduced from gravity studies. Tectonophysics 30, 269-298.

Featherstone, W.E. and Dentith, M.C., 1997. A Geodetic approach to Gravity data reduction for Geophysics. Computers and Geosciences 23, 1063-1070.

Fentaw, H., and Mengistu, T., 2004. The industrial minerals and rocks resource potential of the Ethiopian Rift valley. EARS conference June 20-24, Addis Ababa, Ethiopia.

Fernandes, R.M.S., Ambrosius, B.A.C., Noomen, R., Bastos, L., Combinck, L., Miranda, J.M., Spakman, W., 2004. Angular velocities of Nubia and Somalia from continuous GPS data: Implications on present-day relative kinematics, Earth Planet Science Letters 222, 197-208.

Forsyth, D.W., 1985. Subsurface loading and estimates of the flexural rigidity of continental lithosphere. Journal of Geophysical Research 90, 12623-12632.

Furman, T., Bryce, J.G., Karson, J., Iotti, A., 2004. East African Rift System (EARS) plume structure: insights from quaternary mafic lavas of Turkana, Kenya. Journal of Petrology 45, 1069-1088.

Gashawbeza, E.M., Klemperer, S.L, Nyblade, A.A., Walker, K.T., Keranen, K.M., 2004. Shear-wave splitting in Ethiopia: Precambrian mantle anisotropy locally modified by Neogene rifting. Geophysical Research Letters 31, L18602.

Gass, I.G., 1975. Magmatic and tectonic processes in the development of the Afro-Arabian dome. In Pilger, A., and Rosler, A. (Editors), Afar depression of Ethiopia. Stuttgart, Schweizerbart, 10-18.

Gebremedhin, T., and Allen , A., 2004. Geochemistry of metavolcanics from the Neoproterzoic Tuludimtu orogenic belt, western Ethiopia. Journal of African Earth Sciences 39, 177-185.

George, R., Rogers, N., Kelley, S., 1998. Geology 26, 923-936.

Gettings, M.E., Black M.R, Mooney, W.D., Healy J.H., 1986. Crustal structures of southwestern Saudi Arabia. Journal of Geophysical Research 91, 6491-6512.

Ghebreab W.,1998. Tectonics of the Red Sea region reassessed. Earth-Science Reviews 45,1-44.

Girdler, R.W., Fairhead, J.D., Searle, R.C., Sowebutts, W.T.C., 1969. Evolution of rifting in Africa. Nature 224, 1178-1182.

Girdler, R.W. and McConnell, D.A. 1994. The 1990 to 1991 Sudan Earthquake sequence and the extent of the East African rift system. Science 264, 67-70.

Giese, P., Scheuber, E., Schilling, F.R., Schmitz, M., Wigger, P., 1999. Crustal thickening processes in the central Andes and the different natures of the Moho-discontinuity. Journal of South American Earth Sciences 12, 201-220.

Goodwin, A.M., 1996. Principles of Precambrian Geology, Academic, SanDiego, California, 327p.

Gouin, P., Mohr, P.A., 1964. Gravity traverses in Ethiopia (first interim report). Bulletin of Geophysical Observatory (Ethiopia) 7, 185-239.

Grand, S.P., van der Hilst, R.D., Widiyantoro, S., 1997. Global seismic tomography: a snapshot of convection in the earth. GSA Today 7 (4), 1-7.

Götze, H.-J., 1976. Ein numerisches Verfahren zur Bereschnung der gravimetrischen und magnetischen Feldgrössen für dreidimensionale Modelkörper. Dissertation, T.U. Clausthal.

Götze, H.-J., 1984. Über den Einsatz interaktive Computergraphik im Rahmen 3-dimensionaler Interpretationstechniken in Gravimetrie und Magnetik, Habil. Schrift, TU Clausthal.

Götze, H.-J. and Lahmeyer, B., 1988. Application of three-dimensional interactive modelling in gravity and magnetics. Geophysics 53 (8), 1096-1108.

Götze, H.-J., Meures, B., Schmidt, S., Steinhauser, P., 1991. On the isostatic state of eastern Alps and the central Andes; a statistical comparison. In: Harmon, R.S., Rapela, C.W. (Editors), Andean Magmatism and its Tectonic Setting. Geological Society of America 265, 279-290.

Götze, H.-J, Krause, S., 2001. The central Andean gravity high, a relic of an old subduction complex?. Journal of South American Earth Sciences 14, 799-811.

Götze, H.-J, Woldetinsae, G., Schmidt, S., Tasarova, S, Ebbing, J., Prezzi, C., Lippmann, A., 2004: Integrated Three Dimensional Gravity Modelling in Different Types of Geological Environments. Eos trans. AGU 85(47) fall meet. Supl., Abstract G51C-0096.

Gurnis, M., Mitrovica, J.X., Ritsema, J., and van Heijst, H.-J., 2000. Constraining mantle density structure using geological evidence of surface uplift rates: The case of the African super plume: Geochemistry, Geophysics, and Geosystems 1, 1999G000035.

Hackney, R., 2004. Gravity anomalies, crustal structure and isostasy associated with the Proterozoic Capricorn Orogen, Western Australia. Precambrian Research 128, 219-236.
Hackney, R., Featherstone, W.E., Götze, H.-J, 2004. ASEG 17th Geophysical Conference and Exhibition, Sydney.
Hager, B.H., Clayton R.W., Richards, M.A., Comer, R.P., Dziewonski, A.M, 1985. Lower mantle heterogeneity, dynamic topography and the geoid, Nature 313, 541-545.
Hartley, R., Watts, A.B., Fairhead, J.D., 1996. Isostasy of Africa. Earth and Planetary Science Letters 137, 1-18.
Hautot, S., Whaler, K., Gebru, W., Dessisa, M., 2004. The structure of the Lake Tana basin (Ethiopia) inferred from magnetotelluric imaging (Abstract). EARS conference June 20-24, Addis Ababa, Ethiopia.
Hayward, N. J., Ebinger, C. J., 1996. Variations in the along-axis segmentation of the Afar rift system, Tectonics 15, 244-257.
Hay, D.E, Wendlandt, R.F., Keller, G.R., 1995. Origin of Kenya Rift Plateau-type phonolites: Integrated petrologic and geophysical constraints on the evolution of the crust and upper mantle beneath the Kenya Rift. Journal of Geophysical Research 100, 10549-10557.
Hearn, P., Hare,T., Schruben, P., Sherrill, D., LaMar, C., Tsushima, P., 2001. Global GIS database, Digital Atlas of Africa. USGS publication.
Hébert, H., Deplus, C., Huchon, P., Khanbari, K., Audin, L., 2001.Lithospheric structure of a nascent ridge inferred from gravity data: The western Gulf of Aden, Journal of Geophysical Research 106, 26345-26363.
Heiskanen, W.A., and Vening Meinesz, F.A., 1958. The earth and its gravity field. McGraw-hill NewYork, Toronto and London, 470 pp.
Henry, W.J., Mechie, J., Mahuire, P.K.H., Khan, M.A., Prodell, C., Keller, G.R., Patel, J., 1990. Seismic investigation of the Kenya rift valley, Geophysical Journal International 100, 107-130.
Hubbert, M.K., 1948. A line integral method of computing the gravimetric effects of two-dimensional masses. Geophysics 13, 215-225.
Jestin, F., Huchon, P., Gaulier, M., 1994. The Somalia plate and the East African Rift system: Present-day kinematics. Geophysical Journal International 116, 637-654.
Kampunzu, A.B., Mohr, P., 1991. Magmatism evolution and pertogenesis in the East African Rift system. In: Kampunzu, A.B., Lubala, R.T. (Editors), Magmatism in extensional structural settings, Springer-Verlag, 85-136, Berlin.
Kazmin, V. 1972. The Geology of Ethiopia, EIGS Tech. Report, Addis Ababa, Ethiopia.
Kazmin, V, 1978. Geology of the Ethiopian basement and possible relation between the Mozambique and the Red Sea belts. Egyptian Journal of Geology, 22, 73-86.
Kebede, F., Kulhanek, O., 1991. Source parameters of selected earthquakes on the central and western margin of Afar. Tectonophysics 170, 243-257.
Keller, G.R., Mechie, J., Braile, L.W., Mooney, W.D., Prodehl, C., 1994. Seismic structure of the uppermost mantle beneath the Kenya rift. Tectonophysics 236, 201-216.
Keller, G.R., Harder, S.H., Reilly, B.R., Mickus, K., Tadesse, K., Maguire, P.K.H., 2004. A preliminary analysis of crustal structure variations along the Ethiopian rift. EARS conference, June 20-24, Addis Ababa, Ethiopia.
Kendal, J.M., Stuart, G.W., Ebinger, C.J., Bastow, I.D., Keir, D., 2005. Magma-assisted rifting in Ethiopia, Nature 433, 146-148.
Keranen, K., Klemperer, S.L., Gloaguen, R., 2004. Three-dimensional seismic imaging of a protoridge axis in the Main Ethiopian Rift. Geology 32(11), 949-952.
Kirchner, A., 1997. 3D-Dichtemodellierung zur Anpassung des Schwere-und des Schwerepotentialfeldes der zentralen Anden. Berliner Geowissenschaftliche Abhandlungen (B), Bd. 25, Freie Universität Berlin.
Knox, R.P., Nyblade, A.A., Langston, C.A., 1998. Upper mantle S velocities beneath Afar

and western Saudi Arabia from Rayleigh wave dispersion. Geophysical Research Letters 25, 4233-4236.
Krenkel, E.1922. Die Bruchzonen Ostafrikas. Berlin: Gebr. Borntraeger.184 pp.
KRISP Working Group, 1987. Structure of the Kenya rift from seismic refraction. Nature 325, 239-242.
KRISP Working Group, 1991. Large-scale variation in lithospheric structure along and across the Kenya Rift. Nature 354. 223-227.
Kröner, A., 1985. Ophiolites and the evolution of tectonic boundaries in the late Proterozoic Arabian Nubian Shield of the northeast Africa and Arabia. Precambrian Research 27, 277-300.
Li, X. and Götze, H.-J., 2001. Ellipsoid, geoid, gravity, geodesy, and geophysics. Geophysics 66, 1660-1668.
Lithgow-Bertelloni, C., and Richards, M.A., 1995. Cenozoic plate driving forces. Geophysical Research Letters 22(11), 1317-1320.
Lithgow-Bertelloni, C., Silver, P.G., 1998. Dynamic topography, plate driving forces and the African superswell. Nature 395, 269-272.
Maguire, P., et al., 2003. Geophysical project in Ethiopia studies of continental break-up. EOS, Transaction of American Geophysical Union 84, 337, 342-343.
Mahatsente, R., 1998. Crustal structure of the main Ethiopian Rift from gravity data: 3-dimensional forward modelling and inversion. PhD dissertation, Technische Universität Clausthal, 157 pp.
Mahatsente, R., Jentzsch, G., Jahr, T., 1999. Crustal Structure of the Main Ethiopian Rift from gravity data: 3-dimensional modelling. Tectonophysics 313, 363-382.
Makris, J., Thiele, P., Zimmermann, J., 1969. Crustal Investigation from gravity measurements at the scarp of the Ethiopian Plateau. Zeitschrift für Geophysik, Band 36, 299-311, Physica-verlag, Würzburg.
Makris, J. Menzel, H. and Zimmerman, J., 1972. A preliminary interpretation of the gravity field of Afar, northeast Ethiopia. In: Girdler, R.W. (Editor), East African Rifts. Tectonophysics 15, 31-39.
Makris, J., Ginzburg, A., 1987. The Afar Depression, transition between continental rifting and sea floor spreading. Tectonophysics 141, 199-214.
Makris, J., Menzel, H., Zimmermann, J., Gouin, P., 1975. Gravity field and crustal structure of north Ethiopia. In: Pilger, A., Rosler, A. (Editors), Afar Depression of Ethiopia, Schweizerbart, 135-144, Stuttgart.
Makris, J., Tsirondis, J., Richter, H., 1991. Heat flow density distribution in the Red Sea. Tectonophysics, 198, 383-393.
Mariita, N., 2004. Ranking of Geothermal Potential of volcanic centres of the Northern Kenya Rift (Abstract).EARS conference June 20-24, Addis Ababa, Ethiopia.
Marty, B., Pik, R., Gezahegn, Y., 1996. Helium isotopic variations in Ethiopian plume lavas: nature of magmatic sources and limit on lower mantle contribution. Earth and Planetary Science Letters 144, 223-237.
Mackenzie, G.D., Thybo, H., Maguire, P.K.H., Ebinger, C.J., 2004. evidence for crustal structure influence on the evolution of the Main Ethiopian Rift (abstract). EARS conference, June 20-24, Addis Ababa, Ethiopia.
Mckenzie, D., 1978. Some remarks on the development of sedimentary basins, Earth Planetary Science Letters 40, 25-32.
Mckenzie, D.P., Fairhead, J.D., 1997. Estimates of the effective elastic thickness of the continental lithosphere from Bouguer and free-air anomalies. Journal of Geophysical Research 102, 27523-27552.
McNutt, M.K., 1980. Implications of regional gravity for the state of stress in the earth's crust and upper mantle. Journal of Geophysical Research 85, 6377-6396.

Mechie, J., Keller, G.R., Prodehl, C., Gaciri, S., Braile, L.W., Mooney, W.D., Gajewski, D., Sandmeier, K.-J., 1994. Tectonophysics 236, 179-200.
Mengel, K., and Kern, H., 1992. Evolution of the petrological and seismic Moho implication for the continental crust-mantle boundary. Terra Nova 4, 109-116.
Mogessie, A., Belete, K.H., Hoinkes, G., 2000. Yubdo-Tulu Dimtu mafic-ultrmafic belt, Alaskan-type intrusions in western Ethiopia: its implication to the Arabian-Nubian Shield and tectonics of the Mozambique belt. Journal of African Earth Sciences 30, 62
Mohr, P.A., Gouin, P. 1967. Gravity traverses in Ethiopia. Bulletin of Geophysical Observatory (Ethiopia) 10, 15-52.
Mohr, P.A., and Wood, C.A., 1976. Volcano spacings in the Eastern rift of Africa. Centre for Astrophysics, preprint series No. 510.
Mohr, P.A., 1983. The Ethiopian flood basalt province. Nature 303, 577-584.
Mulugeta, G. and Ghebreab, W., 2001. Modelling heterogeneous stretching during episodic or steady rifting of the continental lithosphere. Geological Society of America 29, 895-898.
Mulugeta, G. 2004, Dynamic models of magma emplacement during rifting of continental lithosphere: implications for the main Ethiopian Rift (MER) (Abstract). EARS conference, June 20-24, Addis Ababa Ethiopia.
Negash, B., and Ayele, A., 1995. Interpretation of gravity data over the Main Ethiopian and southern rift systems. GSE, Tech. Report, Addis Ababa, Ethiopia.
Nyblade, A.A., Pollack, H.N., Jones, D.L., Podmore, F., Mushayandebvu, M., 1990. Terrestrial heat flow in east and southern Africa. Journal of Geophysical Research 65, 17 371-17384.
Nyblade, A.A., Robinson, S.W., 1994. The African superswell. Geophysical Research Letters 21, 765-768.
Nyblade, A.A., and Brazier, R.A., 2002. Precambrian lithospheric controls on the development of the East African rift system. Geology 30, 755-758.
Okabe, M., 1979. Analytical expressions of gravity anomalies due to homogeneous polyhedral bodies and translations into magnetic anomalies. Geophysics 44, 730-741.
Oluma, B. and Zewuge, M., 2001. Notes on a Gravity Survey of North Western Ethiopia. Geological Survey of Ethiopia, Unpublished report, Addis Ababa, Ethiopia.
Pacella, G.B., 1948. Gravity determinations in Ethiopia. Dai Rendicontidell Academia Nationale dei Lincei.
Panasyuk, S.V., and Hager, B.H., 2000. Models of isostatic and dynamic topography, geoid anomalies and uncertainties. Journal of Geophysical Research 105, 28199-28209.
Panasyuk, S.V., Hager, B.H., Forte, A.M., 1996. Understanding the effects of mantle compressibility on geoid kernels. Geophysical Journal International 124 121-133.
Parker, R.L, 1972. The rapid calculation of potential anomalies. Geophysical Journal of Royal astronomical Society 31,447-455.
Partridge, T.C., Maud, R.R., 1987. Geomorphic evolution of southern Africa since Mesozoic. South African Journal of Geology 90, 179-208.
Plouff, D., 1976. Gravity and magnetic fields of polygonal prisms and application to magnetic terrain corrections. Geophysics 41, 727-41.
Pollack, H.N., Hurter, S.J., Johnson, J.R., 1993. Heat flow from the earth's interior: Analysis of the global data set. Review of Geophysics 31, 267-280.
Prodehl, C., Fuchs, K., Mechie, J., 1997. Seismic-refraction studies of the Afro-Arabian Rift System-a brief review. Tectonophysics 278, 1-13.
Purcell, P.G., 1981. the Bouguer gravity field of Ethiopia and the tectonics of the east African rift, M.Sc. Thesis, University of Sydney, Australia.
Ritsema, J., Nyblade, A.A., Owens, T.J., Langston, C. A., VanDecar, J. C., 1998. Upper mantle seismic velocity structure beneath Tanzania, east Africa: implications for the stability of cratonic lithosphere. Journal of Geophysical Research 103, 21201-21213.

Ritsema, J., Van Heijst, H.J., 2000. New seismic model of the upper mantle beneath Africa. Geology 28, 63-66.
Richardson, S.M., and McSween, H.Y., 1989. Geochemistry Pathways and Processes. Prentice-Hall, Inc. P.327-342.
Roberts, A. 2001. Curvature attributes and their application to 3D interpreted horizons, First break 19.2, 85-100.
Rogers, N., Macdonald, R., Fitton, J.G., George, R., Smith, M., Barreiro, B., 2000. Two mantle plumes beneath the east African rift system: Sr, Nd and Pb isotope evidence from Kenya rift basalts. Earth and Planetary Science letters 176, 387-400.
Rooney, T.O, Furman, T., Ayalew, D., Yirgu, G., 2004. Silicate veining above an ascending mantle plume-evidence from new Ethiopian Xenolith localities. EOS Trans. AGU 85(47), Fall meet. Suppl., Abstract V51B-0560.
Ruegg, J.C., 1975. Main results about the crustal and upper mantle structure of the Djibouti region (T.F.A.I). In: Pilger, A., Rösler, A. (Editors), Afar Depression of Ethiopia. Schweizerbart Stuttgart pp. 120-134.
Schilling, F.R., and Partzsch, G.M., 2001. Quantifying partial melt fraction in the crust beneath the central Andes and the Tibetan plateau. Physics and chemistry of the Earth 26, 239-246.
Schmidt, S. and Götze, H.-J., 1998. Interactive visualization and modification of 3D models using GIS functions. Physics and chemistry of the earth, 23, 289-296.
Schmidt, S., and Götze, H.-J., 1999. Integration of data constraints and potential field modelling-an example from southern Saxony, Germany. Physics and Chemistry of the Earth (A) 24(3), 191-196.
Searle, R., Gouin, P., 1972. A gravity survey of the central part of the Ethiopian rift valley. Tectonophysics 15, 41-42.
Simpson, R.W., Jachens, R.C., Blakely, Richard J. Saltus, R.W., 1986. A new isostatic residual gravity map of the conterminous United States with a discussion on the significance of isostatic residual anomalies. Journal of Geophysical Research 91, 8348-8372.
Simyu, S.M. and Keller, G.R., 1997. An integrated analysis of lithospheric structure across the East African plateau based on gravity anomalies and recent seismic studies. Tectonophysics 278, 291-313.
Smith, W. H. F., Sandwell, D.T., 1997. Global seafloor topography from satellite altimetry and ship depth Soundings. Science 277, 1956-1962.
Singh, B. 2002. Simultaneous computation of gravity and magnetic anomalies resulting from 2-D object. Geophysics 67, 801-806.
Sleep, N.H., 1997. Lateral flow and ponding of starting plume material. Journal of Geophysical Research 102, 10001-10012.
Sobolev, S.V., and Babeyko, A.Y.,1994. Modelling of mineralogical composition, density and elastic velocities in anhydrous magmatic rocks. Surveys in Geophysics 15, 515-544.
Sobolev, S.V., Zeyen, H., Stoll, G., Werling, F., Altherr, R., Fuchs, K., 1996. Upper mantle temperatures from teleseismic tomography of French Massif Central including effects of composition, mineral reactions, anharmonicity, anelasticity and partial melt. Earth and Planetary Science letters 139, 147-163.
Stern, R.J., 1994. Arc assembly and continental collision in the Neoproterozoic East African orogen: implications for the consideration of Gondwana land. Annual Review, Earth and Planetary Science Letters 22, 319-351.
Stewart, K., and Rogers, N., 1996. mantle plume and lithospheric contributions to basalts from Southern Ethiopia. Earth and Planetary Science Letters 139, 195-211.
Tadesse, T., 1996. Structures across a possible intra-oceanic suture zone in the low-grade Pan-African rocks of northern Ethiopia. Journal of African Earth Sciences 23, 375-381.
Talwani, M. and Ewing, M., 1960. Rapid computation of gravitational attraction of three-

dimensional bodies of arbitrary shape. Geophysics 25, 203-225.
Tefera, M., Chernet, T., Haro, W., 1996. Geological Map of Ethiopia, 1: 2000000, second edition. EIGS, Addis Abba.
Teklemariam, M., 2004. Overview of geothermal resources utilization and potential in eastern Africa, EARS (Abstract). EARS conference, June 20-24, 2004, Addis Ababa, Ethiopia.
Tesfaye, S., Harding, D., Kusky, T.M., 2003. Early break-up boundary and migration of the Afar Triple junction, Ethiopia. Geological Society of America Bulletin 115, 1053-1067.
Tessema, A., Antoine, L.A.G., 2003. Variations in effective elastic plate thickness of the East Africa lithosphere. Journal of Geophysical Research 108 (B5), 2224, doi: 1029/2002JB002200.
Turcotte, D.L, and Emerman, S.H., 1983. Mechanisms of active and passive rifting, Tectonophysics 94, 39-50.
Turcotte, D.L. and Schubert, G., 2002. Geodynamics (second edition). Cambridge
Ukstins, I., Renne, P., Wolfenden, E., Baker, J., Ayalew, D., Menzies, M.A., 2002. Matching conjugate volcanic rifted margins: $^{40}Ar/^{39}Ar$ chronostratigraphy of pre-and-syn-rift bimodal flood volcanism in Ethiopia and Yemen. Earth and Planetary Science Letters 198, 289-306.
UNDP, 1994. UNDP Project ETH/90/009 Airborne survey processing Report, GSE, Addis Ababa, Ethiopia.
Upcott, N. M., Mukasa, R.K., Ebinger, C.J., Karner, G.D., 1996. Along-axis segmentation and isostasy in the Western rift, East Africa. Journal of Geophysical Research 101, 3247-3268.
Vail, J.R., 1983. Pan African crustal accretion in Northeast Africa. Journal of African Earth Sciences 1, 285-249.
Vearncombe, J.R., 1983. A dismembered ophiolite from the Mozambique Belt, West Pokot, Kenya. Journal of African Earth Sciences 1, 133-143.
Vogel, A., 1964. Least squares in three-dimensional gravity and magnetic interpretation. Geoexploration 2.
Vogt, P.R., 1978. Long wavelength gravity anomalies and interaplate seismicity. Earth and Planetary Science Letters 37, 465-475
Watts, A.B., 2001. Isostasy and flexure of the lithosphere, Cambridge University Press, 451 pp.
Williams, LA.J., 1982. Physical aspects of magmatism in continental rifts. In Palmasson, G (Ed.): Continental and Oceanic rifts. AGU Geodynamics series 8, 193-222.
Willis, B. 1936. East African plateaus and Rift Valleys. Washington D.C. Carnegie Inst. 385 pp.
Woldegabriel, G., 1987. Volcano-tectonic history of the central sector of the Main Ethiopian Rift. PhD thesis, Casewestern reserve University, Cleveland, and USA.
WoldeGabriel, G., Aronson, J., Walter, R., 1990. Geology, geochronology, and rift basin development in the central sector of the Main Ethiopian Rift. Geological Society of America Bulletin 102, 439-458.
Woldegabriel, G., Heiken, G., White, T.D., Asfaw, B., Hart, W.K., Renne, P.R. 2000. Volcanism, tectonism, sedimentation, and the paleoanthropological record in the Ethiopian Rift System. Geological Society of America, special paper 345.
Woldegabriel, G., Renne, P.R., Hart, W.R., Ambrose, S., Asfaw, B., White T.D., 2004. Geoscience methods lead to Paleao-anthropological Discoveries in Afar Rift, Ethiopia. EOS, Transactions of American Geophysical Union 85, 29, 273-276.
Woldetinsae, G., kebede, Y., Tareke, F., Belachew, M., Seifu, A., Yosef, M., Gebreselassie, H., Hailu, A., 2000. Geophysical signatures of Egambo and Baruda prospects, western Ethiopia. Geological Survey of Ethiopia Tech. Report (unpublished), Addis Ababa.
Wondirad, B., 2000. Preliminary report on the gravity survey results of the southeastern

highlands and associated lowlands. Geological Survey of Ethiopia (unpublished), Addis Ababa.

Worku, H., 1996. Geodynamic development of the Adola Belt (Southern Ethiopia) in the Neoproterozoic and its control on gold mineralization. PhD Thesis, Berlin Technical University 156, Verlag Dr. Koster, Berlin.

Yibas, B., Reimold, W.U, Armstrong, R, Koeberl, C., Anhaeusser, C.R, and Phillips, D. 2002. The tectonostratigraphy, granitoid geochronology and geological evolution of the Precambrian of Southern Ethiopia. Journal of African Earth Sciences 34, 57-84.

Yihunie, T., Tesfaye, M., 2002. Structural evidence for allochthonous nature of the Bulbul terrain in southern Ethiopia: A west verging-thrust nappe. Journal of African Earth Sciences 34, 85-93.

Zeyen, H., Volker, F., Wehrle, V., Fuchs, K., Sobolev, S., Altherr, R., 1997. Styles of continental rifting: crust-mantle detachment and mantle plumes. Tectonophysics 278 329-352.